NAT'L INST. OF STAND & TECH R.I.C.
A11103 440665
NIST
PUBLICATIONS

United States Department of Commerce
National Institute of Standards and Technology

NISTIR 90-3939

EMR TEST FACILITIES EVALUATION OF A SMALL REVERBERATING CHAMBER LOCATED AT RADC, GRIFFISS AFB ROME, NEW YORK

Myron L. Crawford
John M. Ladbury
Bill F. Riddle
Ezra B. Larsen

QC
100
.U56
90-3939
1990
C.2

NATIONAL INSTITUTE OF STANDARDS &
TECHNOLOGY
Research Information Center
Gaithersburg, MD 20899

DATE DUE

Demco, Inc. 38-293

NISTIR 90-3939

EMR TEST FACILITIES EVALUATION OF A SMALL REVERBERATING CHAMBER LOCATED AT RADC, GRIFFISS AFB ROME, NEW YORK

Myron L. Crawford
John M. Ladbury
Bill F. Riddle
Ezra B. Larsen

Electromagnetic Fields Division
Center for Electronics and Electrical Engineering
National Engineering Laboratory
National Institute of Standards and Technology
Boulder, Colorado 80303-3328

June 1990

Sponsored by
Compatibility and Measurements Division
RADC/RBC
Griffiss AFB, New York 13441

U.S. DEPARTMENT OF COMMERCE, Robert A. Mosbacher, Secretary
NATIONAL INSTITUTE OF STANDARDS AND TECHNOLOGY, John W. Lyons, Director

CONTENTS

		Page
Abstract		1
1.	Introduction	2
2.	Description of the RADC Small Reverberating Chamber and NIST Evaluation Systems	3
3.	CW Evaluation of the RADC Small Reverberating Chamber	5
	3.1 Antenna Coupling Efficiency and VSWR	5
	3.2 Chamber Q Factor	6
	3.3 Tuner Effectiveness	7
	3.4 Test Zone E-Field Uniformity	7
	3.5 E-Field Amplitude Calibration	8
	3.6 Comparison of Data for the RADC Small Reverberating Chamber with the NIST Anechoic Chamber	9
4.	CW Measurement Uncertainty for the RADC Small Reverberating Chamber	10
	4.1 Estimate of Uncertainty for Establishing a CW E-Field Amplitude in the Chamber	10
	4.2 Comments on CW Measurement Uncertainty	10
5.	Pulsed RF Evaluation of the RADC Small Reverberating Chamber	11
	5.1 Background	11
	5.2 Evaluation of Pulsed RF Measurements in the Mode-Tuned Chamber	12
	5.3 Evaluation of Pulsed RF Measurements in the Mode-Stirred Chamber	13
	5.4 Comments on Pulsed RF Measurements	14
6.	Summary and Conclusions	14
7.	Recommendations	15
8.	Acknowledgments	16
9.	References	16

LIST OF FIGURES

Figure		Page
2.1	Two isometric sketches of the RADC small reverberating chamber	18
2.2	Cross sectional views of the RADC small reverberating chamber showing placement of transmitting and receiving antennas, chamber tuner and isotropic probes for measuring spatial E-field uniformity	19
2.3	Six photographs of the RADC small reverberating chamber	20
2.4	Photograph of NIST equipment used to evaluate the RADC small chamber	21
2.5	Block diagram of instrumentation used in cw evaluation of the RADC small chamber	22
2.6	Block diagram of instrumentation used in pulsed rf evaluation of the RADC small chamber	23
3.1	Measured VSWR of: (a) long wire antennas (0.2 to 18 GHz), and (b) broadband horn antennas (0.8 to 18 GHz), transmitting into the RADC small chamber	24
3.2	Measured coupling efficiency of: (a) long wire antennas (0.2 to 18 GHz), and (b) broadband horn antennas (0.8 to 18 GHz), in the RADC small chamber. Losses determined in (b) are from cw mode-tuned measurements and from pulsed rf measurements	25
3.3	(a) Theoretical and experimental Q of the RADC small chamber, and (b) ratio of theoretical to experimental Q (0.4 to 18 GHz)	26
3.4	Measured tuner effectiveness in the small chamber using: (a) long wire antenna (0.2 to 18 GHz), and (b) broadband horn antenna (0.8 to 18 GHz)	27
3.5a,b	Spatial distribution of E-field components in the small chamber measured with 10 NIST isotropic probes (5 cm dipoles), using long wire antennas for transmitting and receiving: (a) maximum values, and (b) average values. Net transmitted power = 1 W	28,29
3.6a,b	Spatial distribution of E-field components in the small chamber measured with 10 NIST isotropic probes (5 cm dipoles), using broadband horn antennas: (a) maximum, and (b) average values. Net transmitted power = 1 W	30,31
3.7	Average values of E-field components in the small chamber measured with 10 NIST isotropic probes (5 cm dipoles), using long wire antennas: (a) average of the 10 maximum values for each component, and (b) average of the 10 average values. Net transmitted power = 1 W	32

LIST OF FIGURES (CONTD.)

Figure		Page
3.8	Average values of E-field components in the small chamber measured with 10 NIST isotropic probes (5 cm dipoles), using broadband horn antennas: (a) average of the 10 maximum values for each component, and (b) average of the 10 average values. Net transmitted power = 1 W	33
3.9	Maximum and average E-field strengths in the small chamber measured with: (a) 1 cm dipole probe, and (b) received power of long wire antenna. Net transmitted power = 0.1 W	34
3.10	Maximum and average E-field strengths in the small chamber measured with: (a) 1 cm dipole probe, and (b) received power of broadband horn antenna. Net transmitted power = 0.1 W	35
3.11	Maximum responses of NIST 1 cm dipole probe to an E-field of 37 dBV/m using: (a) RADC small reverberating chamber, and (b) NIST anechoic chamber	36
3.12	Maximum powers received by a broadband (1 to 18 GHz) horn antenna in an E-field of 37 dBV/m using: (a) RADC small reverberating chamber, and (b) NIST anechoic chamber	37
3.13	Comparison of: (a) free-space gain of a broadband horn antenna, with (b) difference in maximum responses of the horn measured in NIST anechoic chamber minus RADC small reverberating chamber	38
5.1a-j	Maximum and average values of received rf pulse waveforms in the mode-tuned RADC small reverberating chamber using no rf absorber (chamber empty) and 1 piece of absorber;	
	(a) F = 0.9 GHz	39
	(b) F = 1.3 GHz	40
	(c) F = 2.0 GHz	41
	(d) F = 2.9 GHz	42
	(e) F = 4.2 GHz	43
	(f) F = 5.65 GHz	44
	(g) F = 8.9 GHz	45
	(h) F = 12 GHz	46
	(i) F = 16 GHz	47
	(j) F = 18 GHz	48
5.2	Graphs of data from figure 5.1 showing the time required for 3 μs rf pulses transmitted into the mode-tuned chamber to rise to 63 % of the steady state amplitude, using: (a) no absorber, and (b) 1 piece of 7.6 cm x 61 cm x 61 cm rf absorber	49
5.3	Graphs of data from figure 5.1 showing the time required for 3 μs rf pulses transmitted into the mode-tuned chamber to rise to 90 % of the steady state amplitude, using: (a) no absorber, and (b) 1 piece of 7.6 cm x 61 cm x 61 cm rf absorber	50

Figure		Page
5.4a,b	Graphs of correction factors for response ammplitude of rf pulses in the mode-tuned chamber as a function of frequency, at selected pulse duration, using: (a) no absorber, and (b) 1 piece of 7.6 cm x 61 cm x 61 cm rf absorber	51,52
5.5a-j	Maximum values of received rf pulse waveforms in the mode-stirred RADC small reverberating chamber using no rf absorber (chamber empty) and 1 piece of absorber;	
	(a) F = 0.9 GHz	53
	(b) F = 1.3 GHz	54
	(c) F = 2.0 GHz	55
	(d) F = 2.9 GHz	56
	(e) F = 4.2 GHz	57
	(f) F = 5.65 GHz	58
	(g) F = 8.9 GHz	59
	(h) F = 12 GHz	60
	(i) F = 16 GHz	61
	(j) F = 18 GHz	62
5.6	Graphs of data from figure 5.5 showing the time required for 3 μs rf pulses transmitted into the mode-stirred chamber to rise to 63 % of the steady state amplitude, using: (a) no absorber, and (b) 1 piece of 7.6 cm x 61 cm x 61 cm rf absorber	63
5.7	Graphs of data from figure 5.5 showing the time required for 3 μs rf pulses transmitted into the mode-stirred chamber to rise to 90 % of the steady state amplitude, using: (a) no absorber, and (b) 1 piece of 7.6 cm x 61 cm x 61 cm rf absorber	64
5.8a,b	Graphs of correction factors for response amplitude of rf pulses in the mode-stirred chamber as a function of frequency, at selected pulse durations, using: (a) no absorber, and (b) 1 piece of 7.6 cm x 61 cm x 61 cm rf absorber	65,66

LIST OF TABLES

Table		Page
3.1	Spatial variation of the cw E-field average and maximum values measured in the RADC small reverberating chamber -----	67
4.1	Summary of estimated uncertainties for determining the cw field strength inside the mode-tuned RADC small reverberating chamber (0.5 to 2.0 GHz)----------	68
4.2	Summary of estimated uncertainties for determining the cw field strength inside the mode-stirred RADC small reverberating chamber (2 to 18 GHz)----------	69
5.1a,b	Mode-tuned data obtained from figure 5.1, giving rise times and correction factors for rf pulses in the RADC small reverberating chamber ----------	70,71
5.2a,b	Mode-stirred data obtained from figure 5.5 giving rise times and correction factors for rf pulses in the RADC small reverberating chamber ----------	72,73

EMR Test Facilities: Evaluation of a Small Reverberating Chamber Located at RADC, Griffiss AFB, New York

Myron L. Crawford
John M. Ladbury
Bill F. Riddle
Ezra B. Larsen

Electromagnetic Fields Division
National Institute of Standards and Technology
Boulder, Colorado 80303

This report describes measurement procedures and results from evaluating a small reverberating chamber located at Rome Air Development Center (RADC), Rome, New York. The chamber was developed for measuring and analyzing the electromagnetic susceptibility/vulnerability (EMS/V) of weapon systems and the radio frequency (rf) shielding effectiveness of enclosures and materials. A brief description of the facility is given, including instrumentation for its evaluation and calibration by the National Institute of Standards and Technology (NIST). Work was done earlier at NIST to evaluate the RADC large reverberating chamber. A follow-on project to construct and evaluate a small chamber is discussed in this report. Measurements include: (1) voltage standing wave ratio (VSWR) of the transmitting and receiving antennas; (2) coupling efficiency of the chamber; (3) effectiveness of the chamber tuner; (4) E-field uniformity in the test zone; (5) calibration of test E-fields based on receiving antenna power measurements and calibrated dipole probe voltage measurements; (6) responses of standard equipment under test (EUT) to test fields in the RADC reverberating chamber and the NIST anechoic chamber; and (7) performance of the reverberating chamber excited by rf pulses at ten frequencies from 0.9 to 18 GHz, four pulse widths from 0.1 to 3 μs, and for two values of chamber Q. Conclusions are that the chamber can be used at frequencies down to 500 MHz for cw testing, and for pulsed rf immunity testing with pulse widths as short as 0.3 μs. Estimates of measurement uncertainties are given.

Key words : electromagnetic radiated susceptibility/vulnerability testing ; pulsed rf measurements ; reverberating chamber .

1. Introduction

The use of a reverberating chamber for performing EMS/V measurements is relatively new. Considerable work has been done to evaluate and document methods for using this technique [1-3]. Research work has also been done at the National Institute of Standards and Technology (NIST) to evaluate, develop, describe, and document the methodology for performing radiated susceptibility/vulnerability (EMS/V) measurements using a reverberating chamber. This effort is described in an NIST publication [4] and an IEEE Proceedings paper [5]. In addition, work was performed to determine the feasibility of using such a chamber for pulsed rf immunity testing [6,7]. Finally a project for the present sponsor covered the evaluation of a large reverberating chamber (9.78 m x 5.18 m x 3.69 m). This work is summarized in an interagency report sent to the sponsor in December 1987 [8]. The measurements described in that report are similar to those discussed in the present report, which pertains to a small chamber (1.75 m x 1.41 m x 1.57 m), based on the sponsor's guideline. Both the "large" and "small" reverberating chambers are now located at Griffiss Air Force Base (AFB), but the data for the small chamber were taken by NIST personnel while the chamber was at its original location at NIST in Boulder, Colorado.

The incentive for performing this work stems from numerous advantages suggested for the use of a reverberating chamber. These include:

1. Electrical isolation from or to the external environment;
2. Convenience (indoor test facility) compared with an open field test site;
3. Ability to generate high level fields over a large test volume with relatively small power;
4. Broad frequency coverage;
5. Cost effectiveness;
6. Potential use for both radiated susceptibility and emission testing with minor instrumentation changes;
7. No requirement of physical rotations of the equipment under test (EUT); and
8. Security.

These advantages are somewhat offset by limitations, which include loss of polarization and directivity information relative to the EMC/EMI profile of the EUT, and limited measurement accuracy. However, this technique does offer a time-efficient, cost-effective way to evaluate the EMS/V performance of large equipment using an existing shielded enclosure with minor modifications. The measurement concept utilizes the shielded, high-Q, multimoded environment to obtain time-averaged field strengths that simulate "real world" near-field environments. Also, it is sometimes the only technique by which high exposure fields can be generated safely to perform EM susceptibility tests required by the Department of Defense for some of their applications.

These considerations, along with others, motivated RADC to invest in the research and development of this methodology. They then constructed and placed into operation two reverberating chamber facilities, one of which is described in this report.

Measurements described in this report were performed between January and May, 1989.

2. Description of the RADC Small Reverberating Chamber and NIST Evaluation Systems

The RADC small reverberating chamber is a rectangular shielded enclosure 1.75 m x 1.41 m x 1.57 m (5.75 ft x 4.625 ft x 5.15 ft) in size, constructed from sheet aluminum welded together at the edges. Cross sectional views of the chamber are shown in figure 2.1. It is equipped with two bulkhead access panels and an access door located at the end of the chamber. The chamber is also equipped with a tuner shown in figure 2.2 consisting of a rectangular blade about 1 m in cross section. The tuner is rotated in a step-wise fashion under computer control.

The locations and orientations of the chamber's excitation (transmitting) and reference (receiving) antennas are shown in figure 2.2. The antennas are placed so as to be cross polarized or in the corners of the chamber and oriented toward the corners to ensure that the transmitted signal couples into all possible modes and to monitor the reference received signal from all possible modes as efficiently and uniformly as possible. This must be done without favoring particular modes or transmitting directly into the chamber's test zone, or coupling the signal directly between the transmitting and receiving antennas. This is necessary to obtain a statistically uniform, spatial distribution of the field in the chamber's test zone. Photographs of six different views of the chamber are shown in figure 2.3. Captions are given for each photograph describing the particular view.

Figure 2.4 is a photograph of the NIST equipment used to perform the chamber evaluations. Figure 2.5 is a block diagram of the NIST system used for the cw evaluation measurements and figure 2.6 is the block diagram of the NIST system used for the pulsed rf evaluation measurements of the chamber. A test field is established inside the chamber by means of an rf source (cw or pulsed, depending on the tests being performed) connected to the appropriate transmitting antenna. The term "cw" used here stands for continuous wave and refers to a single-frequency sinusoidal signal, and the term "pulsed rf" refers to pulse-modulated cw with characteristics similar to a pulsed radar signal. Modes excited inside the chamber are stirred by rotating the tuner, which functions as a field-perturbing device.

The test zone in the chamber is defined as the total volume minus a minimum separation from the walls and ceiling of approximately 30 cm. Placement of the equipment under test (EUT) should fall within this volume except, possibly, relative to the floor. The separation distance between the EUT and the floor may be less than 30 cm depending upon the intended EUT configuration relative to the ground plane. Test leads and cables are routed to appropriate monitors, etc., outside the chamber through shielded feed-through connectors. Coaxial cables are used for rf signals, and high resistance lines are used for dc signals. This is done to prevent leakage of the EM energy to the outside environment or into the instrumentation room. To minimize impedance mismatching, a 10-dB attenuator was used whenever possible between the receiving antenna and the 50-Ω power sensor or spectrum analyzer.

The chamber was evaluated using two different operational approaches referred to as mode-tuned and mode-stirred [4]. For the mode-tuned tests, the tuner is stepped in uniform increments and measurements are made at each tuner position of the net input power supplied to the transmitting antenna, the receiving antenna power, the field-measuring probe responses and the

equipment under test (EUT) response. Corrections are then made for the changes in the transmitting antenna's input impedance as a function of tuner position and frequency. The measurement results are then normalized to a constant net input power value. The number of tuner steps used per revolution was 200 (increments of 1.8 degree).

For the mode-stirred tests, the tuner was continuously rotated while sampling the reference antenna received power, the field probe response and the EUT response at rates much faster than the tuner revolution rate. These measurements were made using a spectrum analyzer (cw tests), or transient digitizer (pulsed rf tests) with diode detectors and "smart" voltmeters capable of data storage and calculation of statistical functions. Large data samples (up to 9,999) are obtained for a single tuner revolution. Tuner revolution rates are adjusted to meet the EUT output monitor, diode probe response time, and sampling rate requirements of the instrumentation. Typical rates used were approximately 3 to 6 minutes per revolution. For mode-stirred tests, the input power was measured only at the beginning of each measurement cycle. For the cw tests, as shown in figure 2.5, a calibrated bidirectional coupler was used at the input to the transmitting antenna to measure the net input power. For the pulsed rf tests, only the incident signal was measured as shown in figure 2.6. Details of how the measurement cycles proceed under computer control, and how the data are recorded, managed, and processed for presentation, are contained in [4,8].

The transmitting and reference receiving antennas used for the cw tests were long wire antennas (0.2 - 1.0 GHz), and broadband horn antennas (0.8 - 18.0 GHz).

For the pulsed rf tests, the mode-tuned approach was used to optimize absolute measurement accuracy, to obtain complete statistical information for evaluating the time domain response characteristics of the reference antenna's received signal, and to determine total energy content in the received pulse relative to the normalized energy in the transmitted pulse. The mode-stirred approach was used for relative measurements, with the digitizing oscilloscope placed in its maximum-hold mode of operation. This approach is much faster than the mode-tuned approach and results in much larger data sampling than the mode-tuned approach; however, it does not provide complete statistical results, since only maximum values are recorded. The approach used was determined by the final results needed. In some cases both approaches were used, and the results are given for comparison. The mode-tuned approach was required for complete statistical data and total energy (transmitted-versus-received) analysis. The mode-stirred approach was used to analyze relative information such as charge and decay time and to determine test field amplitude correction factors for input rf pulse widths too short for the chamber to charge up to its steady state or cw response value. The digitizing oscilloscope used is capable of measuring signals with rise times of approximately 30 ps, at a sampling rate of 50 kHz, with sample sizes up to 1024 per scan.

3. CW Evaluation of the RADC Small Reverberating Chamber

How well a shielded enclosure can be made to operate as a reverberating chamber depends upon a number of considerations. The major requirement is that the enclosure be large compared to the wavelength of the lowest frequency intended for use so that sufficient modes, necessary to obtain statistical spatial field uniformity, exist. Other considerations include mode density and quality factor [9]. These requirements should be fulfilled for the RADC chamber described above at frequencies above approximately 500 MHz.

3.1 Antenna Coupling Efficiency and VSWR

The efficiency with which energy can be injected into or coupled out of the chamber via the transmitting and receiving antennas is determined by: (a) the VSWR of the antennas (that is, the impedance match between the rf source and the transmitting antenna or between the receiving antenna and its output detector), and (b) the ability of the antennas to couple energy into or out of the particular modes that exist at the test frequencies of interest. Rotating the tuner changes the characteristics of the field inside the chamber, which in turn influences the effective VSWR of the antennas. Hence the net input power supplied to the chamber's transmitting antenna and the power accepted by the receiving antenna vary as a function of tuner position. That is, the impedance match between the rf source and transmitting antenna, and between the receiving antenna and its termination, affect the power transfer between the two antennas. This can result in errors in determining the amplitude of the field inside the enclosure.

Variations, determined statistically, in the VSWR of the two transmitting antennas used to excite the RADC small chamber are shown in figure 3.1. The receiving antenna's VSWRs should be similar. The figures show the maximum, average, and minimum VSWR obtained by rotating the tuner through a complete revolution at frequencies from 200 MHz to 18 GHz (long wire antennas) and from 800 MHz to 18 GHz (broadband horn antennas). Large variations and high values of VSWR exist, especially at the lower frequencies. At higher frequencies the variations become less and the VSWR values are lower, approaching the free-space VSWR of the antennas.

The coupling efficiency of the antennas placed inside the chamber is defined as the ratio of the net input power delivered to the transmitting antenna to the power available into a 50-Ω matched impedance at the terminals of the receiving antenna. These ratios (insertion loss), referred to as chamber loss, are given in figure 3.2. The curves show: (a) the average and minimum losses measured for the mode-tuned approach when using a pair of long wire antennas, and (b) the average and minimum losses using a pair of broadband ridged-waveguide rectangular horn antennas. Impedance mismatch between the receiving antenna and power detector used to measure the received power are not accounted for in these measurements. The magnitude of the error resulting from this is discussed in [4,8] and included in tables 4.1 and 4.2.

3.2 Chamber Quality Factor

The chamber's quality factor (Q) influences the operation of the chamber in a number of ways. Examples are tuner effectiveness, rf input power requirements and the accuracy with which test field levels can be established inside the chamber. Another important factor is the time required for the chamber to charge up to a steady-state condition after the input pulsed signal is applied. This influences the chamber's response characteristics for pulsed rf testing, as will be discussed later.

From resonant cavity theory the chamber's "composite Q", ($\vec{Q}$), can be determined [9] from the equation

$$\vec{Q} = \frac{3\,V}{2\,S\delta_s\mu_r}\left[\frac{1}{1 + \frac{3\lambda}{16}\left(\frac{1}{a} + \frac{1}{b} + \frac{1}{c}\right)}\right] , \qquad (1)$$

where V is the volume inside the chamber in m^3, S is the internal surface area in m^2, and $\delta_s = [2/(\omega\mu\sigma)]^{1/2}$ is the skin depth in m, λ is the wavelength in m, and a, b, and c are the chamber's internal dimensions in m.

The chamber's composite $\vec{Q}$ is determined by averaging the 1/Q values of all possible modes within a small frequency interval about the frequency of interest. Equation (1) is considered a maximum or upper bound because it assumes the chamber losses are due only to finite wall conductivity. In reality, other factors such as rf energy leakage from the chamber, loss in antenna support structures, and loss in the chamber wall coatings also contribute to the total losses.

An alternative means of determining the chamber Q is to measure the insertion loss between a transmitting and receiving antenna pair. If the rf energy is uniformly distributed throughout the volume of the reverberating chamber, an empirical value of Q can be obtained [10] from the equation

$$Q' = 16\,\pi^2\left(\frac{V}{\lambda^3}\right)\left(\frac{P_r}{P_t}\right) , \qquad (2)$$

where P_r is the power available at the receiving antenna in W and P_t is the net input power delivered to the transmitting antenna in W.

Results obtained using (1) to calculate the composite Q and by using the chamber loss data shown in figure 3.2 together with (2) to calculate the experimental Q are shown in figure 3.3. Figure 3.3 (a) gives the theoretical Q and experimental Q for the RADC small chamber, and figure 3.3 (b) shows the ratio of theoretical to experimental Q. At the higher frequencies the ratio approaches a value roughly equal to 2. This indicates that at frequencies where (1) and (2) are valid, there are relatively small losses other than loss in the chamber walls.

3.3 Tuner Effectiveness

A consideration in the operation of a reverberating chamber is the effectiveness of the tuner to obtain randomness in the distribution of the test signal inside the chamber. To achieve this the tuner must be electrically large and be shaped or oriented to distribute energy equally into all possible chamber modes. A test to determine how well the tuner is functioning is to measure the ratio of the maximum to minimum power in the receiving antenna as a function of tuner position. This is done while maintaining a constant net input power to the transmitting antenna. A large power ratio indicates that the tuner is effective in redistributing the scattered fields inside the chamber.

Measurement results for the RADC small chamber are given in figure 3.4. Figure 3.4 (a) gives the ratio of maximum to minimum received power using the long wire antennas over the frequency range 0.2 to 18 GHz. Figure 3.4 (b) gives the same type of data using broadband horns over the frequency range 0.8 to 18 GHz. A number of factors related to the design of the tuner can influence the magnitude of this ratio. Also, a reduction in this ratio caused by placing rf absorber and/or an EUT inside the chamber is a measure of the loading effect. A minimum ratio of 20 dB is recommended to assure proper operation of the chamber [4]. As seen in figures 3.4 (a) and (b), a tuner effectiveness greater than 20 dB was achieved for the RADC small chamber at all frequencies for both types of antennas.

3.4 Test Zone E-Field Uniformity

Tests were made to determine the E-field uniformity in the chamber as a function of spatial position and frequency, again, using both long-wire and broadband horn antennas. Ten small NIST isotropic probes [11,12,13] designed to operate at frequencies up to 2 GHz were placed at various locations inside the chamber as shown in figure 2.2. Each probe has three orthogonally oriented dipoles which are aligned with the three axes of the chamber, namely transverse (Ex), longitudinal (Ey), and vertical (Ez). Measurements were made of the field strength of each orthogonal component at the ten locations for each tuner position (200 steps of 1.8 degree for frequencies 200 - 1000 MHz and 400 steps of 0.9 degree for frequencies 1.0 - 2.0 GHz). These data were normalized for a net input power of 1 W applied at the input terminals of the transmitting antennas. The maximum and average values for each field component and the "total magnitude" (root-sum-squared or RSS value of the three components) were then determined from the complete data sets. The results of these measurements are shown in figures 3.5 and 3.6. The spread in the data shows the amount of spatial field variation inside the chamber at the indicated frequencies. The field strength in the graphs of figure 3.5 drops significantly at frequencies below 0.5 GHz. This is due to the decrease in efficiency of the long wire transmitting antenna used and to the lower number of modes available in the chamber. The chamber appears to be operating properly at frequencies down to at least 500 MHz, but with rather large spatial variations at the lower frequencies. The spatial variations at selected frequencies are summarized in Table 3.1. The average values, determined statistically from all ten locations, for the average and maximum E-fields of each component and their

composite total are summarized in figures 3.7 and 3.8. The relative amplitudes of the field components of each figure are approximately the same. The composite total of the average E-field components in figures 3.7 (b) and 3.8 (b) are approximately 4.8 dB or the ratio of $\sqrt{3}$ greater than the individual components. This indicates that the average component values are randomly polarized in the chamber. The composite total maximum amplitudes in figures 3.7 (a) and 3.8 (a), however, are only about 3 dB greater than the individual components. This indicates that the maximum components' values are not completely independant of each other. This is similar to the results obtained in the RADC large reverberating chamber and in the NIST reverberating chamber and appears to be inherent in the measurement method. The implication is that if multiple receptors are used (for example an isotropic probe whose output is a function of all three orthogonal dipoles) in establishing the test field amplitude inside a reverberating chamber, the results will be biased either 3 dB for maximum response data or 4.8 dB for average response data.

A comparison of figures 3.7 and 3.8 indicates slightly higher E-field amplitudes in the chamber when using broadband transmitting antennas, as compared with long wire antennas for the same input power. This is because of the horn's higher efficiency. As mentioned earlier, the E-field amplitude in the chamber is influenced by the chamber Q. Inserting the 10 probes into the chamber with their lossy transmission lines lowers the chamber Q and hence the field strength in the chamber compared to the field strength that would be present without the loading effect of the multi-probe system.

3.5 E-Field Amplitude Calibration

The field strength in the chamber can be determined in two ways. The first technique is to measure the power received by the reference antennas, and then determine the equivalent power density in the enclosure using the equation [4]

$$\bar{E}_a = \sqrt{\bar{\eta}\,\bar{P}_d} \approx \frac{4\pi}{\lambda}\sqrt{30\,\bar{P}_r} \quad , \qquad (3)$$

where $\bar{E}_a$ is the equivalent electric field in V/m, $\bar{\eta}$ is the average wave impedance of the chamber in Ω, $\bar{P}_d$ is the equivalent power density in W/m^2, in the enclosure, λ is the wavelength in m, and $\bar{P}_r$ is the average measured received power in W. The average wave impedance is assumed to be approximately equal to $120\pi\ \Omega$. The validity of (3) has been verified and is discussed in section 2.3.1 of [4]. The maximum and average electric field strengths inside the chamber determined from the receiving antenna power measurements and (3) are shown in figures 3.9 and 3.10. These data were normalized to 0.1 W net input power to the transmitting antenna.

The electric field strength inside the chamber can also be determined by measuring it with one or more calibrated probes. Data obtained using a 1-cm dipole probe fabricated at NIST are also shown on figures 3.9 and 3.10. The probe was calibrated in a planar field using a TEM cell [14] at frequencies up to 500 MHz and in an anechoic chamber at frequencies from 500 MHz to 18 GHz [15]. The assumption is made that the field strength over the aperture of the probe inside the reverberating chamber will approximate the planar field used to calibrate the probe. This is reasonable, at least at frequencies for which the probe is electrically small. Also, the open-space far-field gain of an electrically small dipole is small (1.76 dB). Thus, the probe-measured fields should be equivalent, within approximately 1.76 dB, to the E-fields determined using a receiving antenna. This is true if the equivalent gains for the probe and receiving antenna, after being placed inside the chamber, are assumed to be 0 dB. The agreements shown in figures 3.9 and 3.10 are typical of those observed in the data when determining field strengths inside reverberating chambers.

3.6 Comparison of Data for the RADC Small Reverberating Chamber with the NIST Anechoic Chamber

Comparisons of the response or EMS/V characteristics of EUT obtained using an anechoic chamber, with those obtained using a reverberating chamber, are typically made in terms of maximum (peak) values. The main reason for this is that the EUT's worst-case performance or susceptibility is typically the desired quantity. Also, it is very difficult to obtain a true average response for an EUT from anechoic chamber data. Even determining the EUT's peak response in an anechoic chamber (depending upon how well behaved the EUT receiving pattern characteristic is) requiresconsiderable effort and may involve complete pattern measurements.

The benefit of making the above type of comparison is to obtain a "correlation factor" between results obtained in the reverberating chamber and in an anechoic chamber. This should first be done for reference standard EUTs and then for an EUT which is more typical of operational equipment. For this effort, two reference EUTs were used. These were: (a) a 1 cm dipole probe referred to earlier, and (b) a small broadband horn antenna similar to what is used at frequencies from 0.8 to 18 GHz as the transmitting and receiving antennas in the chamber. The measurements were performed in both the RADC small reverberating chamber and in the NIST 4.9 m x 6.7 m x 8.5 m anechoic chamber in Boulder, CO.

The maximum response values obtained using the 1 cm dipole probe are given in figure 3.11. The probe response in the anechoic chamber is greater than its response in the reverberating chamber by an average of about 2 dB. This is expected, since it corresponds approximately to the free space gain of an electrically short dipole. That is, the expected correction factor between the EUT EMS/V response measurements, in the two facilities, is the free-space gain of the EUT [4].

Measurements of the maximum response of a broadband horn antenna obtained using the two chambers are shown in figure 3.12. For the anechoic chamber measurements, the horn was aligned on the boresight (main beam) of the transmitting antenna to obtain the maximum response. The horn response is greater in the anechoic chamber than in the reverberating chamber by

approximately its free-space gain. This is shown in figure 3.13, which compares the difference in the horn's maximum response in the two chambers with the horn's calibrated free-space gain. As expected, the results are in general agreement.

4. CW Measurement Uncertainty for the RADC Small Reverberating Chamber

4.1 Estimate of Uncertainty for Establishing a CW E-Field Amplitude in the Chamber

As indicated in section 3, EMS/V test fields can be established in a reverberating chamber in the following two ways: using a reference receiving antenna or using a calibrated transfer probe. If a reference receiving antenna is used, the field strength is determined using eq. (3). If an E-field probe is used, the field strength is determined in terms of the probe response, after its calibration in a known E-field. Estimates of the uncertainties in these methods as determined for the RADC small reverberating chamber are summarized in tables 4.1 and 4.2 for the mode-tuned and mode-stirred approaches, respectively. These results are similar to those determined for both the NIST and RADC large reverberating chambers, details of which are given in [4,8]. General comments given in section 5.1 of [8], explaining the sources of uncertainty, are also applicable to the RADC small chamber; however, the lower useful frequencies are higher because of the chamber's smaller size.

4.2 Comments on CW Measurement Uncertainty

Some general comments on interpreting uncertainties of immunity measurements are given as follows:

(a) If corrections are not made for impedance mismatch of the transmitting or receiving antenna, absolute amplitude measurements of the test field strength inside the chamber will be too low. This will cause an error in determining the EUT response, which will also be too low. For example, the low frequency data of figures 3.9 and 3.10 for the field determined from the received power measurements should be corrected (response increased) to account for the impedance mismatch between the receiving antenna and power detector.

(b) The wave impedance, when measuring the maximum response of an EUT, appears to be higher than 377 Ω, especially for frequencies lower than 2 GHz. This means that if a wave impedance of 377 Ω is assumed when determining the maximum amplitude of an exposure field, there will be a systematic error resulting in too low a calculated E-field value. Since the actual E-field is higher than the calculated value, this results in too high an EUT response indication for a specified E-field exposure. If the field strength is determined by using a calibrated E-field probe, there is still some uncertainty, since the wave impedance is different in the probe calibration environment than in the reverberating chamber. An estimate of this error is included in tables 4.1 and 4.2.

(c) The spatial variation of the E-field values in the mode-tuned chamber decreases with increasing frequency from as great as ± 7 dB at 500 MHz to less than ± 3 dB at 2 GHz. This variation is expected to continue to decrease as the frequency increases. However, other variations and uncertainties were found, using the reference standard EUTs (1 cm dipole and broadband horn), at high frequencies where the spatial E-field variation is small. These are due to other sources of error as shown in tables 4.1 and 4.2. One technique to reduce the total error would be to increase the number of frequencies at which data are taken, or increase the number of receiving probes used to measure the exposure field, and then average the data taken.

5. Pulsed Rf Evaluation of the RADC small Reverberating Chamber

5.1 Background

Parameters of electromagnetic interference (EMI) signals that can contribute to upset in electronic equipment include: (a) total energy, (b) peak amplitude, and (c) transient time characteristics. All these parameters are modified, relative to free space, for signals transmitted inside a reverberating chamber. Their characterization inside a reverberating chamber, particularly for pulsed rf fields, provides information required to determine correction factors as a function of the input pulse parameters. It also provides insight into the inherent limitations associated with using this complex environment for pulsed rf EMS/V testing. Obviously, these factors are influenced by the Q factor of the chamber, since the time required for the pulsed wave's amplitude to rise to its steady-state value inside the chamber and to decay to zero after the input signal is removed, is a function of the chamber's Q. These "charge" and "decay" times can be reduced by artificially lowering the chamber's Q, for example, by inserting small amounts of rf absorber. However, this reduces the accuracy in determining the test field amplitude. Results of work to evaluate the response characteristics of the chamber when excited by pulsed rf of various pulse widths and frequencies, and with the chamber loaded with a small amount of absorber, are contained in this section.

Because of the advantages of using the reverberating-chamber method for cw EMS/V pre-testing of an EUT, there is considerable interest in using this technique also for pulsed rf EMS/V testing. Work was performed earlier at NIST to evaluate the RADC large reverberating chamber response to pulsed rf excitation [8]. The results of similar work performed for the RADC small chamber are described in this report.

All the pulsed rf measurements for the small chamber were taken at 10 different frequencies between 0.9 to 18 GHz. Data taken for the mode-tuned approach include three pulse widths of 3, 1, and 0.3 μs. The data for the mode-stirred approach include four pulse widths of 3, 1, 0.3 and 0.1 μs. Broadband ridged-waveguide horn antennas were used for both transmitting and receiving the rf pulses in the chamber.

5.2 Evaluation of Pulsed Rf Measurements in the Mode-Tuned Chamber

The mode-tuned measurement approach was used to determine: (a) the chamber loss for rf pulse excitation compared with cw excitation, and (b) the ratio of the received pulse amplitude to the transmitted pulse amplitude, as a function of time after the input pulse is turned on. These two parameters were determined for the chamber empty (no absorber) and with the chamber loaded with 1 piece of 7.6 cm x 61 cm x 61 cm (3" x 24" x 24") rf absorber. The absorber was placed in the center of the chamber on top of a 15 cm high platform of plastic foam.

Measurements were made with short repetitive rf pulses having pulse widths of 0.3, 1.0 and 3.0 μs, to determine the ratio of energy received by the chamber receiving antenna, to the energy supplied to the transmitting antenna. The total energy was determined from numerical integration of the voltage as a function of time. A sample result of the ratio of the input pulse energy to received pulse energy (loss) is shown on figure 3.2 (b). The chamber losses for cw and rf pulses are equal within 2 dB at all frequencies. One can conclude from these measurements that even with significant pulse dispersion as a function of time, as seen by examining figure 5.1, that the energy associated with the field inside the reverberating chamber is approximately the same for cw and pulse testing.

Figure 5.1 shows the mode-tuned received pulse measurements for 3 pulse widths and 2 Q factors. These graphs give an indication of the time required for the chamber to charge up to its steady state amplitude, and to decay to zero after the input pulse is turned on and off. The results show the dependence on frequency and chamber Q. Charge-up time is the time required for the pulse input signal, radiated from the transmitting antenna, to complete all significant multiple reflections inside the chamber. Each graph of power measurement data shows two curves: one for the average value of received power for all tuner positions (at each instant of time), and one for the maximum value of received power (at each instant of time). Curves have been added to the maximum curves to give an approximated smooth result.

By examining the curves in figure 5.1 at the selected frequencies and pulse widths, the approximate charge or decay times can be determined for the empty (no absorber) chamber and for the chamber loaded with the one piece of rf absorber. The data extracted from the curves of figure 5.1 are summarized in table 5.1. Graphs displaying these data are shown in figures 5.2, 5.3, and 5.4. The results of figures 5.2 and 5.3 are given in terms of the time required for the received signal to rise to 63 % and 90 % of the steady state amplitude. The steady-state amplitude is achieved if the pulse duration is sufficient for the chamber to charge up to 100 % of its amplitude (approximately the cw level). Curves drawn in are the estimated results derived from curve fitting to the raw data.

If the transmitted pulse duration is not longer than the charge time of the chamber, an error will result in establishing a known maximum amplitude of the test signal in the chamber. An estimate of the correction factor to apply for this condition can be found by determining the difference (dB) in the calculated ratio of the received signal amplitude to the transmitted signal amplitude as a function of time after turning on the transmitted pulse. Figures 5.4 (a) and (b) give these results for the chamber empty and

with 1 piece of absorber. Again, smooth curves derived from an estimated fit of the raw data are shown. The corrections correspond approximately with the ratio of the received signal amplitude, as a function of time after the pulse is turned on, to the steady state amplitude. Graphs shown in figures 5.4 (a) and (b) are for pulse durations of 1 and 0.3 μs. The correction factor is significantly lower for the chamber loaded with rf absorber (lower Q factor). Figures 5.4 (a) and (b) are used to correct for field-strength reductions in the chamber caused by insufficient time duration of the transmitted pulses. These correction factors should be verified further by comparing the measured responses of a well-characterized EUT to cw fields and to pulsed rf fields of varying pulse widths, using both anechoic and evaluated (calibrated) reverberating chambers.

5.3 Evaluation of Pulsed RF Measurements in the Mode-Stirred Chamber

Measurements were also made using the mode-stirred approach with the chamber. Again, as in the mode-tuned approach, two sets of data were taken, one for the empty chamber (high Q) and the other for the chamber loaded with one piece of rf absorber. Measurements were made at the ten different frequencies from 0.9 to 18 GHz but with four input pulse widths, 0.1, 0.3, 1, and 3 μs. Results of these measurements are given in figures 5.5 to 5.8. The graphs of figure 5.5 show oscilloscope traces for the selected frequencies for the 4 input pulse widths. Each graph has two traces. The upper trace is an envelope of the input pulses applied to the chamber transmitting antenna; that is, the "painted" envelope derived from all the input pulses during one complete rotation of the tuner. The signal shown is the reduced voltage values measured on the side arm of the directional coupler using a calibrated diode detector connected to one channel of the digitizing oscilloscope. The lower trace is the time-domain envelope of the pulses received by the chamber's reference receiving antenna and measured with a second calibrated diode detector connected to the second channel of the digitizing oscilloscope. The polarity of this pulse has been reversed to separate the two traces. The diode detectors have built-in 50 Ω load resistors for impedance matching to 50 Ω. The spread in the top trace (input signal) is due to variations in signal amplitude caused by variations in antenna VSWR (input mismatch) as a function of tuner position. The magnitude of this variation is frequency dependent, decreasing as the frequency increases.

The approximate risetimes and correction factors can be determined from the graphs shown in figure 5.5. These results are summarized in table 5.2. Figures 5.6 and 5.7 give the time required for the signal to rise to 63 % and 90 % of the steady state amplitude. Smooth curves were drawn giving the estimated results derived from a curve fit of the raw data. These data are similar to the results shown in figures 5.2 and 5.3. Graphs displaying the correction factors for field-strength reductions caused by insufficient time duration of the transmitted pulses are shown in figure 5.8. Again these are similar to figure 5.4, determined for the mode-tuned case.

5.4 Comments on Pulsed RF Measurements

Mode-tuned data are generally considered to be more accurate than mode-stirred data for absolute measurements such as chamber loss and test field strength. This is because appropriate corrections can be made for impedance mismatch, cable loss, coupler coupling factors , etc.. The more complete data acquisition for mode-tuned operation makes it possible to obtain maximum, average and minimum response values, whereas only the maximum values can be determined from the mode-stirred measurements. Mode-tuned measurements are taken for each of the (stopped) tuner positions, and sampled at each instant of time during the pulse, so that a maximum value (or minimum or average) can be extracted from the total data taken. Each pulse is digitized at 512 samples in time, for each of the 200 angular positions of the tuner during a 360^0 rotation. Then corrections can be made to each measurement for cable loss, coupling ratio of the directional coupler, attenuator calibrations, and diode detector readings according to previous calibration of power response versus signal frequency and indicated voltage levels. Mode-stirred data cannot be corrected in the same manner; hence, representative values only are obtained. However, results derived from mode-stirred data usually have better definition and are believed to be more accurate for determining relative parameters, such as charge time and relative amplitude correction factors. This is because large data sampling approaching continuous sampling as a function of tuner position is possible, compared to the limited (200 tuner position) sampling of the mode-tuned approach. These conclusions are particularly apparent when comparing figures 5.4 and 5.8.

It was observed in much of the pulsed rf data that the maximum value of field strength measured as a function of time after the pulse turn-on, appears to be slightly greater than the steady-state value. It is conjectured that this "overshoot" is due to the imperfect (non-instantaneous) leading edge of the pulse produced by the pin diode switch in the pulse source. The overall trend, however, is for the shorter pulses to have a smaller value of peak detected voltage. This is because the on-time is not sufficient for the EM energy in the reverberating chamber to reach its steady-state value. Thus, data were taken for a range of pulse durations to determine the correction factor to be applied when using the chamber to take EMS/V data for very short radar-type pulses.

6. Summary and Conclusions

(a) Spatial variations of the E-field maximum and average values in the test volume of the chamber are summarized at selected discrete frequencies in table 3.1. These data were obtained using the NIST multiprobe system and the mode-tuned approach with 200 tuner increments per revolution at frequencies from 0.2 to 1 GHz, and 400 tuner increments at frequencies from 1 to 2 GHz. The limitation for determining the spatial E-field variation depends on the increasing mode density and hence field complexity in the chamber as a function of increasing frequency. At higher frequencies the sample size becomes insufficient to determine the maximum value with sufficient accuracy. The spatial E-field variations should decrease as frequency increases above 2 GHz to less than the ± 3 dB shown at 2 GHz in the table.

(b) The maximum E-field strength established inside the chamber is about 7-8 dB greater than the average E-field. This is consistent with previous results obtained for other reverberating chambers such as the RADC large chamber, the Naval Surface Weapons Center (NSWC), Dahlgren, VA, chambers and the NIST reverberating chambers.

(c) Results of reference standard EUT responses determined using the RADC small reverberating chamber are approximately the same for the same EUT at the same field levels as using NSWC and NIST reverberating chambers.

(d) The "correlation factor" between free-space (anechoic chamber) and reverberating chamber results appears to be the free-space (far-field) gain of the EUT. This implies that susceptibility criteria determined for an EUT using a reverberating chamber must include an additional factor proportional to the EUT's open-field estimated gain as a function of frequency.

(e) Item (d) implies that the directional characteristics of an antenna or EUT placed inside a reverberating chamber are lost, resulting in an equivalent gain of unity (0 dB) in this complex highly reflective environment.

(f) If a reverberating chamber is used for pulsed rf EMS/V testing, and the duration of the input pulses to the chamber is shorter than the chamber's charge time, an error will result in establishing a known maximum amplitude of the test signal. An estimate of the correction factors to apply for shorter pulses is given in figures 5.4 and 5.8.

(g) The use of rf absorbing material inside a reverberating chamber significantly reduces the Q and, hence, charge time of the chamber and can be used to improve the fidelity of the pulse waveshape of the test field in the chamber. However, the absorber should not reduce the Q so much that the reference antenna received power drops more than 6 dB, or the tuner effectiveness is reduced to less than 20 dB.

7. Recommendations.

(a) The practical lower frequency limit recommended for using the RADC small reverberating chamber shown in figure 2.1 is approximately 500 MHz.

(b) The mode-tuned approach is recommended for use at frequencies below 2 GHz if absolute levels of the test field are required. The mode-stirred approach is recommended for use at frequencies above 2 GHz for absolute measurements or at all frequencies above 500 MHz if only relative measurements are made.

Based upon antenna VSWR and EUT response data obtained from the evaluation measurements, the following approaches and number of samples per tuner(s) revolution are suggested for performing EMS/V testing requiring absolute determination of test field amplitudes for EUT response parameters.

Frequency Range	Method	Number of Tuner Positions or Samples
0.5 - 1 GHz	Mode-Tuned	200
1 - 2 GHz	Mode-Tuned	400
2 - 4 GHz	Mode-Stirred	> 3000
4 - 18 GHz	Mode-Stirred	> 5000

(c) Antennas for transmitting rf energy into the chamber and for measuring the test E-field amplitude should not be used outside their specified frequency range. (For example the 0.8 to 18 GHz ridged-horn antennas should not be used outside their specified band.)

(d) Additional work is needed to verify experimentally the correction factors shown in tables 5.1 and 5.2 and figures 5.4 and 5.8. This could be accomplished by comparing the measured responses of a well-characterized EUT to cw and pulsed rf fields as a function of frequency and pulse durations, using both an anechoic chamber and an evaluated/calibrated reverberating chamber.

8. Acknowledgments

Work described in this report was sponsored by RADC, Griffiss AFB, NY, with Charles Blank as project monitor. The authors wish to acknowledge his assistance in making this project possible. In addition, the authors express appreciation to Dr. Mark Ma and Dr. Motohisa Kanda for their support and helpful comments and editorial review.

9. References

[1] Cummings, J.R. Translational electromagnetic environment chamber, a new method for measuring radiated susceptibility and emissions. Proc. IEEE Int. Symp. on EMC; 1975; San Antonio, TX.

[2] Corona, P.; Latmiral, G.; Paolini, E.; Piccioli, L. Performance of a reverberation enclosure for power measurements in the microwave range. 2nd Symp. Tech Exhibition on EMC; 1977; Montreux, Switzerland.

[3] Bean, J.L.; Hall, R.A. Electromagnetic susceptibility measurements using a mode-stirred chamber. Proc. IEEE Int. Symp. on EMC; 1978; Atlanta, GA.

[4] Crawford, M.L.; Koepke, G.H. Design, evaluation and use of a reverberation chamber for performing electromagnetic susceptibility/vulnerability measurements. Nat. Bur. Stand. (U.S.) Tech. Note 1092; 1986 April. 148 p.

[5] Ma, M.T.; Kanda, M.; Crawford, M.L.; Larsen, E.B. A review of electromagnetic compatibility/interference measurement methodologies. Proc. of IEEE; Vol. 73, No. 3; 1985 March.

[6] Project Progress Report - Final Report FY86 "EMR test facilities - Evaluation of reverberation chamber method for performing EMC measurements", prepared for RADC/RBCM, Griffiss AFB, NY. by NBS, Boulder, CO. Report NO. SR-723-1-87. 1987 January.

[7] Crawford, M.L.; Koepke, G.H. Preliminary evaluation of reverberation chamber method for pulsed rf immunity testing. IEEE Int. Symp. on EMC; 1986; San Diego, CA.

[8] Crawford, M.L.; Koepke, G.H.; Ladbury, J.M. EMR test facilities - Evaluation of reverberating chamber located at RADC, Griffiss AFB, Rome New York. Nat. Bur. Stand. (U.S.) NBSIR 87-3080; 1987 December. 80 p.

[9] Liu, B.H.; Chang, D.C.; Ma, M.T. Eigenmodes and the composite quality factor of a reverberating chamber. Nat. Bur. Stand. (U.S.) Tech Note 1066; 1983 August.

[10] Corona, P.; Latmiral, G.; Paolini, E. Performance and analysis of reverberating enclosures with variable geometry. IEEE Trans. on EMC; EMC-22. 1980 February.

[11] Larsen, E.B.; Ries, F.X. Design and calibration of the NBS isotropic electric-field monitor [EFM-5], 0.2 to 1000 MHz. Nat. Bur. Stand. (U.S.) Tech. Note 1033; 1981 March.

[12] Kanda, M.; Driver, L.D. An isotropic electric-field probe with tapered resistive dipoles for broad-band use, 100 kHz to 18 GHz. IEEE Trans. on MT&T. Vol. MTT-35(2); 1987 February.

[13] Bensema, W.D.; Reeve, G.R.; Koepke, G.H. A multisensor automated EM field measurement system. Proc. IEEE IMTC/85 Conf; 1985; Tampa, FL.

[14] Crawford, M.L. Generation of standard EM fields for calibration of power density meters: 20 kHz to 1000 MHz. Nat. Bur. Stand. (U.S.) NBSIR 75-804; 1975 January. 40 p.

[15] Bowman, R.R. Calibration techniques for electromagnetic hazard meters: 500 MHz to 20 GHz. Nat. Bur. Stand. (U.S.) NBSIR 75-805; 1976 April. 33 p.

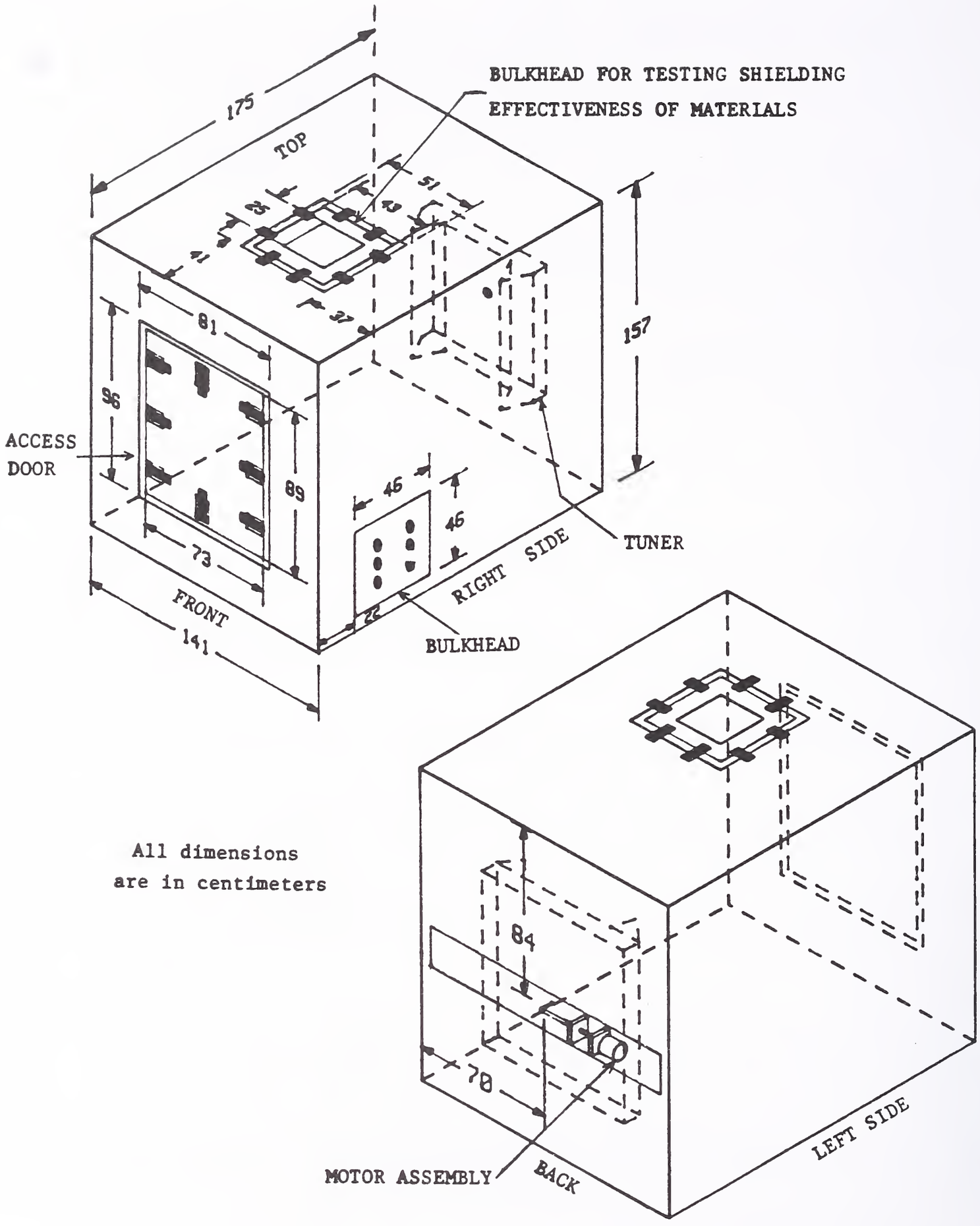

Figure 2.1 Two isometric sketches of the RADC small reverberating chamber.

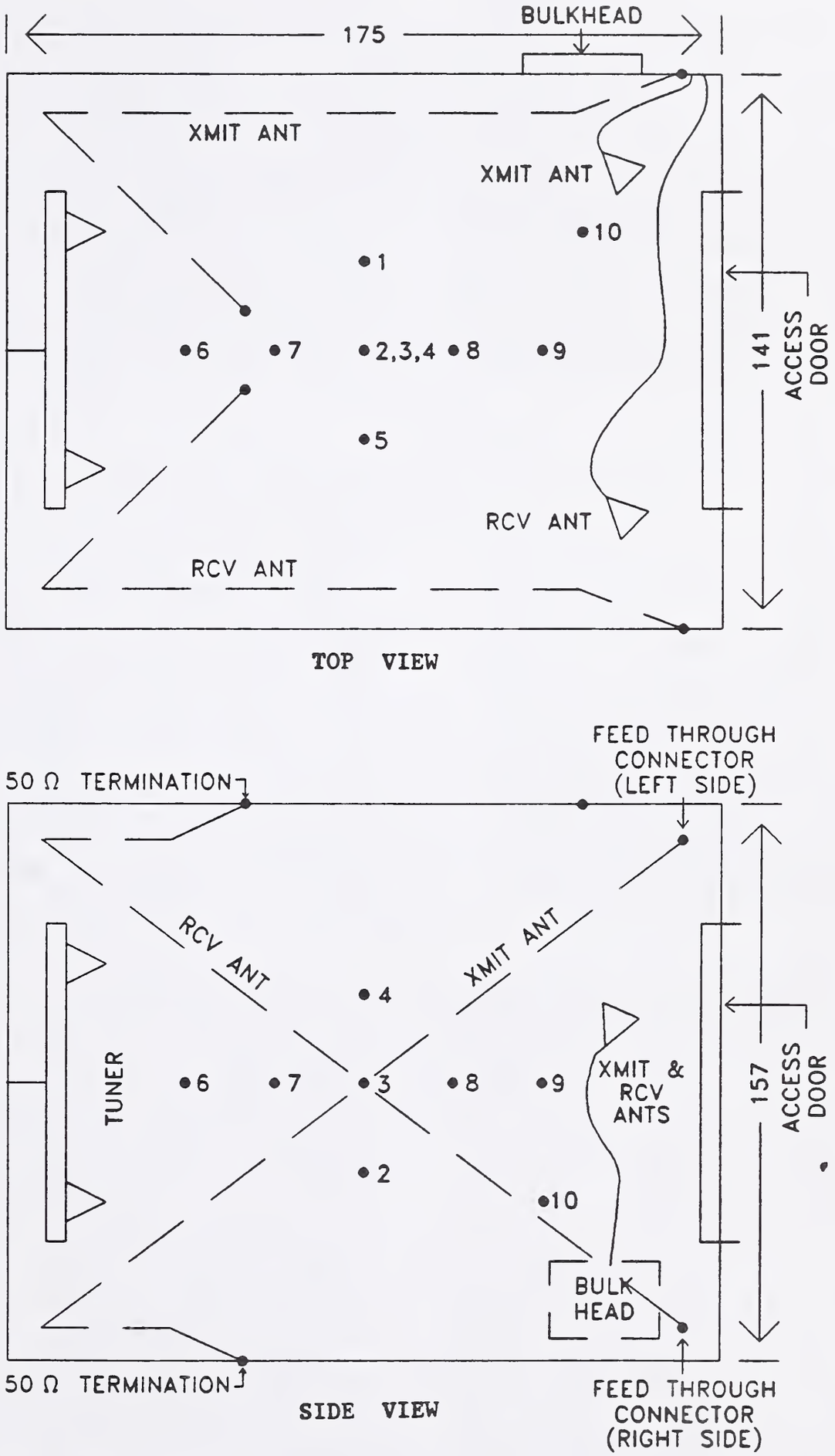

Figure 2.2 Cross sectional views of the RADC small reverberating chamber showing placement of transmitting and receiving antennas, chamber tuner and isotropic probes for measuring spatial E-field uniformity.

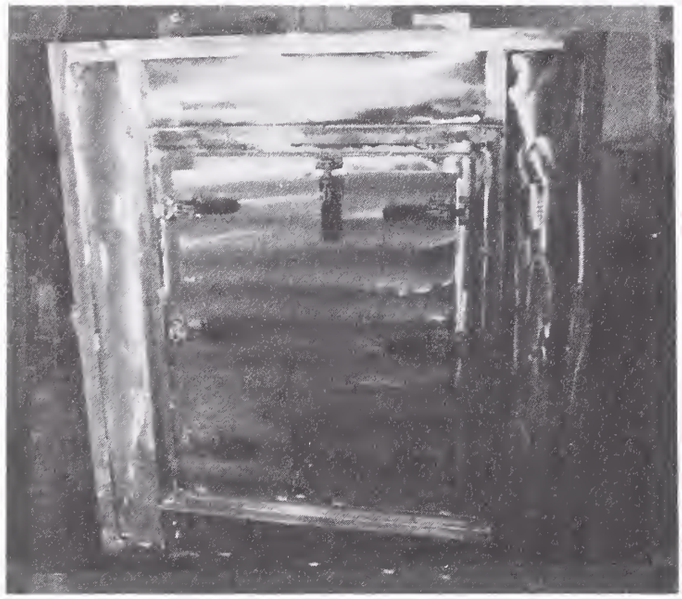

(a) Front view of the reverberating chamber with access door in place.

(b) Front view of the chamber with access door removed.

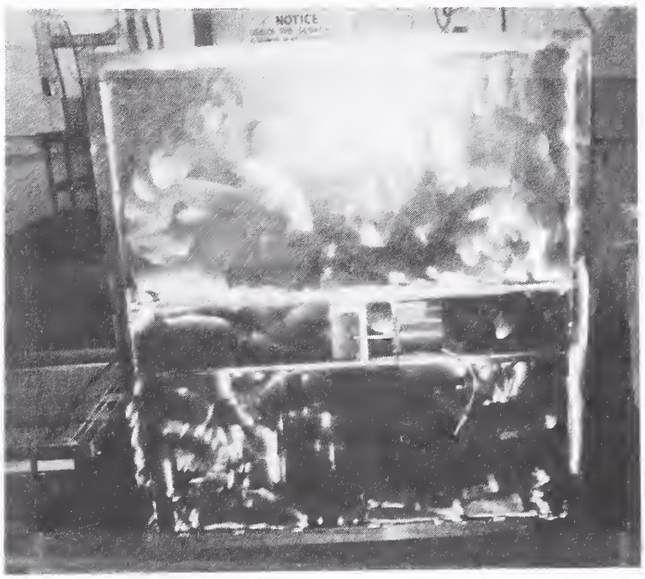

(c) Rear view of the chamber showing the tuner motor assembly.

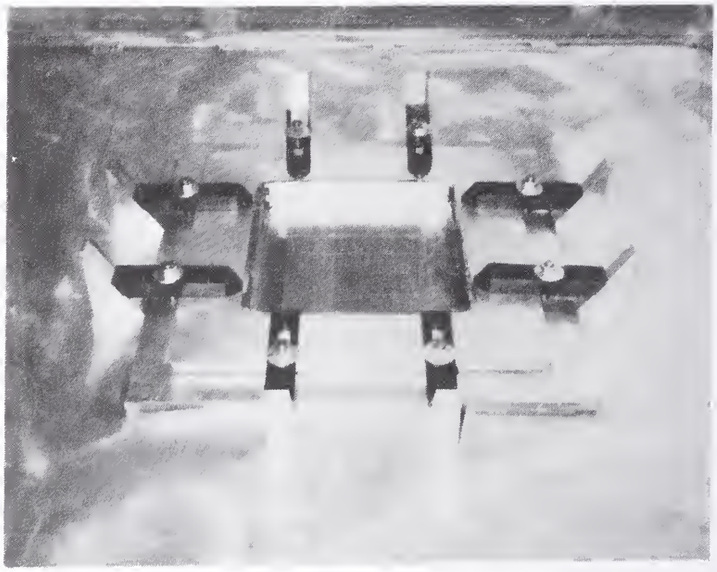

(d) Top view showing the bulkhead for shielding-effectiveness measurement.

(e) View inside the chamber showing probes, long wire antenna, and tuner.

(f) Side view of the chamber showing the access bulkhead.

Figure 2.3 Six photographs of the RADC small reverberating chamber.

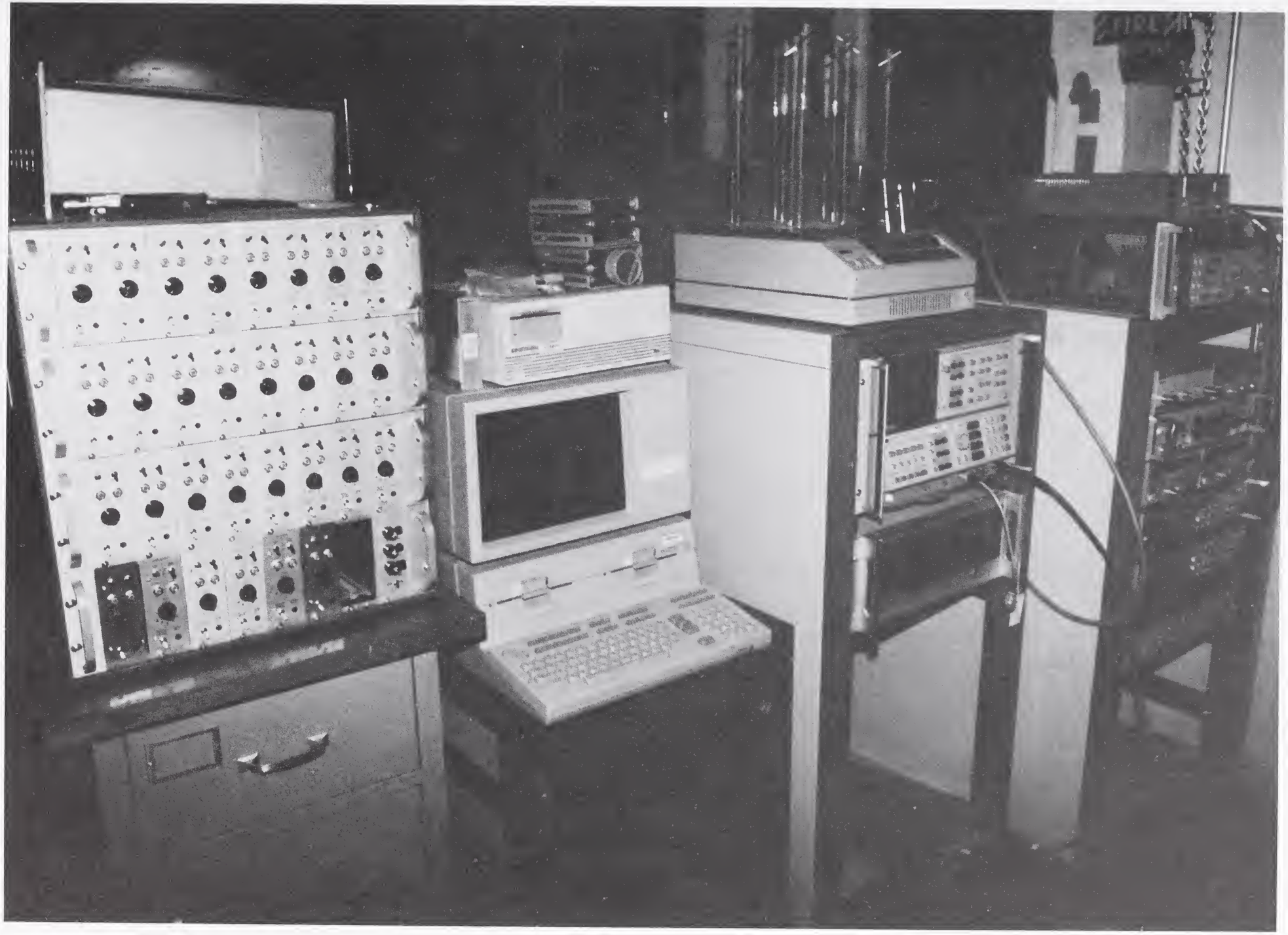

Figure 2.4 Photograph of NIST equipment used to evaluate the RADC small chamber.

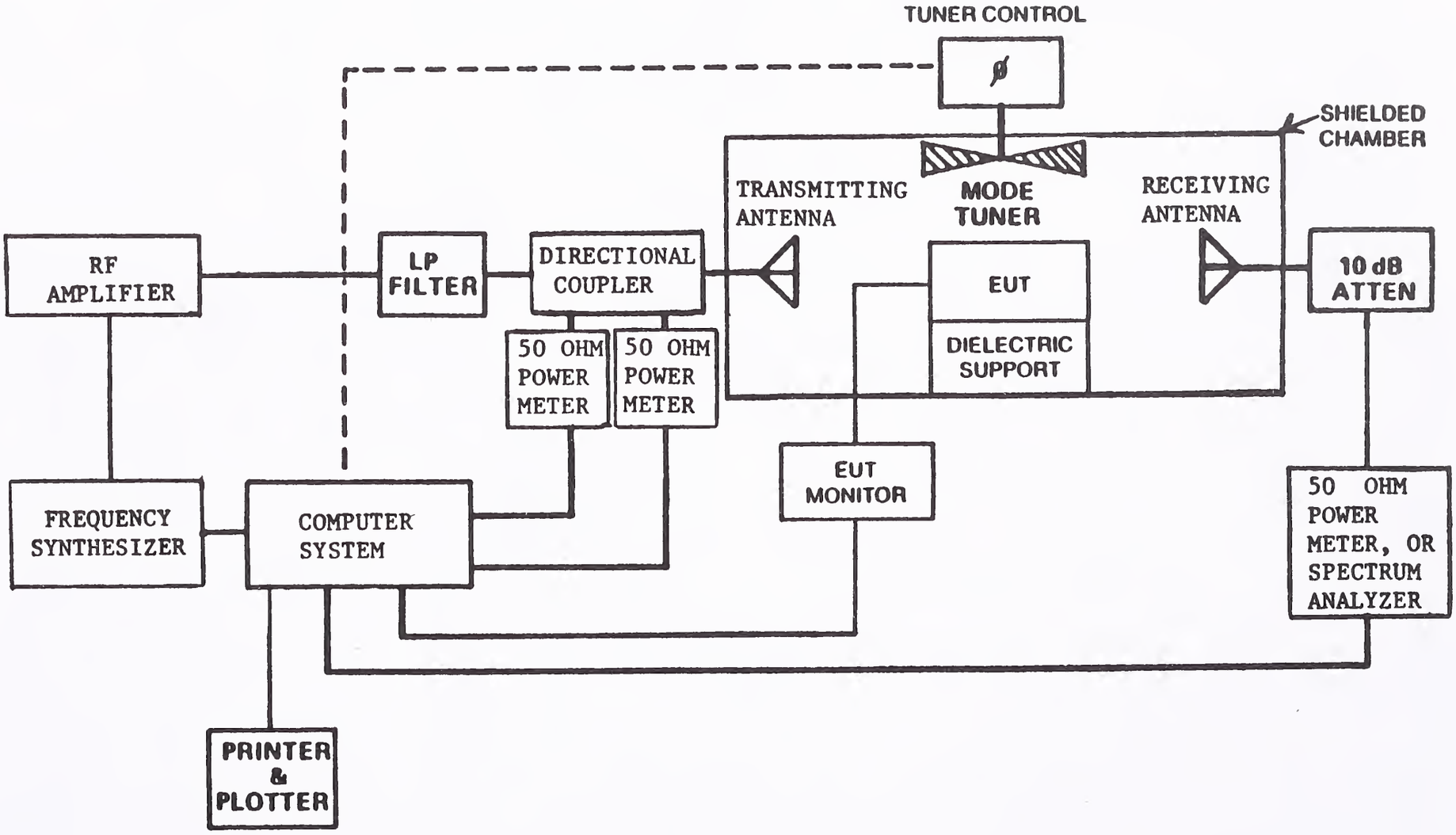

Figure 2.5 Block diagram of instrumentation used in cw evaluation of the RADC small chamber.

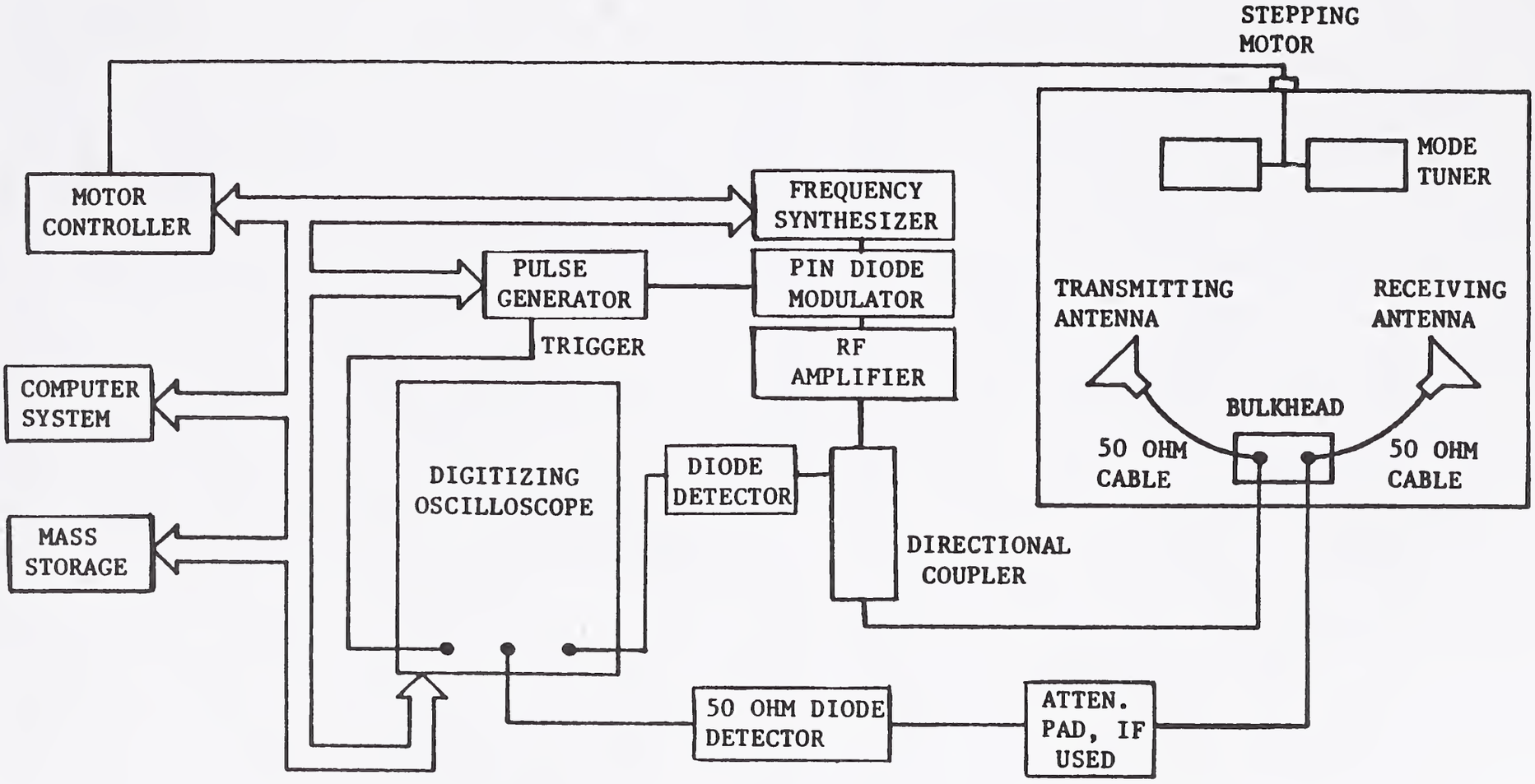

Figure 2.6 Block diagram of instrumentation used in pulsed rf evaluation of the RADC small chamber.

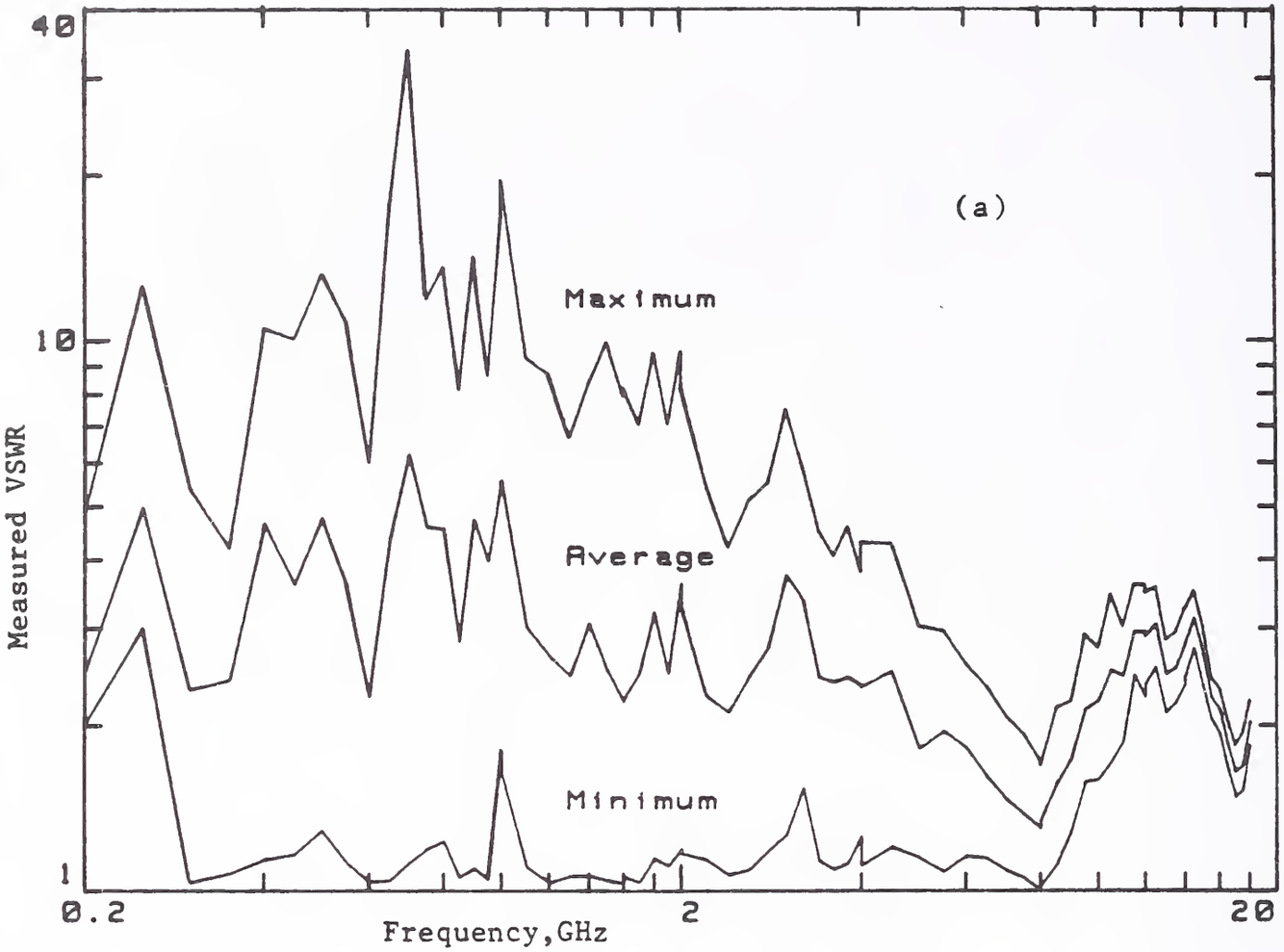

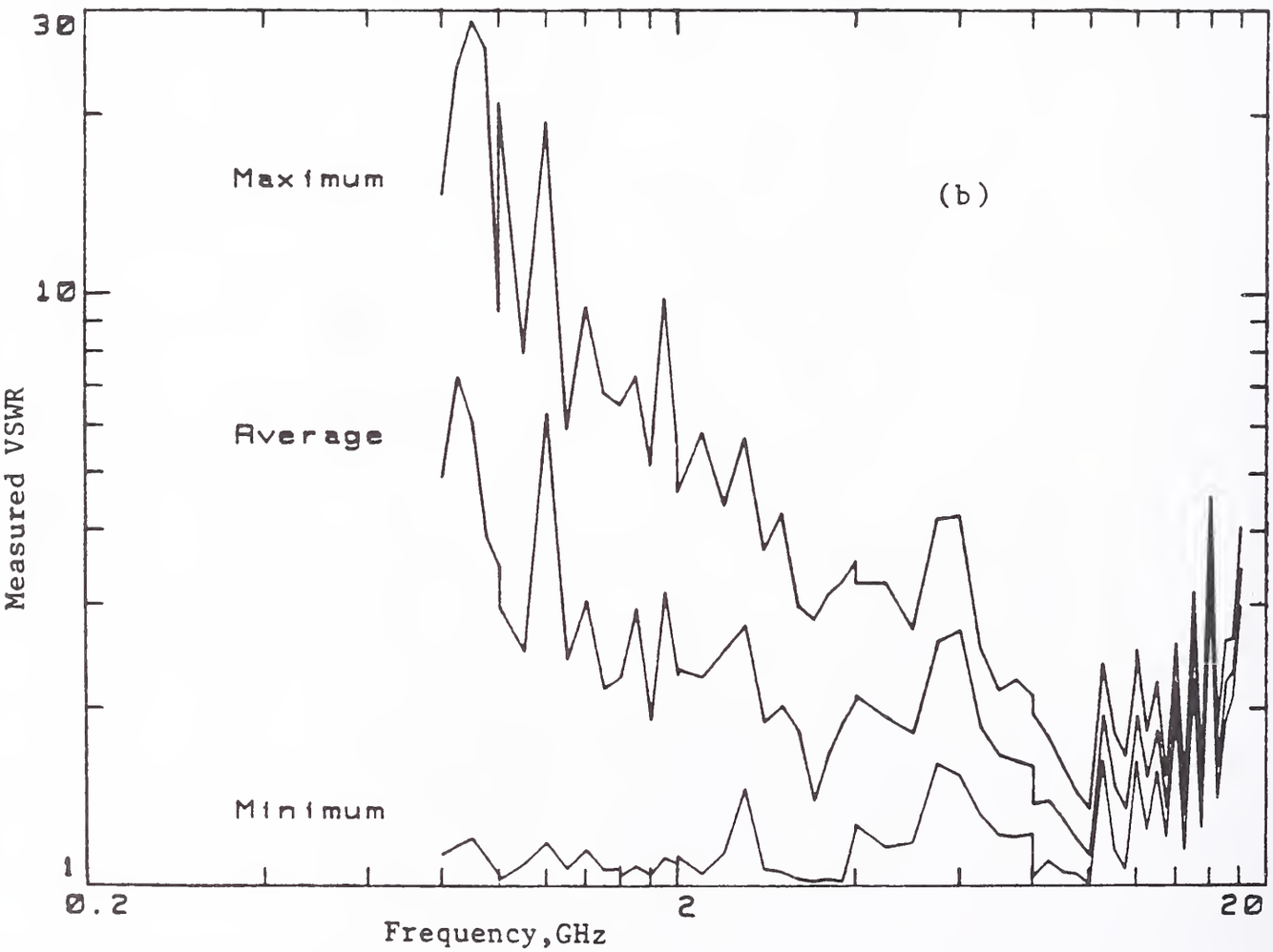

Figure 3.1 Measured VSWR of: (a) long wire antennas (0.2 to 18 GHz), and (b) broadband horn antennas (0.8 to 18 GHz), transmitting into the RADC small chamber.

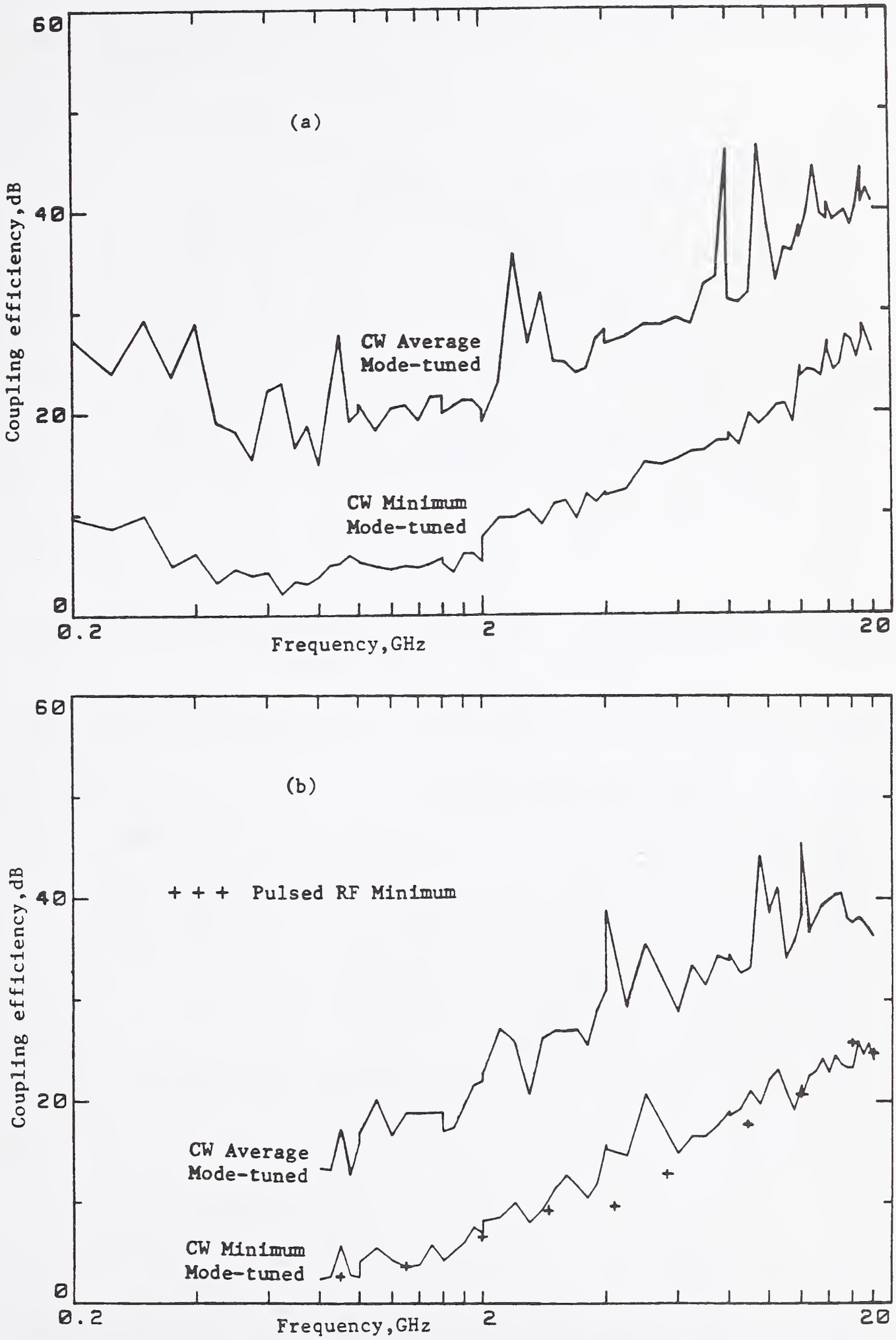

Figure 3.2 Measured coupling efficiency of: (a) long wire antennas (0.2 to 18 GHz), and (b) broadband horn antennas (0.8 to 18 GHz), in the RADC small chamber. Losses determined in (b) are from cw mode-tuned measurements and from pulsed rf measurements.

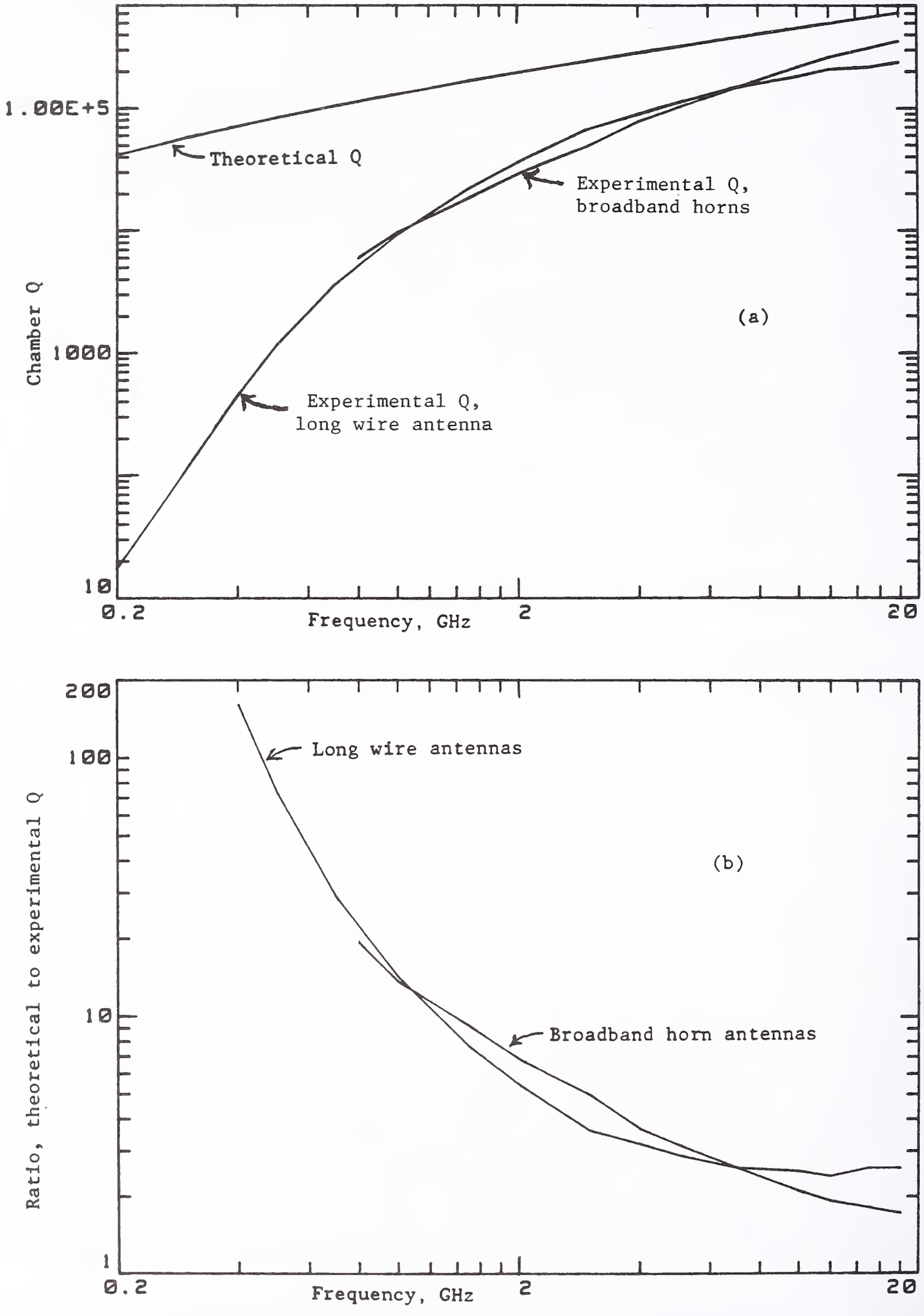

Figure 3.3 (a) Theoretical and experimental Q of the RADC small chamber, and (b) ratio of theoretical to experimental Q (0.4 to 18 GHz).

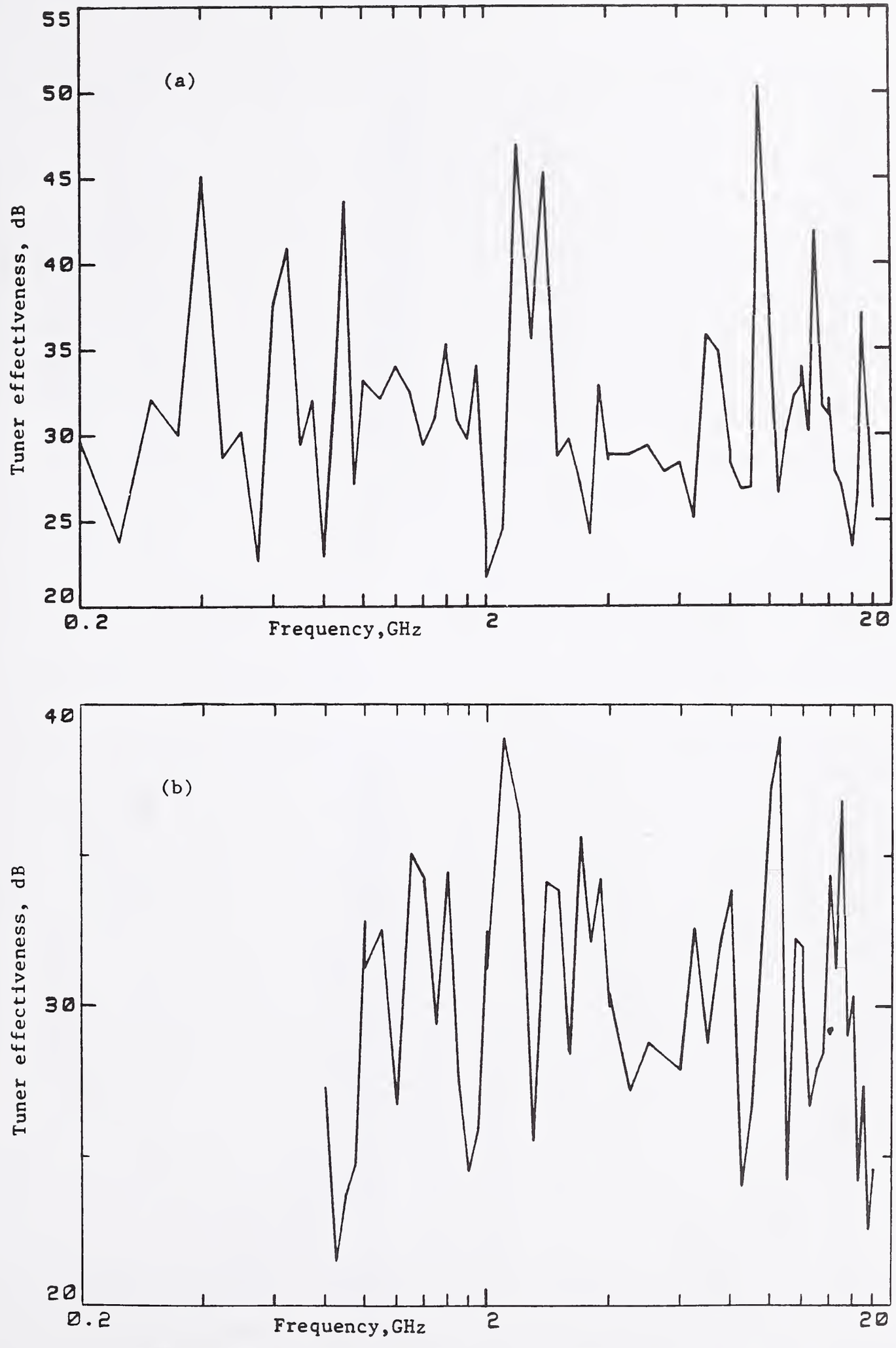

Figure 3.4 Measured tuner effectiveness in the small chamber using: (a) long wire antenna (0.2 to 18 GHz), and (b) broadband horn antenna (0.8 to 18 GHz)

(a) Maximum values

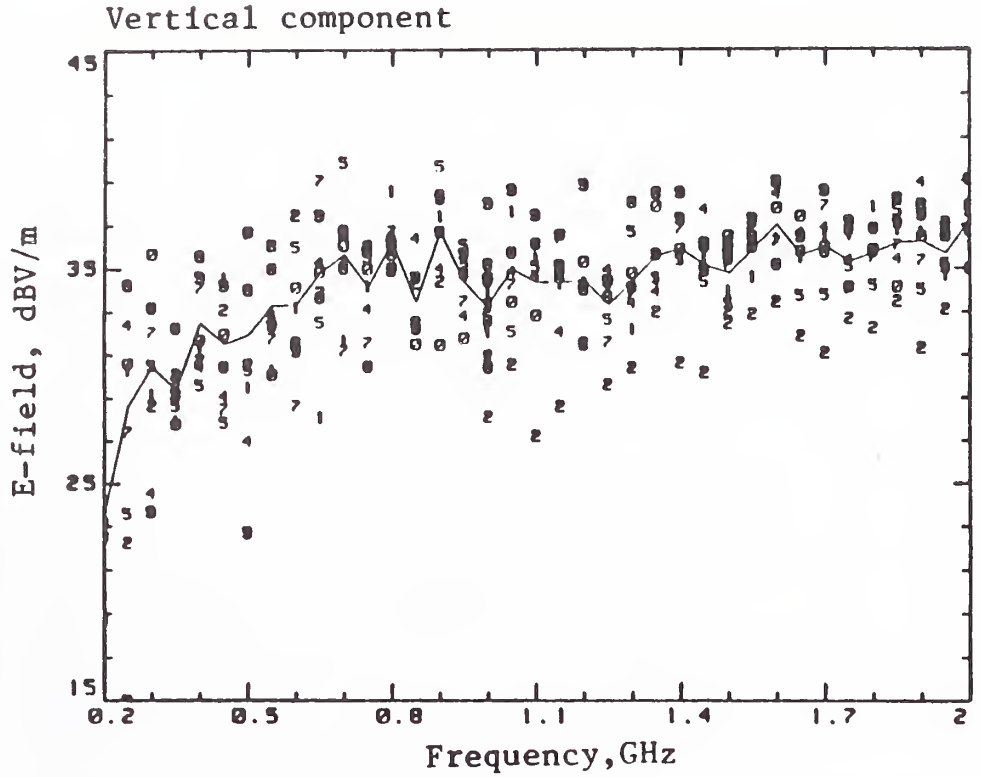

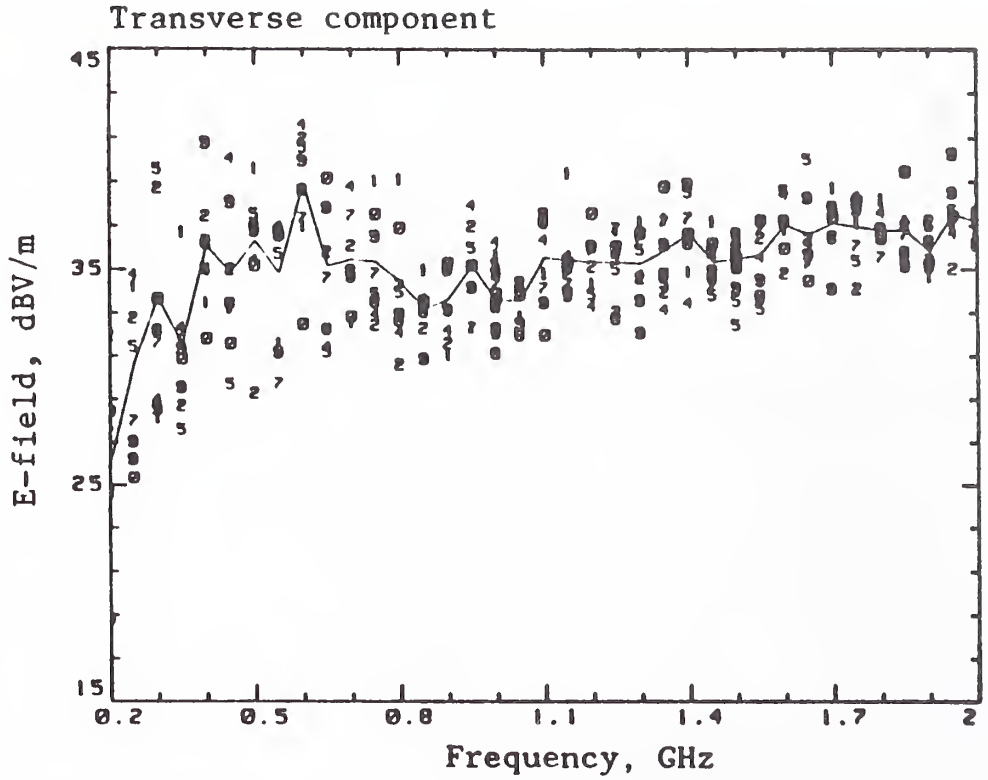

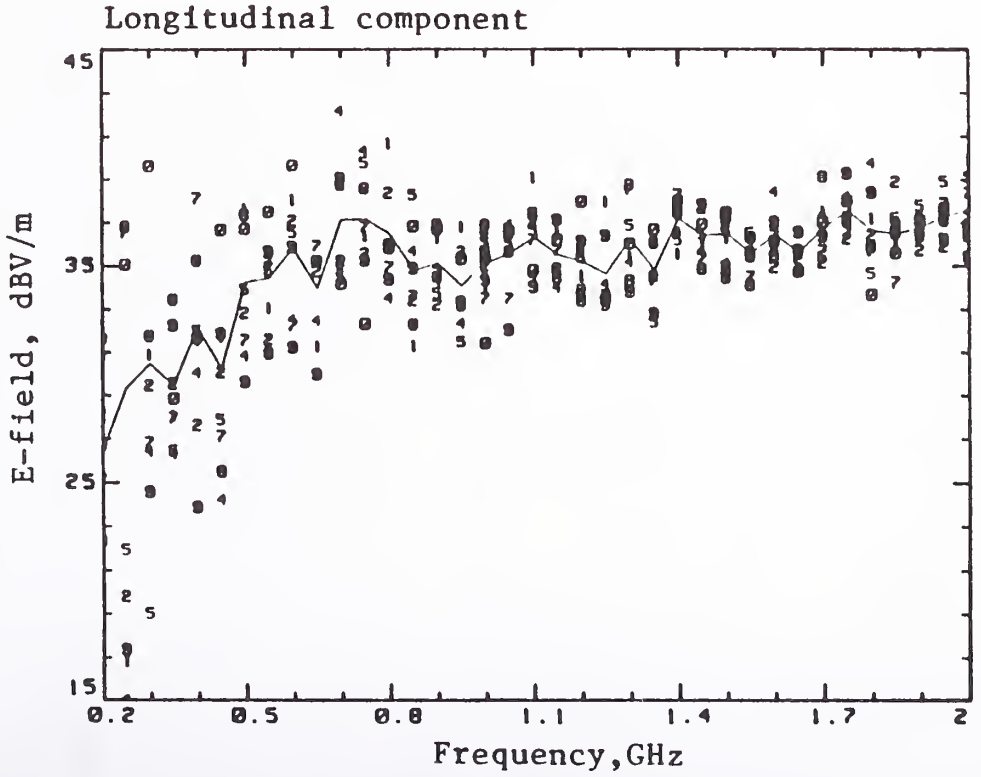

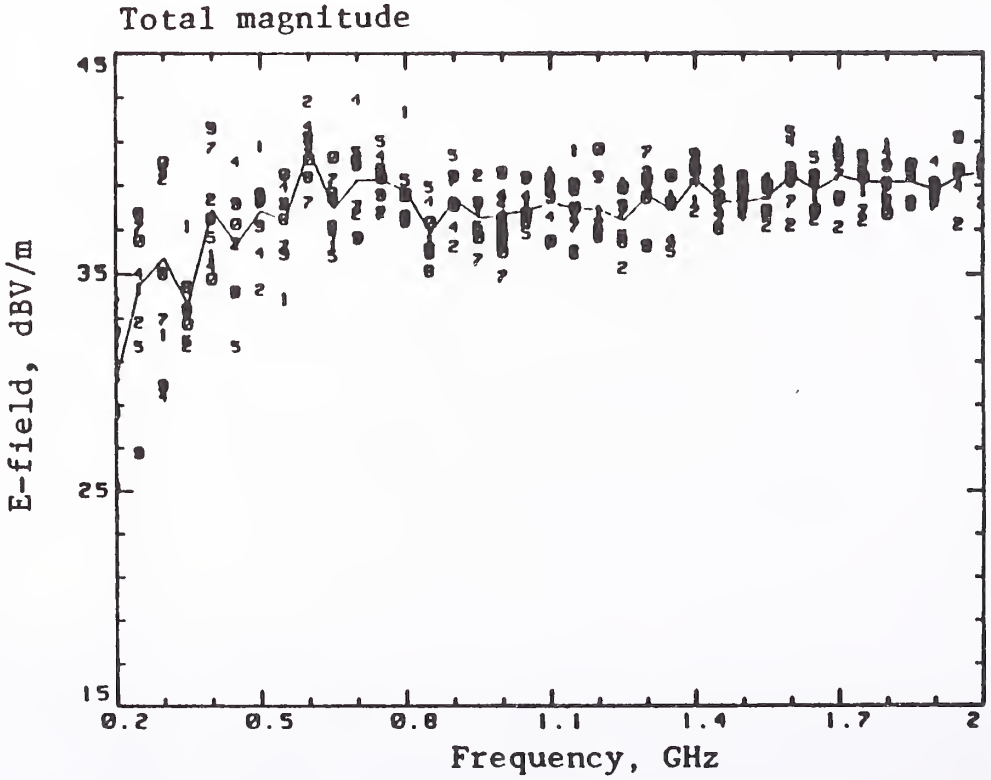

Figure 3.5(a) Spatial distribution of E-field components in the small chamber measured with 10 NIST isotropic probes (5 cm dipoles), using long wire antennas for transmitting and receiving: (a) maximum values, and (b) average values. Net transmitted power = 1 W.

(b) Average values

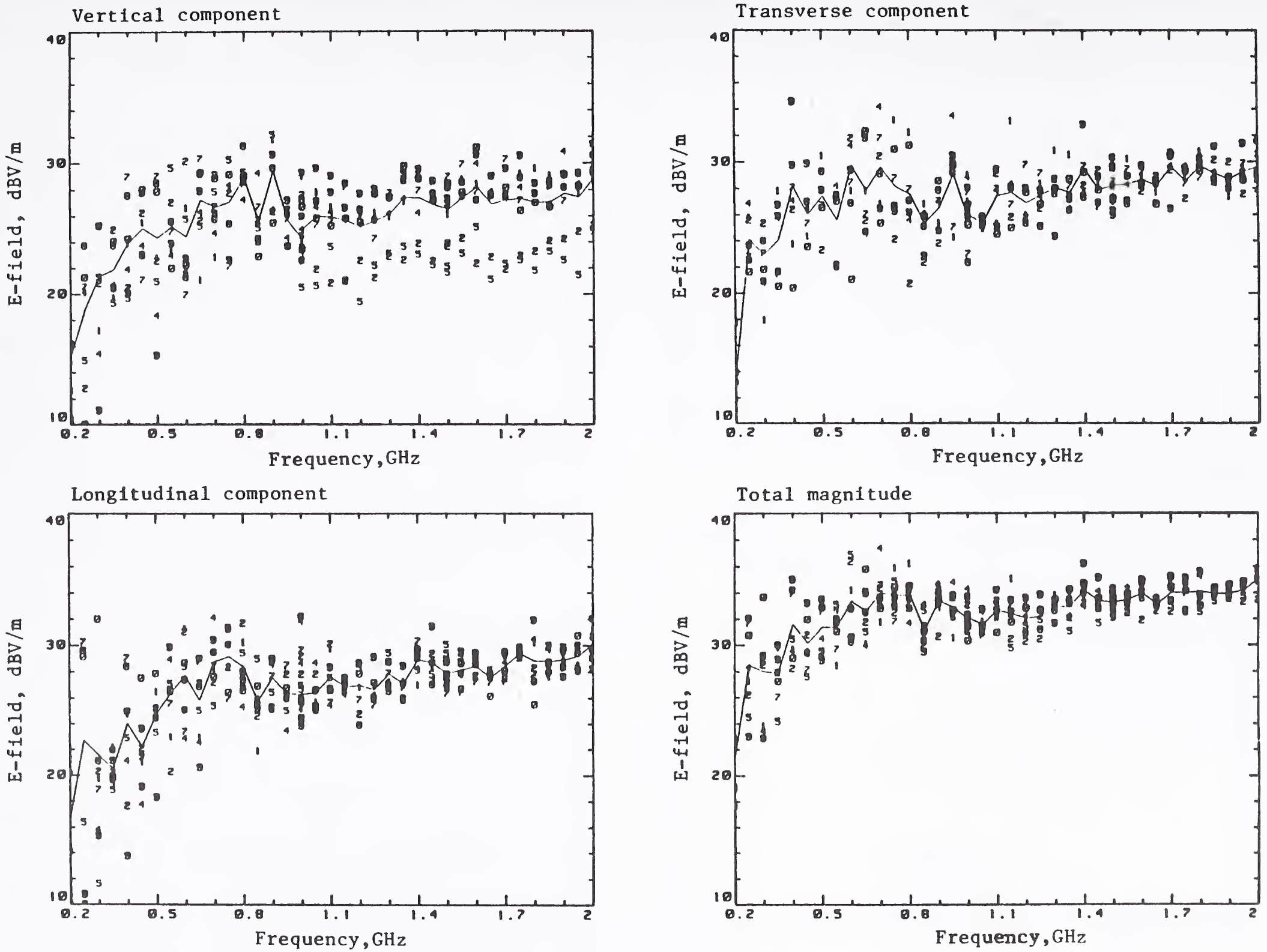

Figure 3.5(b) Spatial distribution of E-field components in the small chamber measured with 10 NIST isotropic probes (5 cm dipoles), using long wire antennas for transmitting and receiving: (a) maximum values, and (b) average values. Net transmitted power = 1 W.

(a) Maximum values

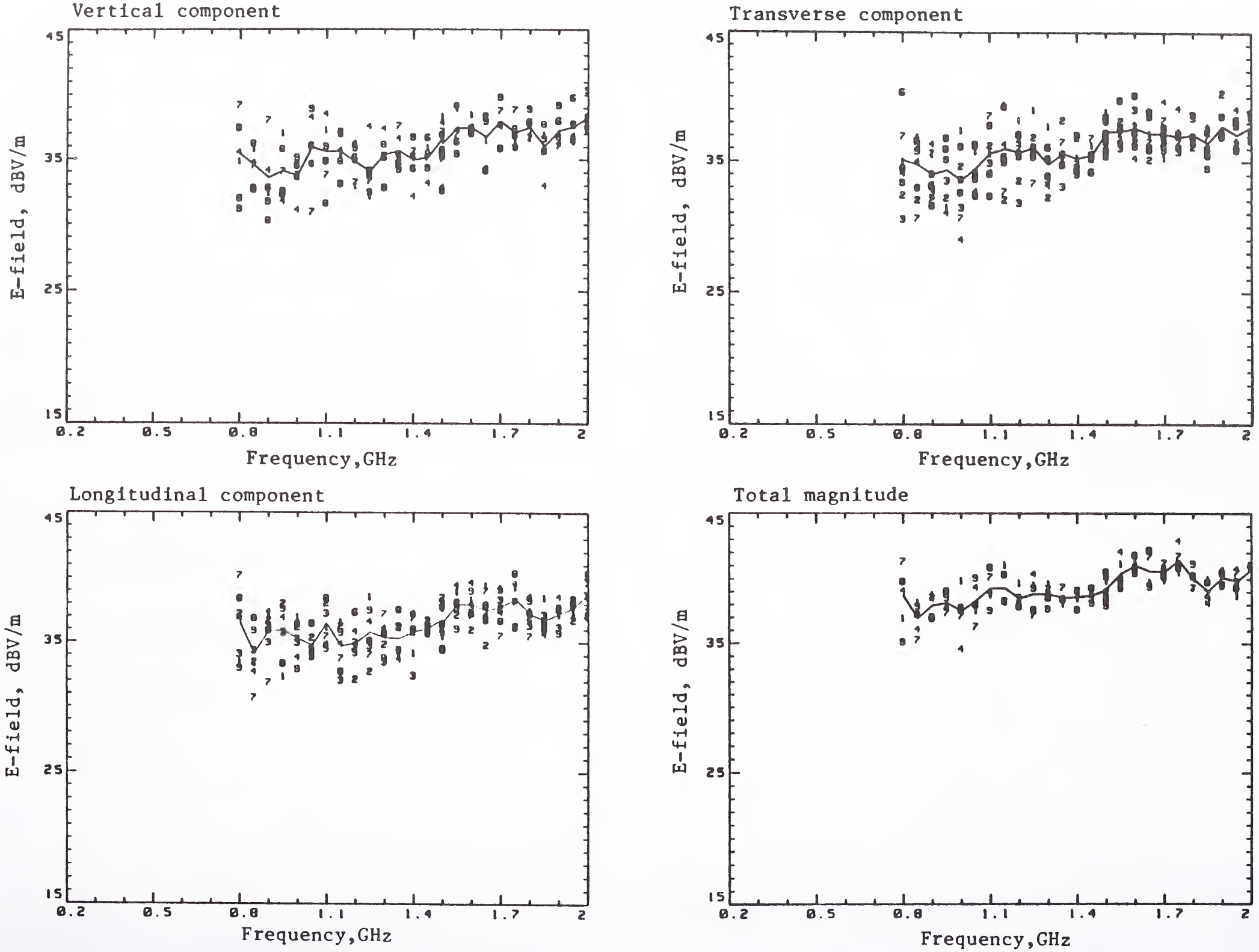

Figure 3.6(a) Spatial distribution of E-field components in the small chamber measured with 10 NIST isotropic probes (5 cm dipoles), using broadband horn antennas: (a) maximum, and (b) average values. Net transmitted power = 1 W.

(b) Average values

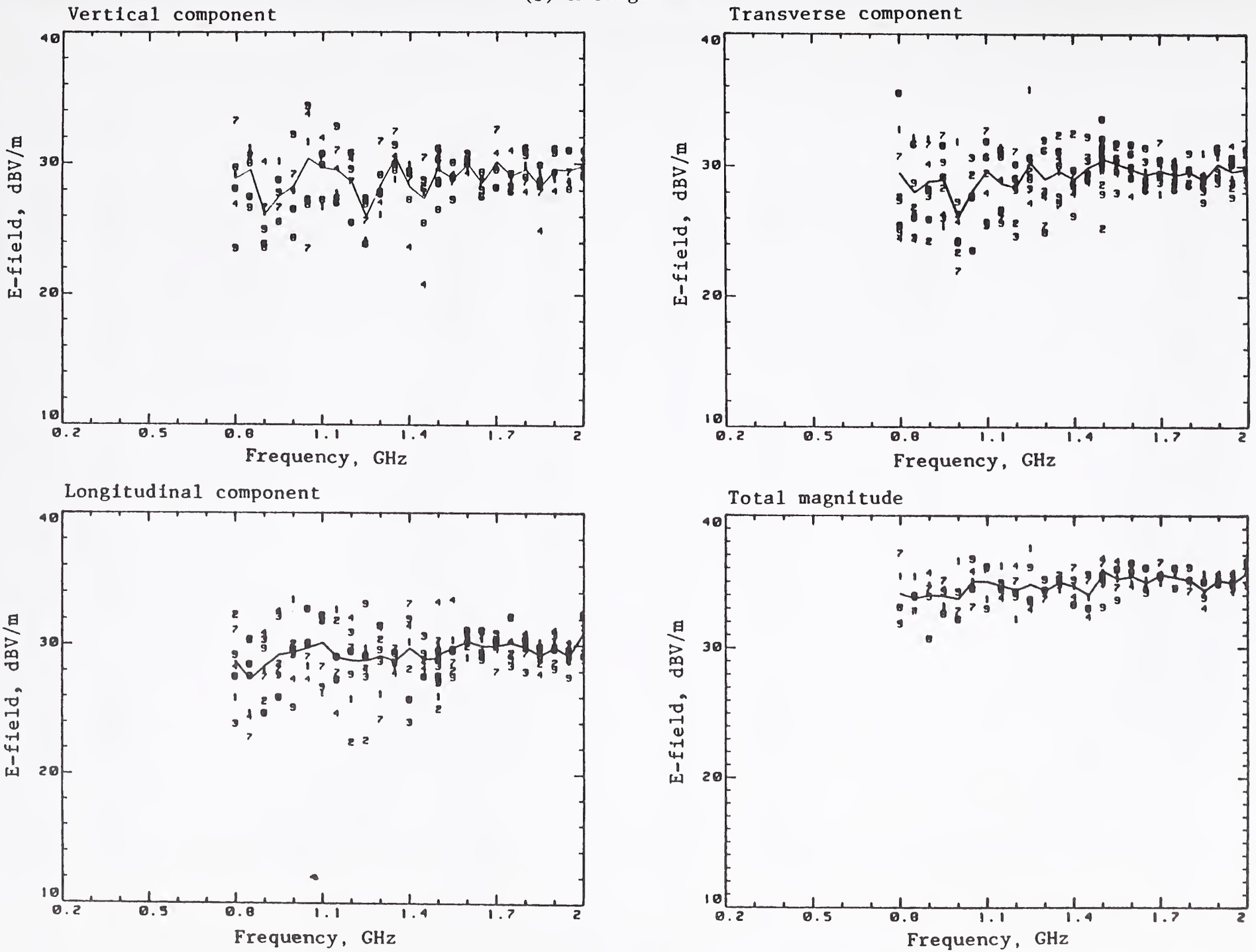

Figure 3.6(b) Spatial distribution of E-field components in the small chamber measured with 10 NIST isotropic probes (5 cm dipoles), using broadband horn antennas: (a) maximum, and (b) average values. Net transmitted power = 1 W.

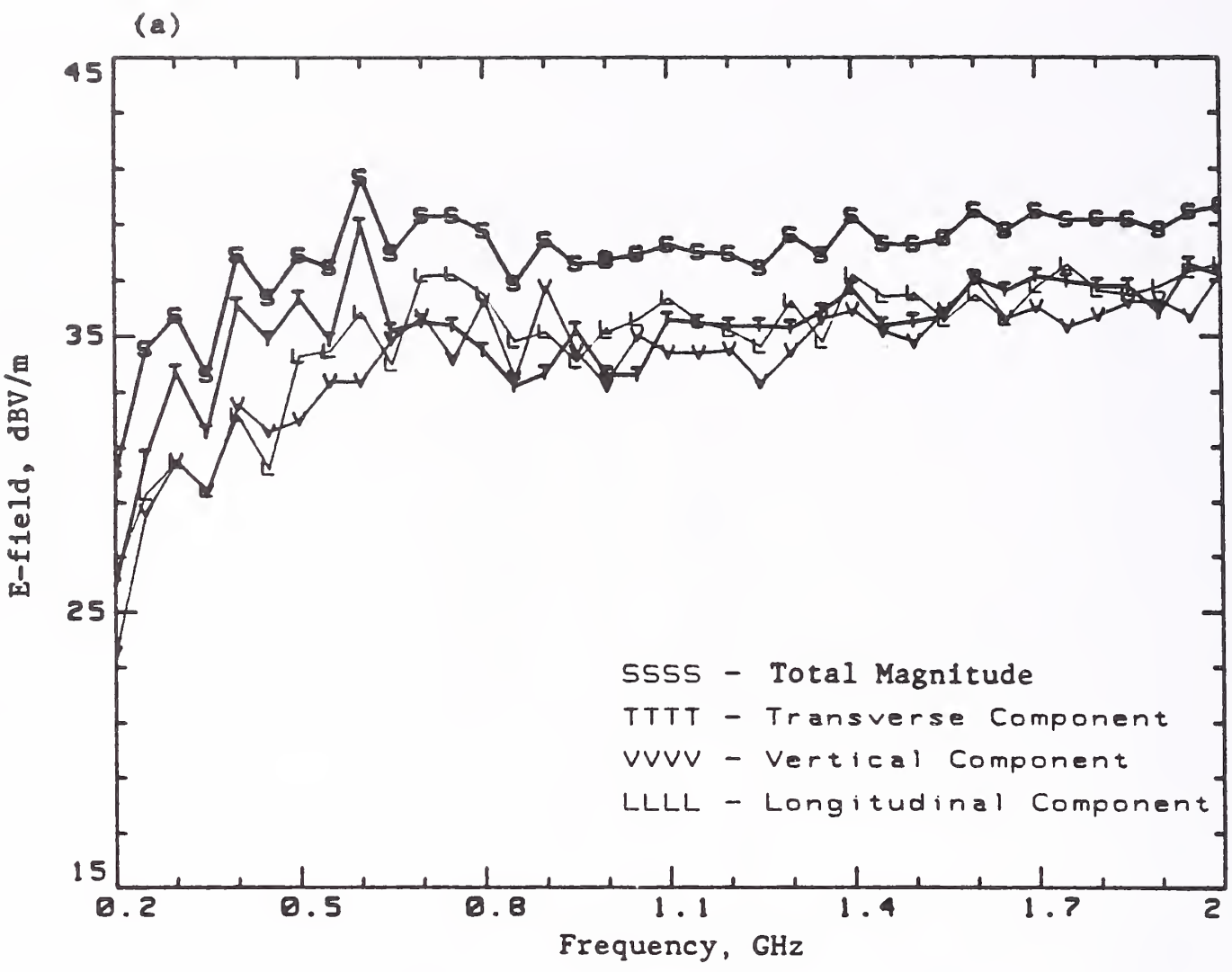

Figure 3.7 Average values of E-field components in the small chamber measured with 10 NIST isotropic probes (5 cm dipoles), using long wire antennas: (a) average of the 10 maximum values for each component, and (b) average of the 10 average values. Net transmitted power = 1 W.

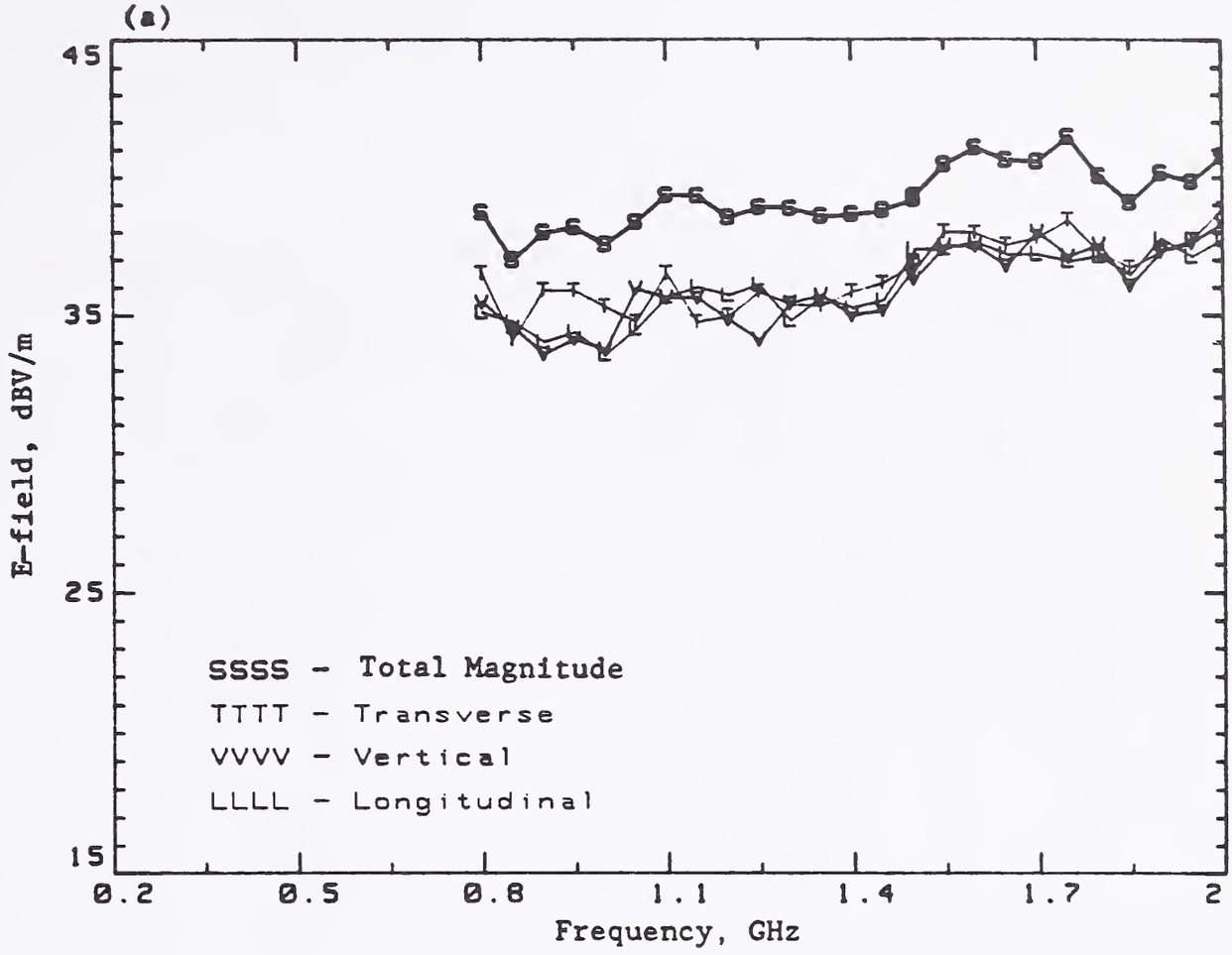

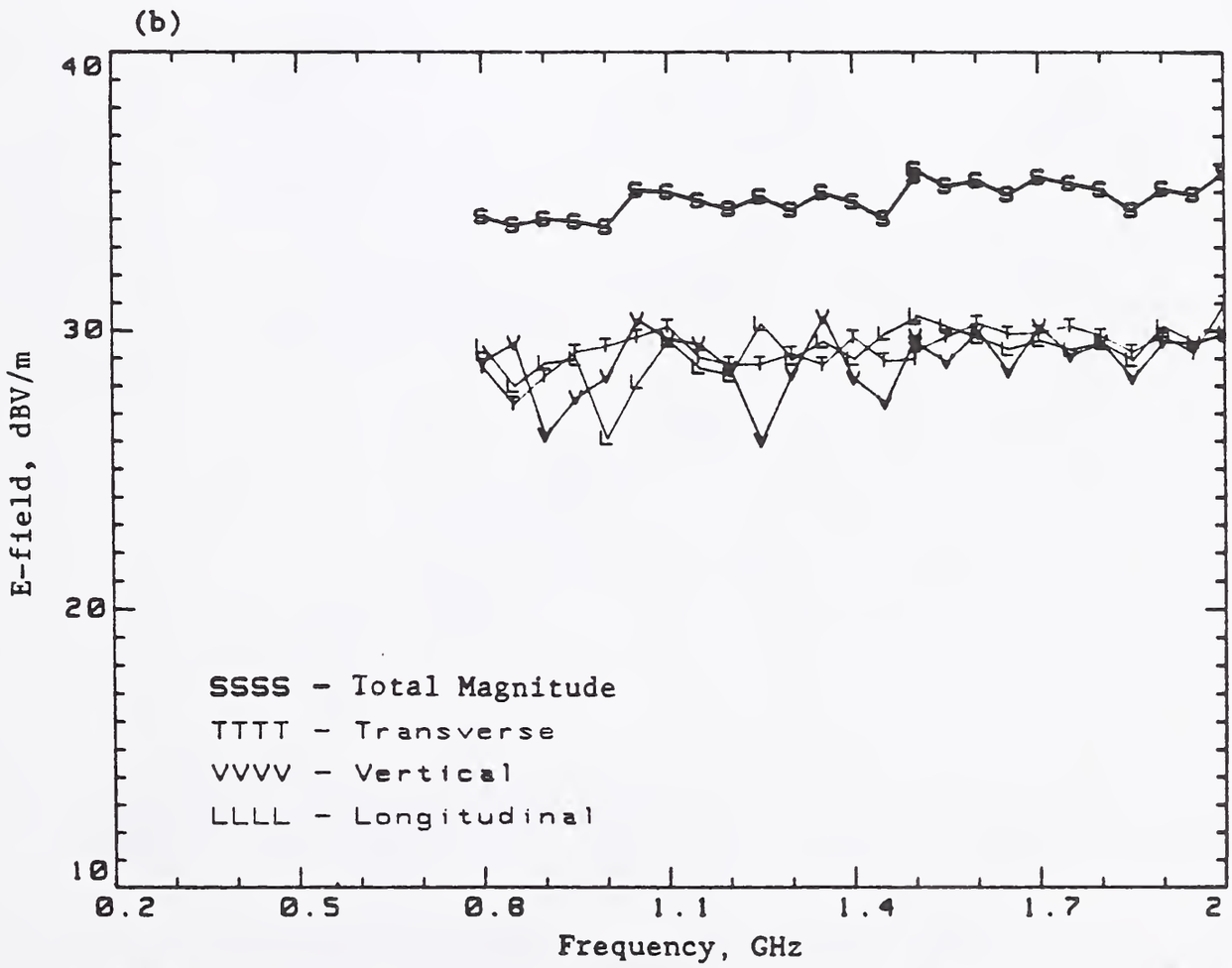

Figure 3.8 Average values of E-field components in the small chamber measured with 10 NIST isotropic probes (5 cm dipoles), using broadband horn antennas: (a) average of the 10 maximum values for each component, and (b) average of the 10 average values. Net transmitted power = 1 W.

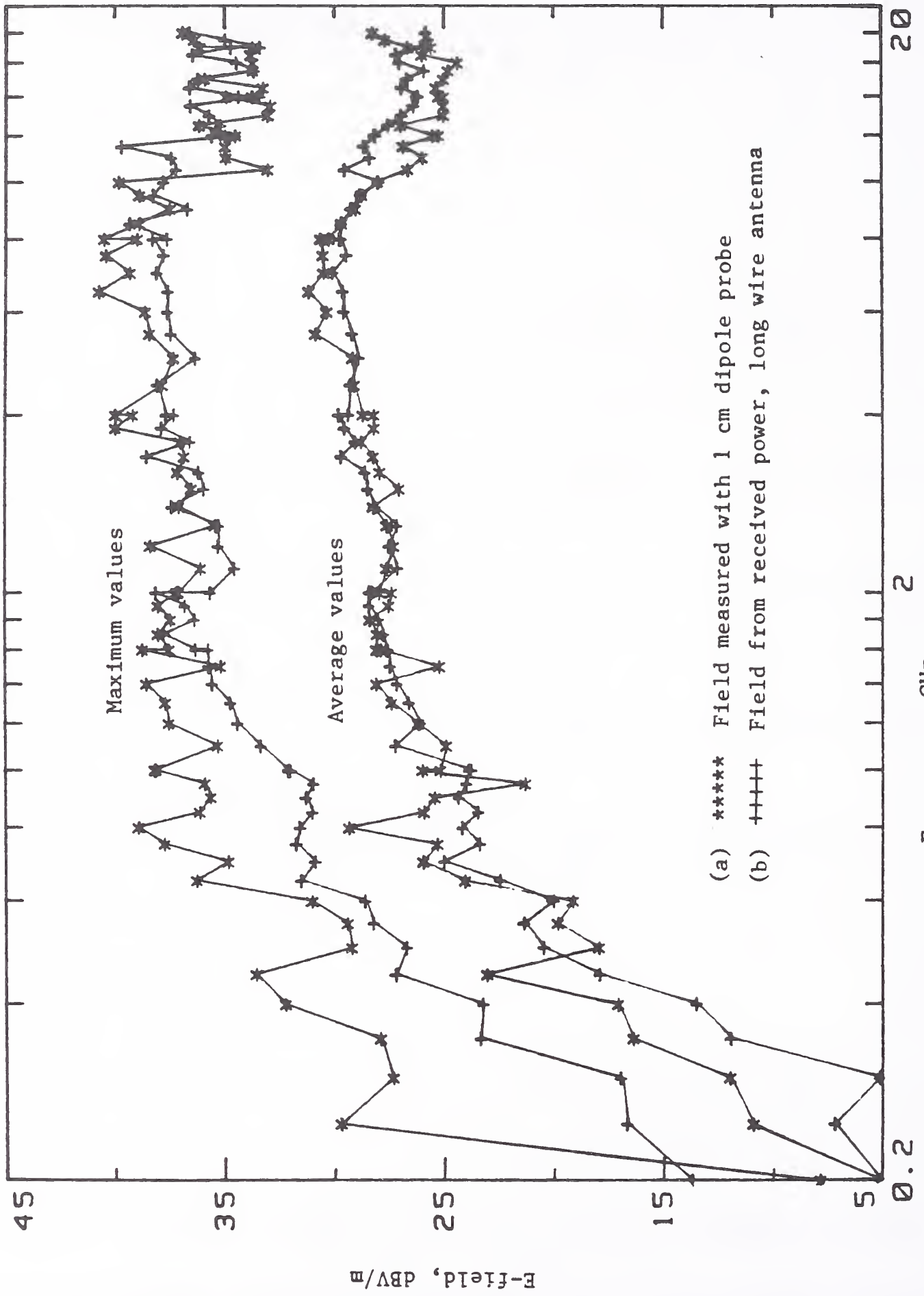

Figure 3.9 Maximum and average E-field strengths in the small chamber measured with: (a) 1 cm dipole probe, and (b) received power of long wire antenna. Net transmitted power = 0.1 W.

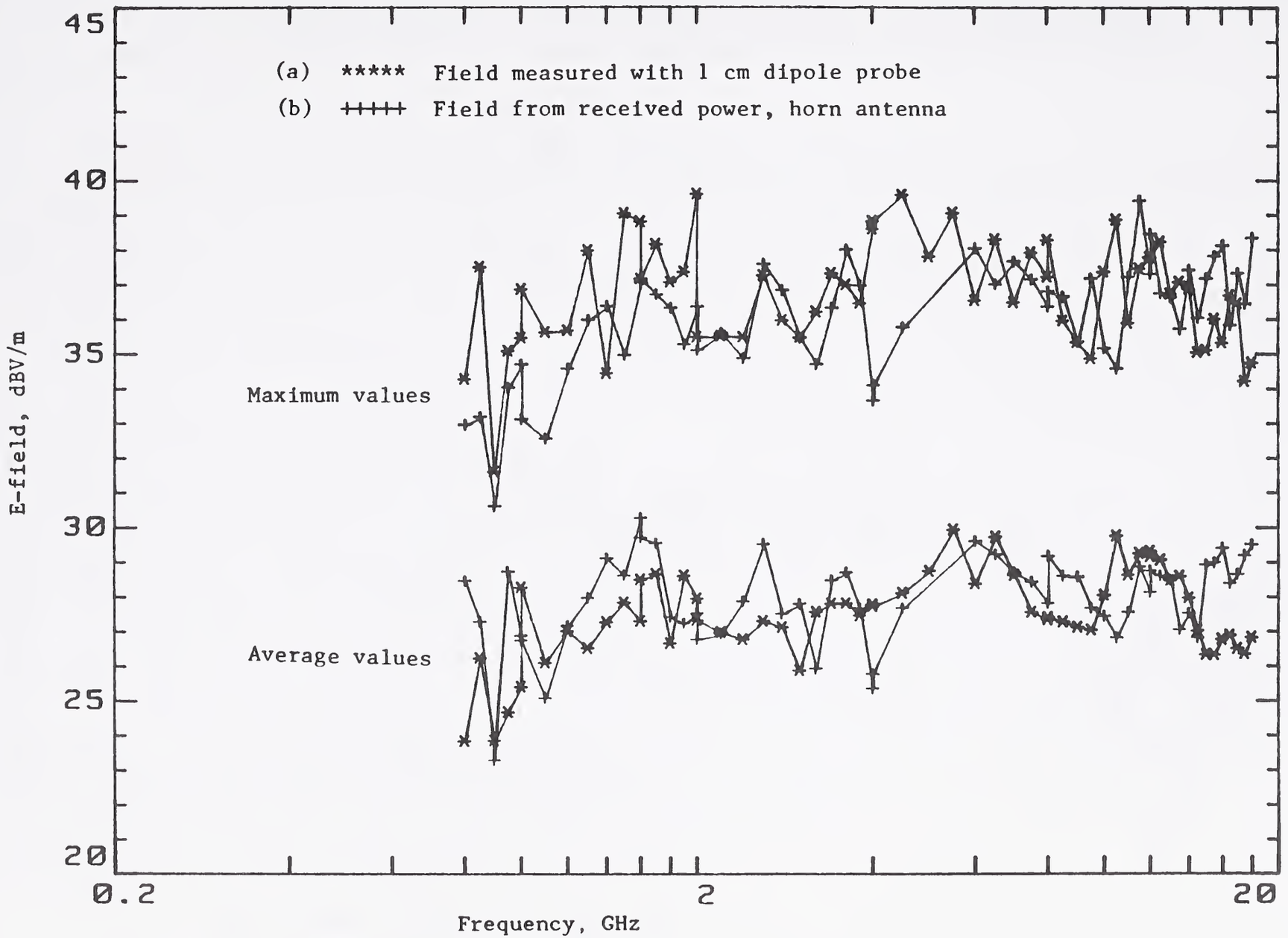

Figure 3.10 Maximum and average E-field strengths in the small chamber measured with: (a) 1 cm dipole probe, and (b) received power of broadband horn antenna. Net transmitted power = 0.1 W.

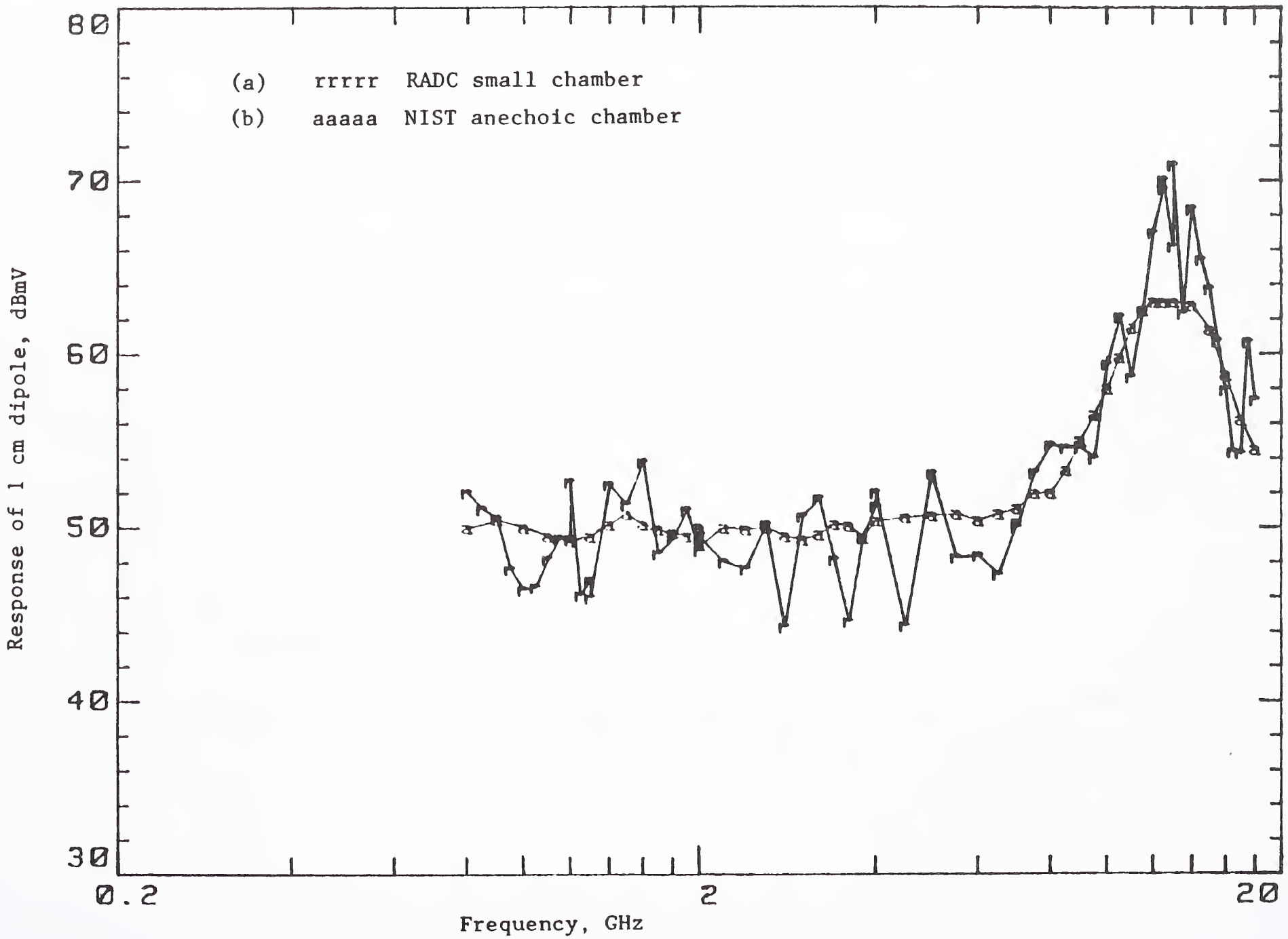

Figure 3.11 Maximum responses of NIST 1 cm dipole probe to an E-field of 37 dBV/m using: (a) RADC small reverberating chamber, and (b) NIST anechoic chamber.

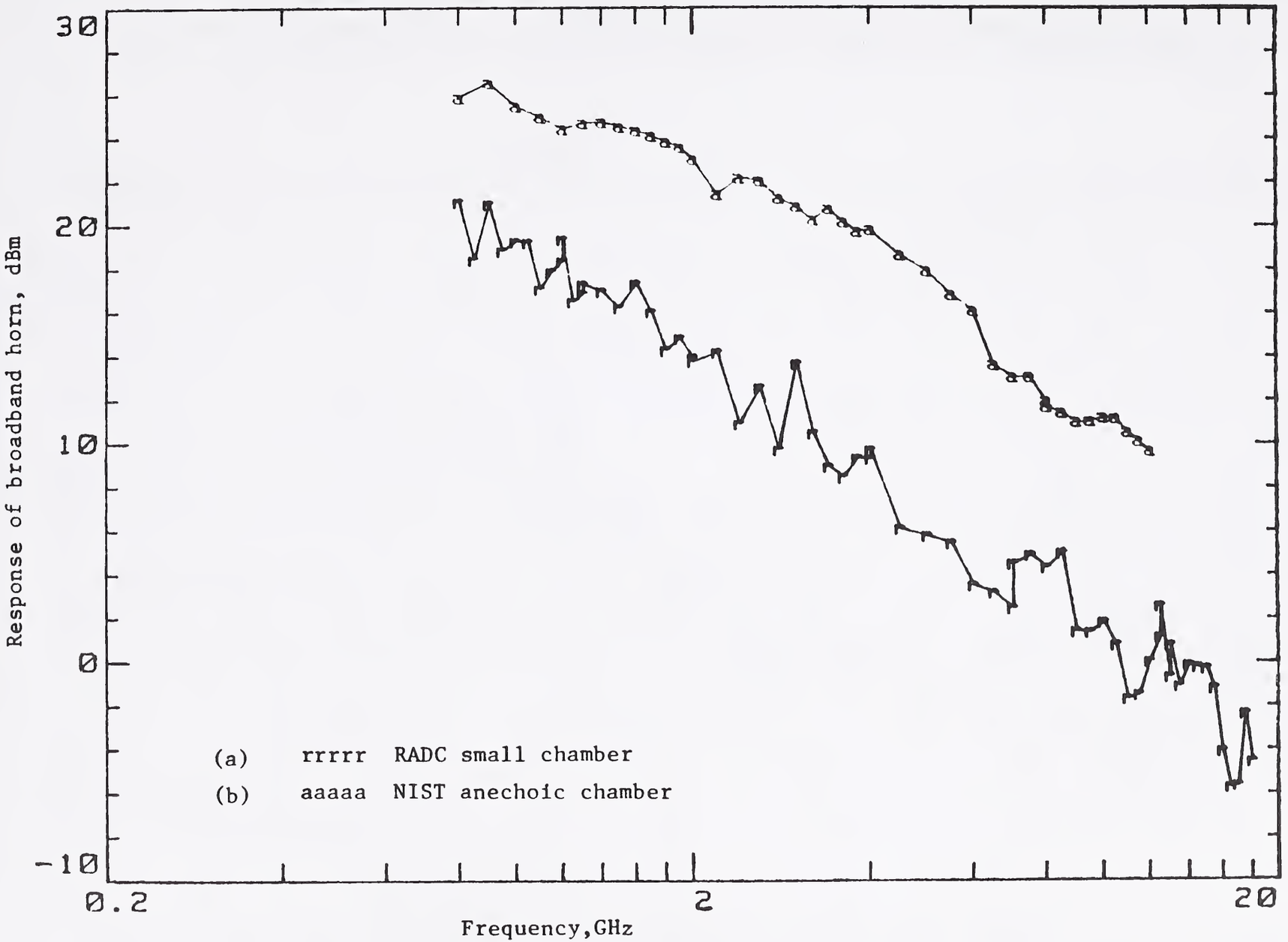

Figure 3.12 Maximum powers received by a broadband (1 to 18 GHz) horn antenna in an E-field of 37 dBV/m using: (a) RADC small reverberating chamber, and (b) NIST anechoic chamber.

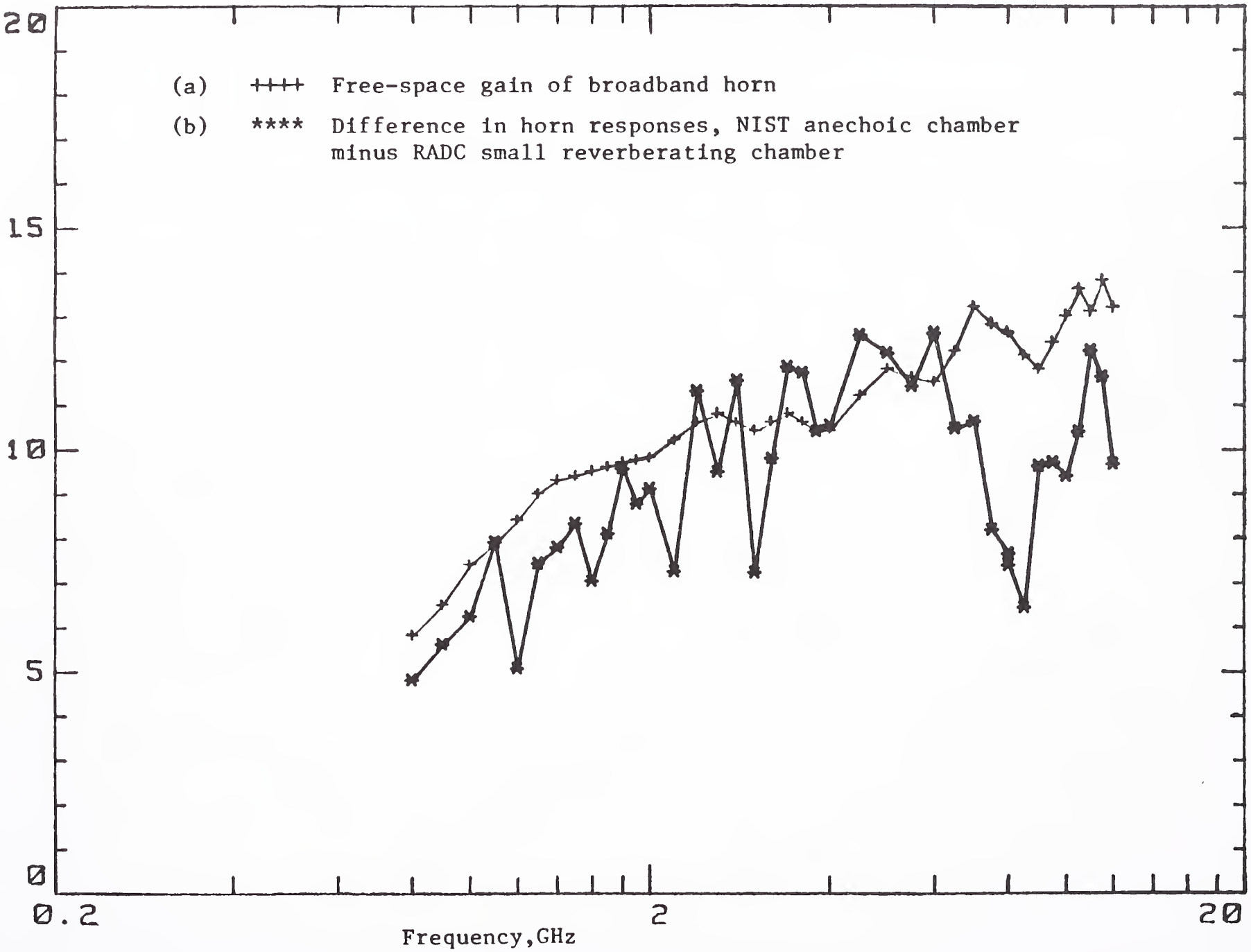

Figure 3.13 Comparison of: (a) free-space gain of a broadband horn antenna, with (b) difference in maximum responses of the horn measured in NIST anechoic chamber minus RADC small reverberating chamber.

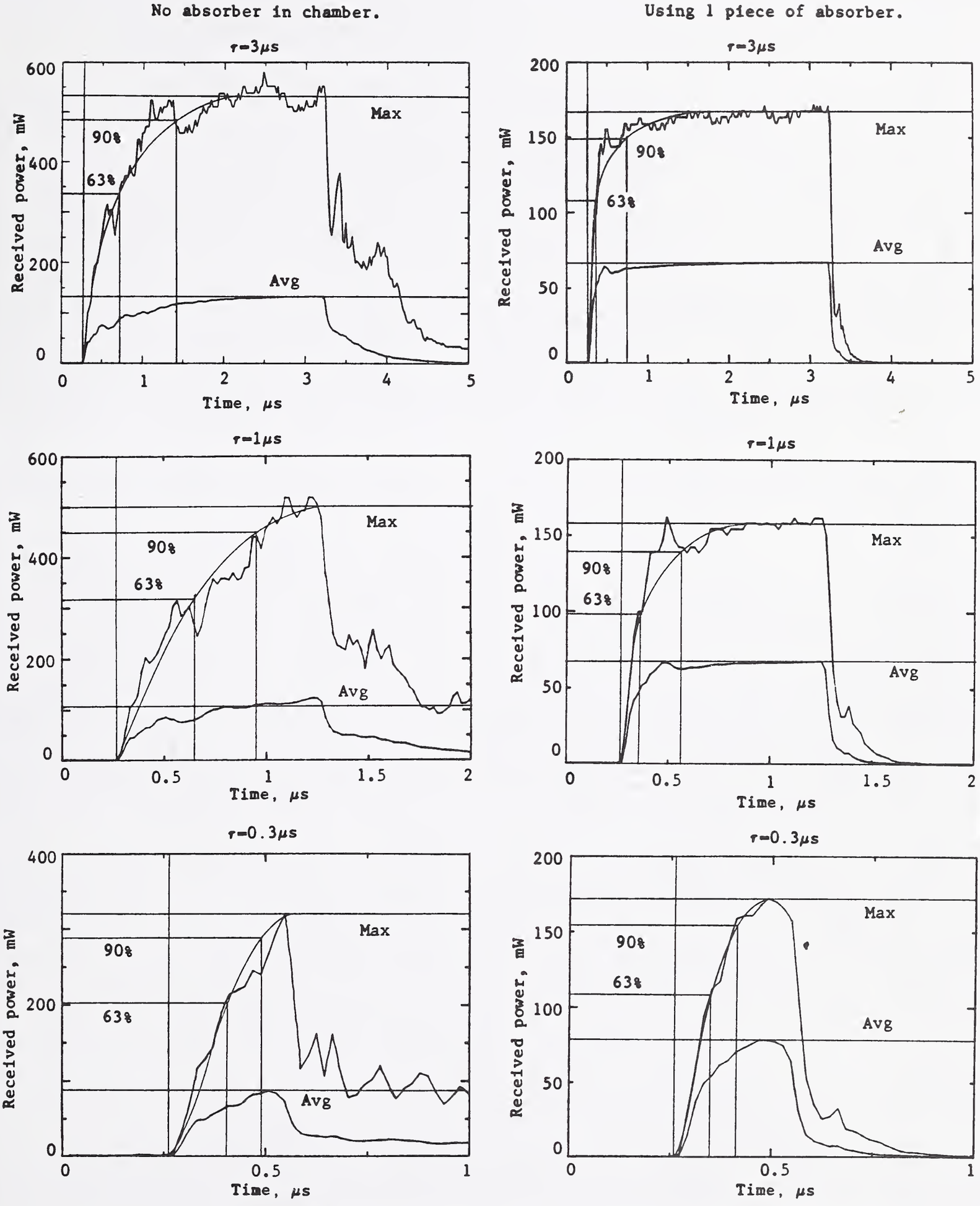

Figure 5.1(a) Maximum and average values of received rf pulse waveforms in the mode-tuned RADC small reverberating chamber using no rf absorber (chamber empty) and 1 piece of absorber; F = 0.9 GHz.

No absorber in chamber.

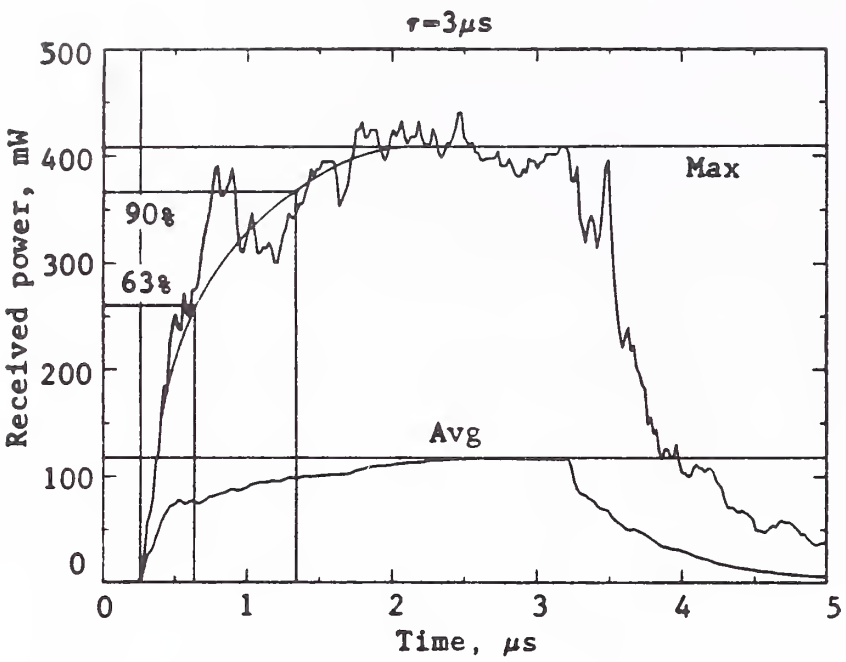

Using 1 piece of absorber.

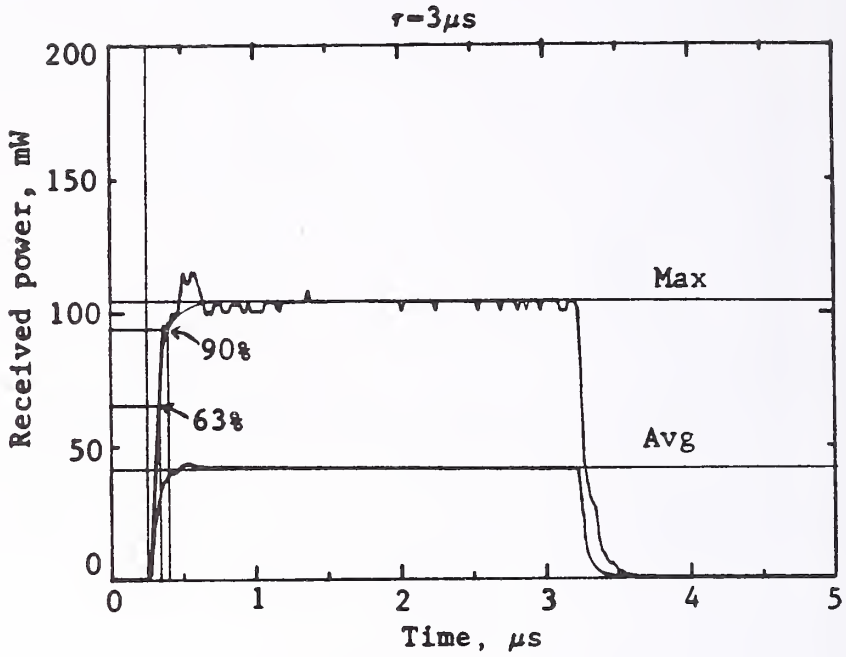

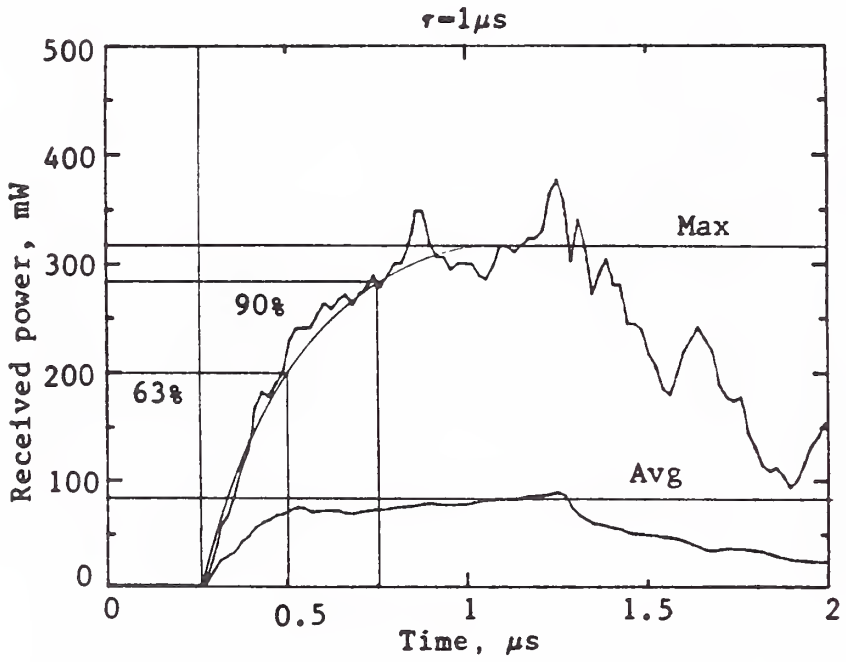

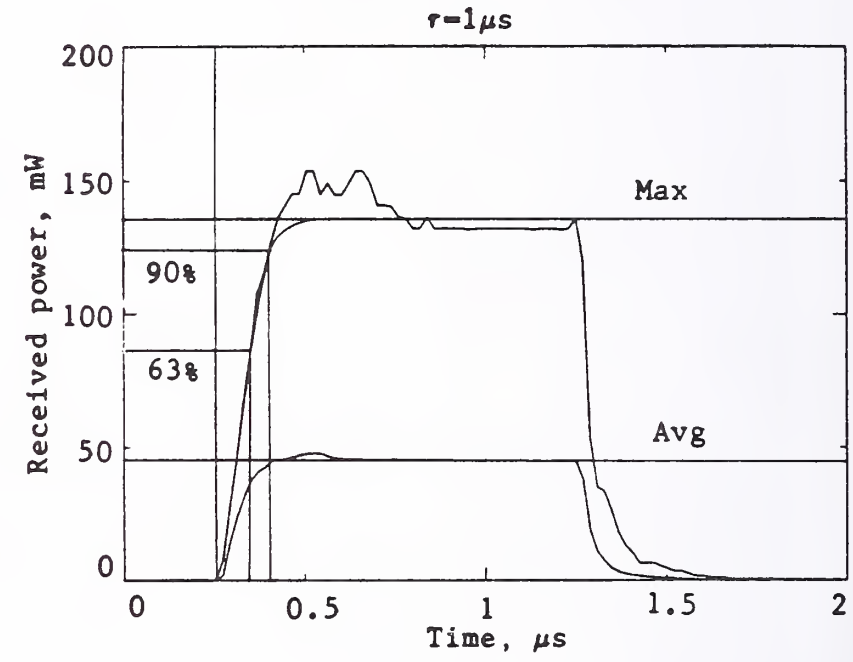

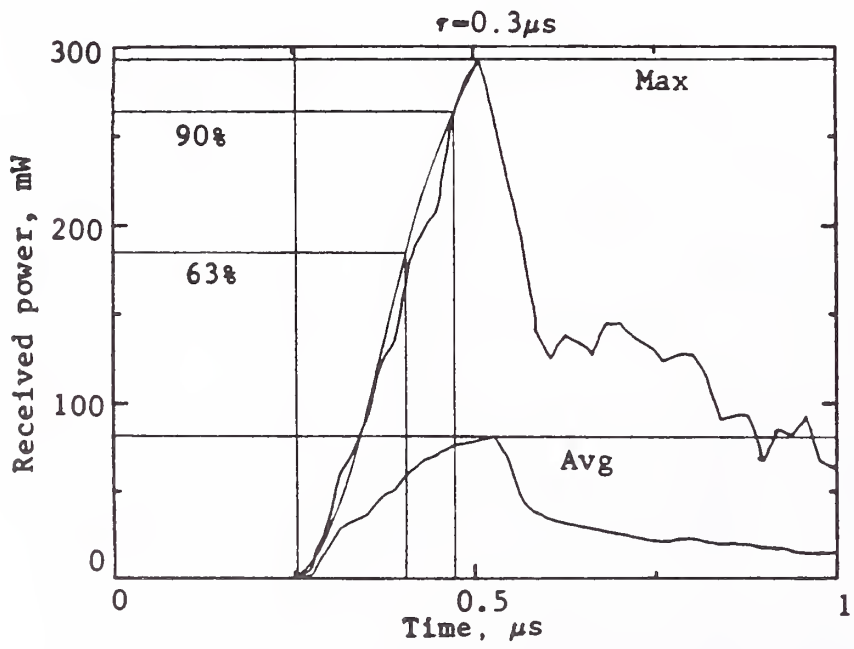

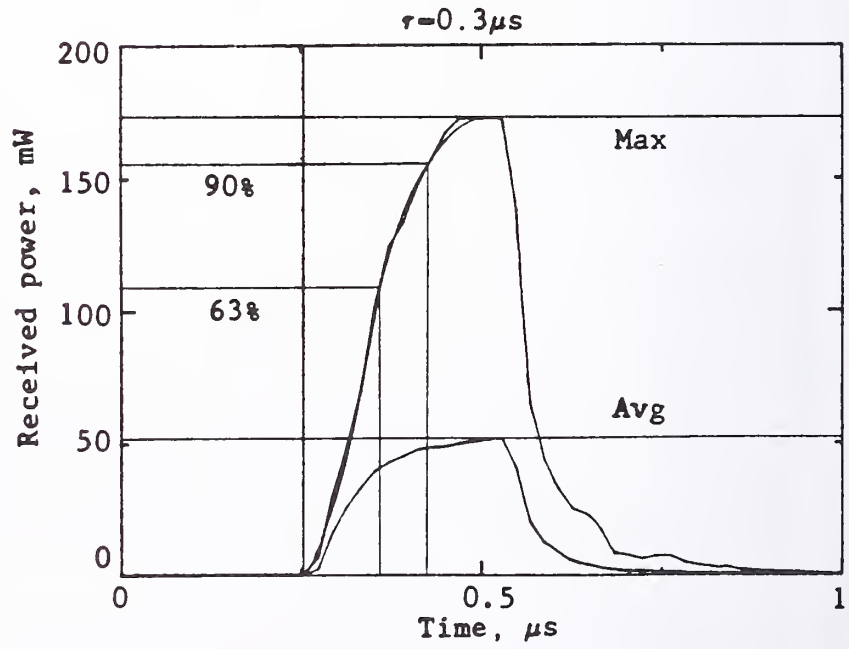

Figure 5.1(b) Maximum and average values of received rf pulse waveforms in the mode-tuned RADC small reverberating chamber using no rf absorber (chamber empty) and 1 piece of absorber; F = 1.3 GHz.

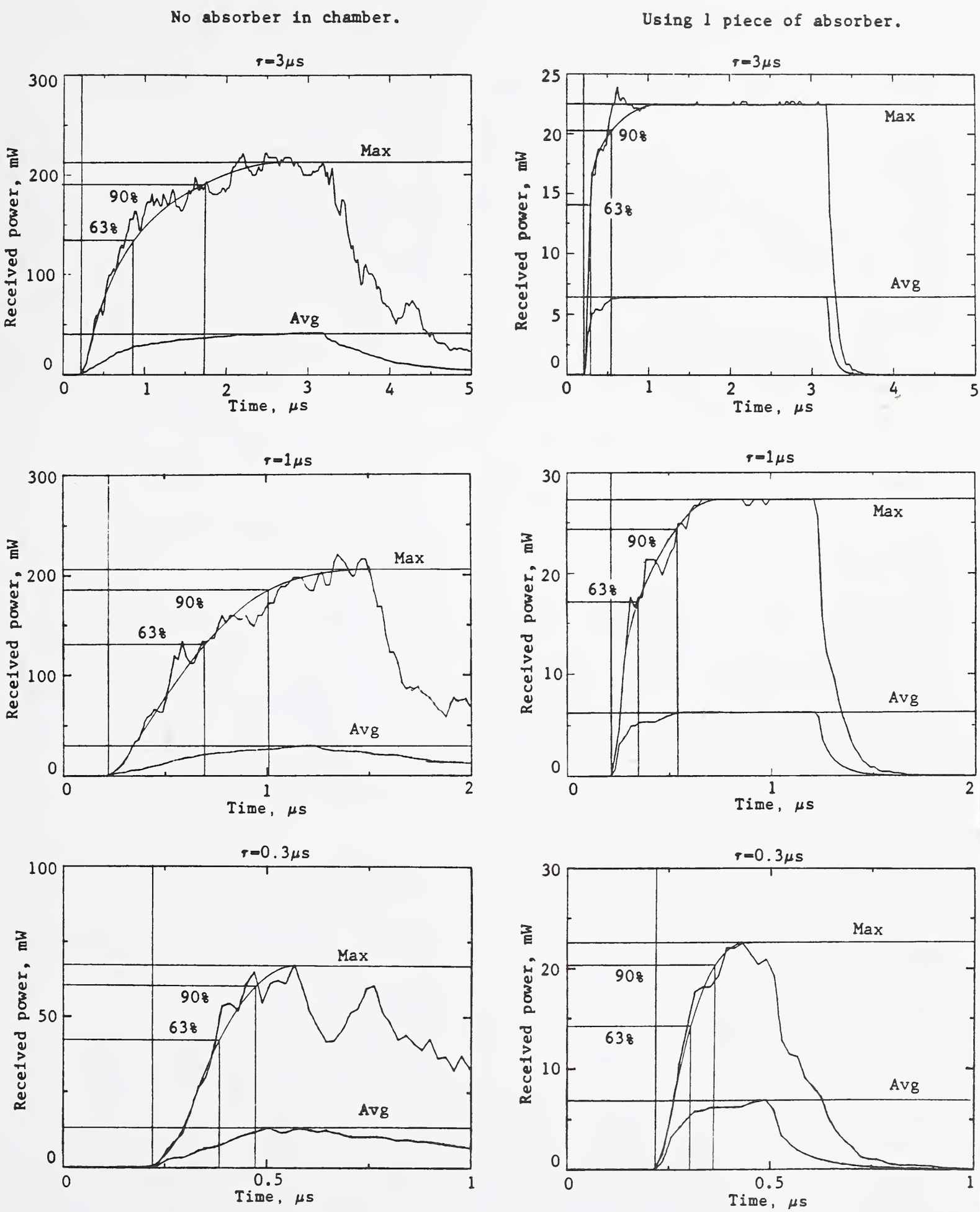

Figure 5.1(c) Maximum and average values of received rf pulse waveforms in the mode-tuned RADC small reverberating chamber using no rf absorber (chamber empty) and 1 piece of absorber; F = 2.0 GHz.

No absorber in chamber.

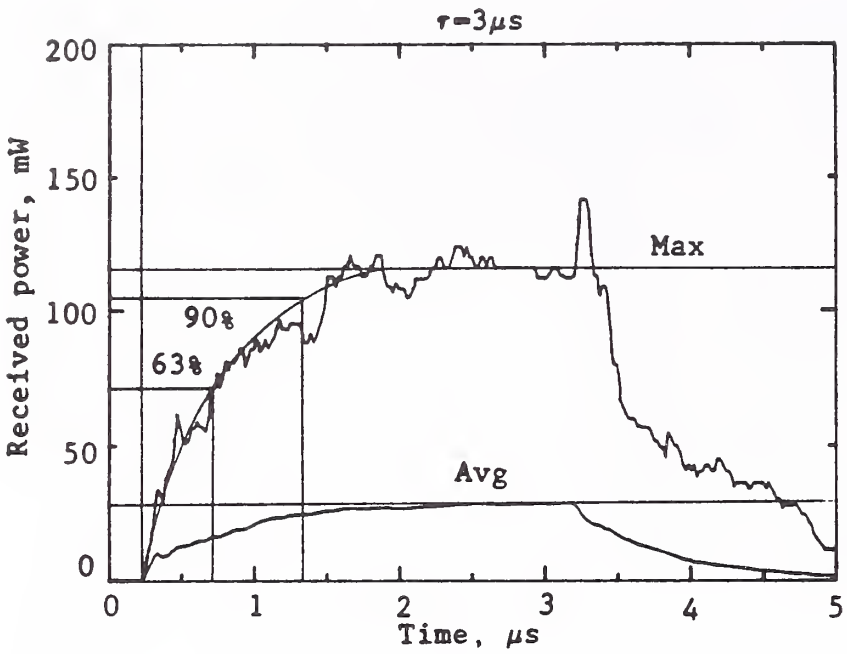

Using 1 piece of absorber.

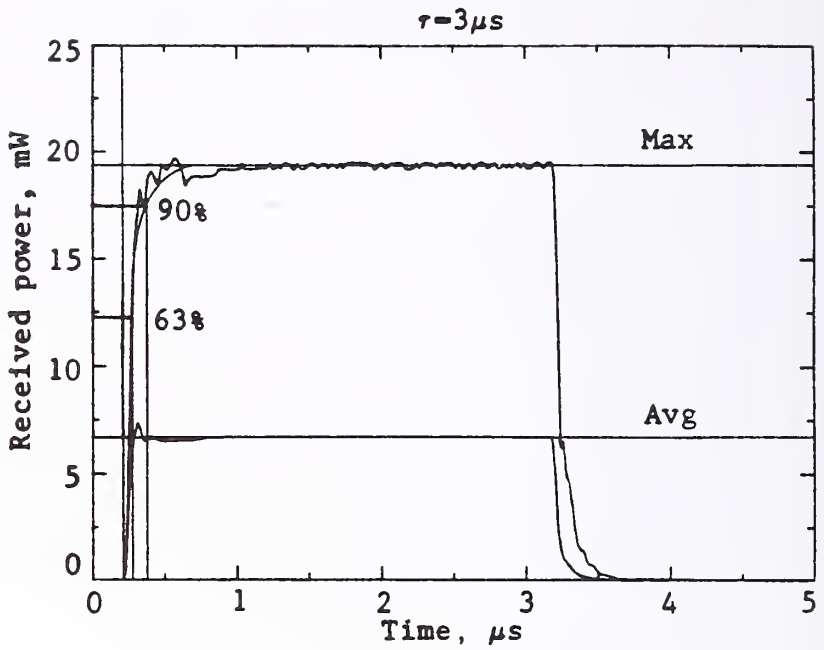

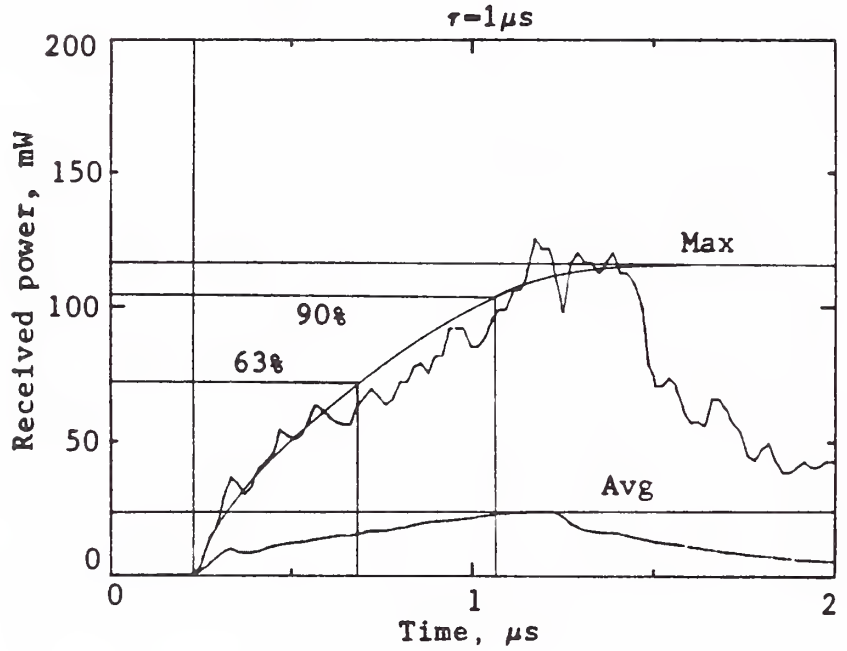

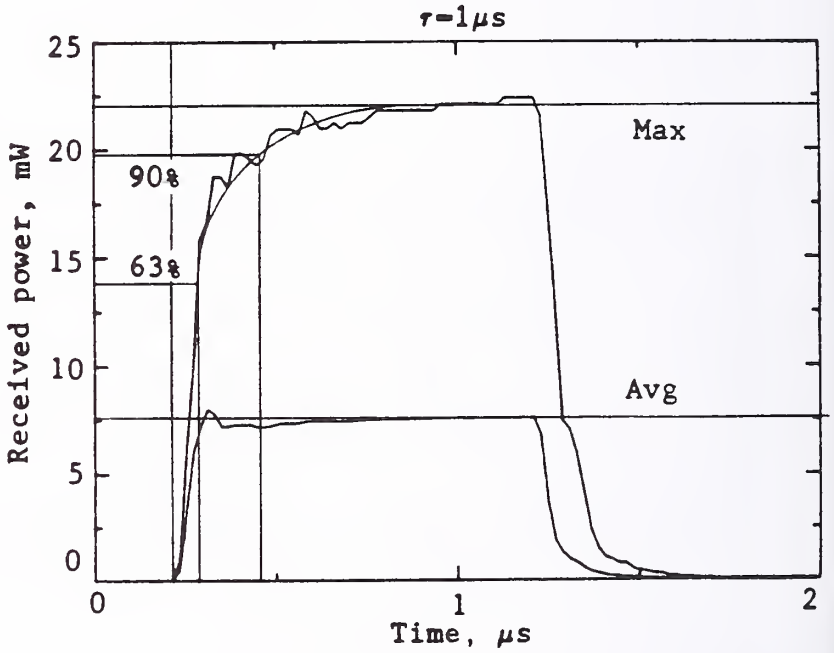

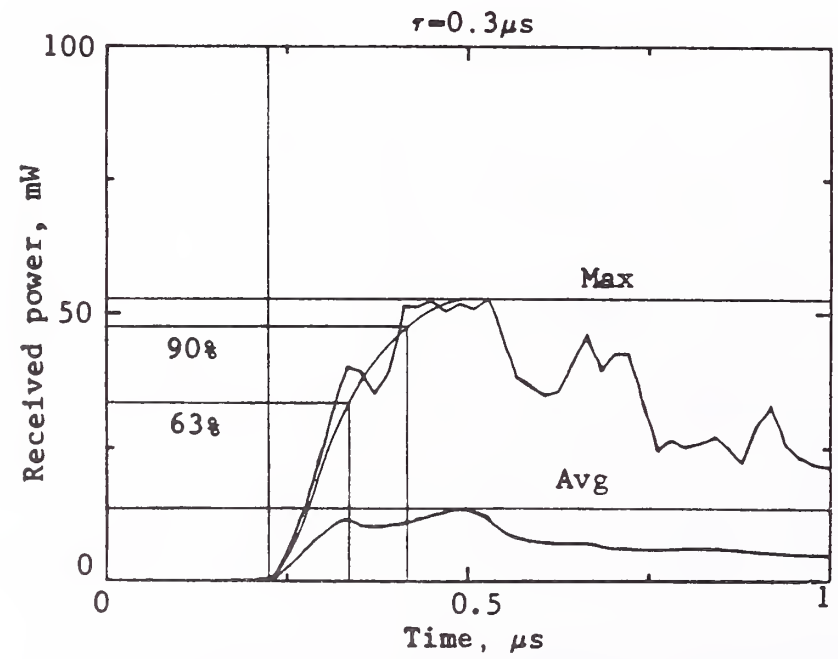

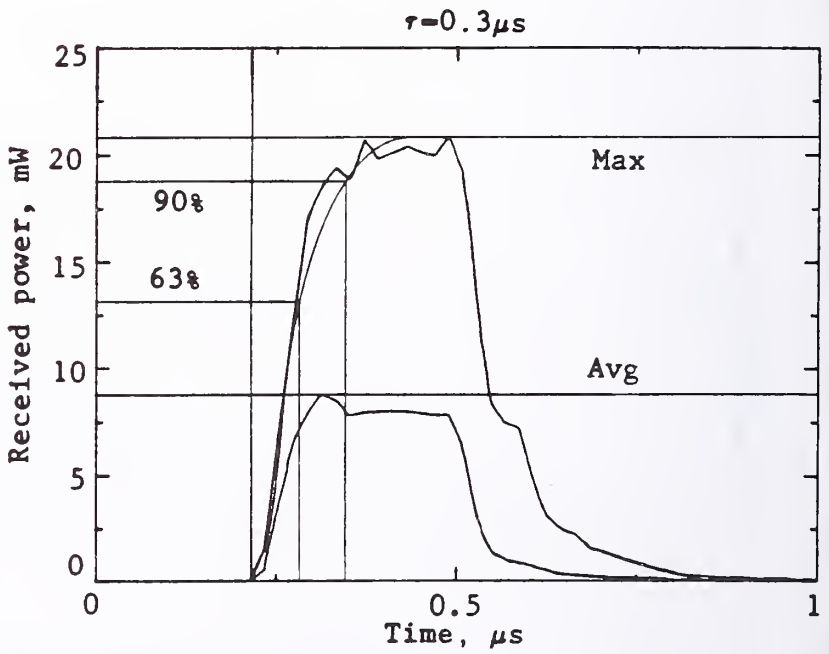

Figure 5.1(d) Maximum and average values of received rf pulse waveforms in the mode-tuned RADC small reverberating chamber using no rf absorber (chamber empty) and 1 piece of absorber; F = 2.9 GHz.

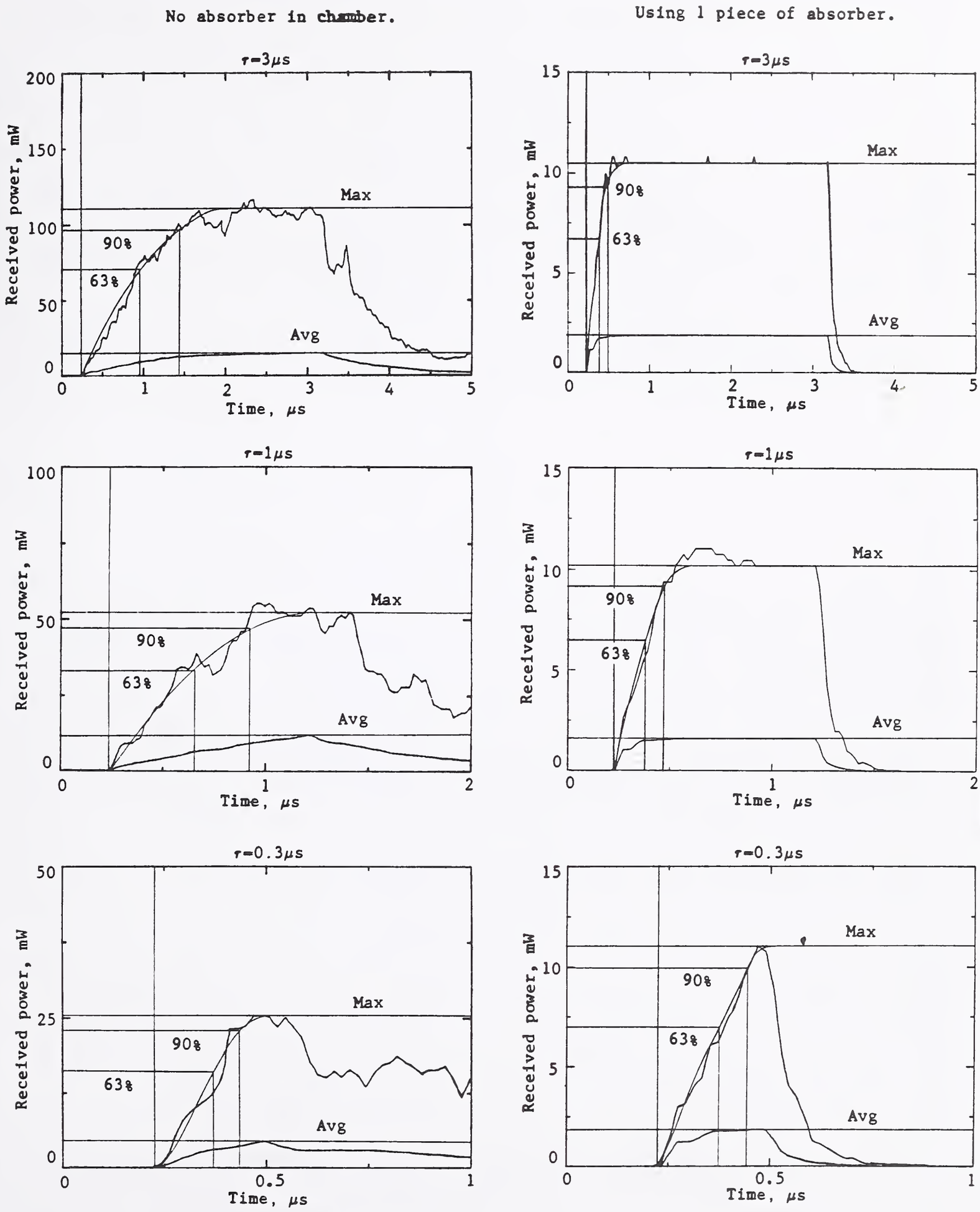

Figure 5.1(e) Maximum and average values of received rf pulse waveforms in the mode-tuned RADC small reverberating chamber using no rf absorber (chamber empty) and 1 piece of absorber; F = 4.2 GHz.

No absorber in chamber.

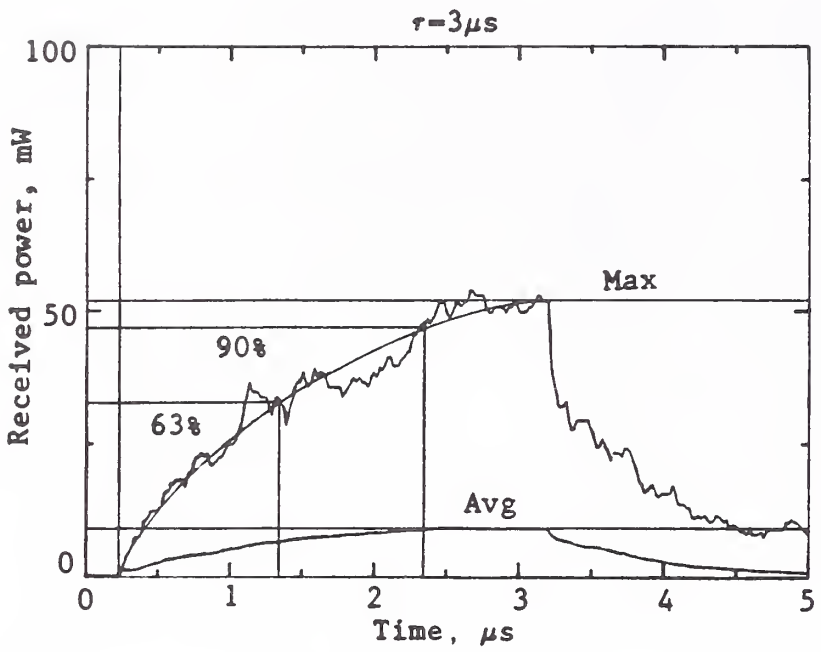

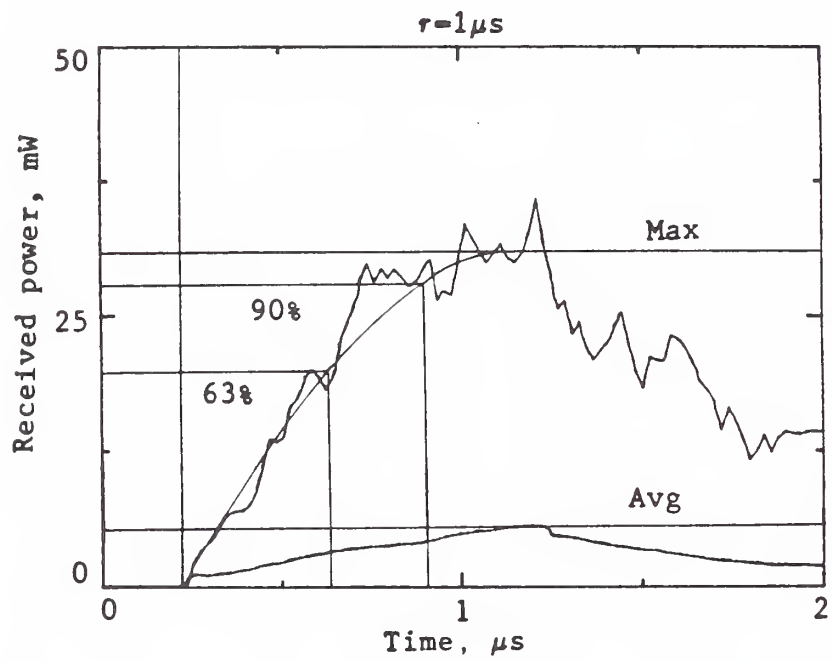

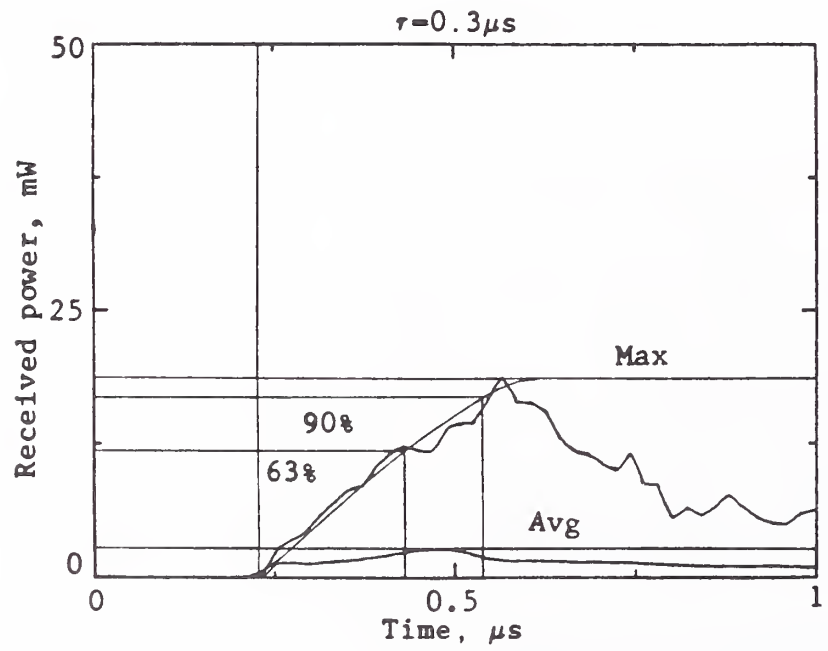

Using 1 piece of absorber.

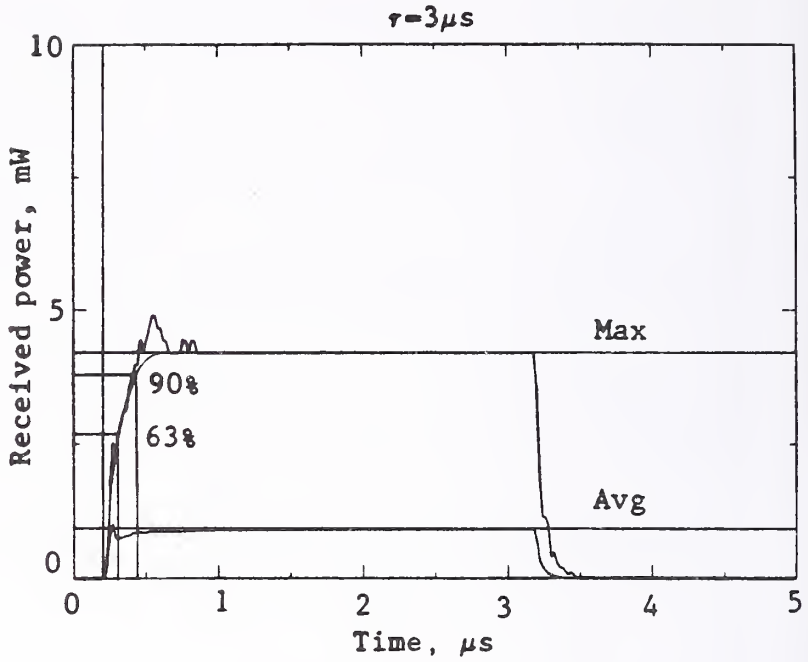

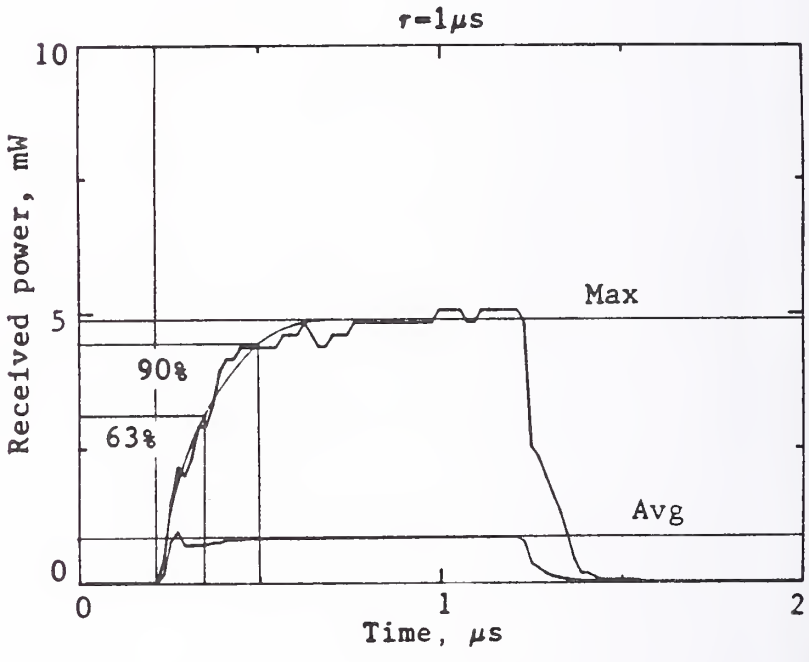

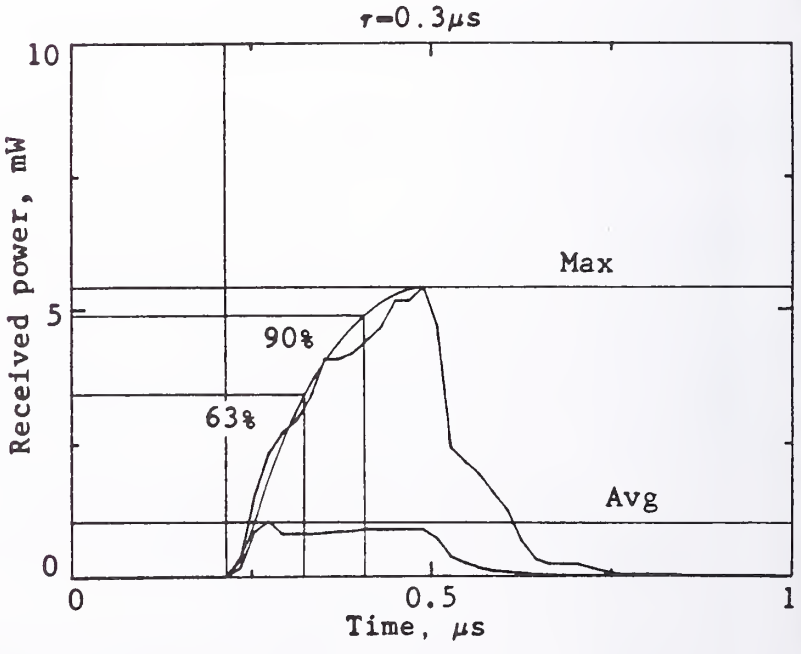

Figure 5.1(f) Maximum and average values of received rf pulse waveforms in the mode-tuned RADC small reverberating chamber using no rf absorber (chamber empty) and 1 piece of absorber; F = 5.65 GHz.

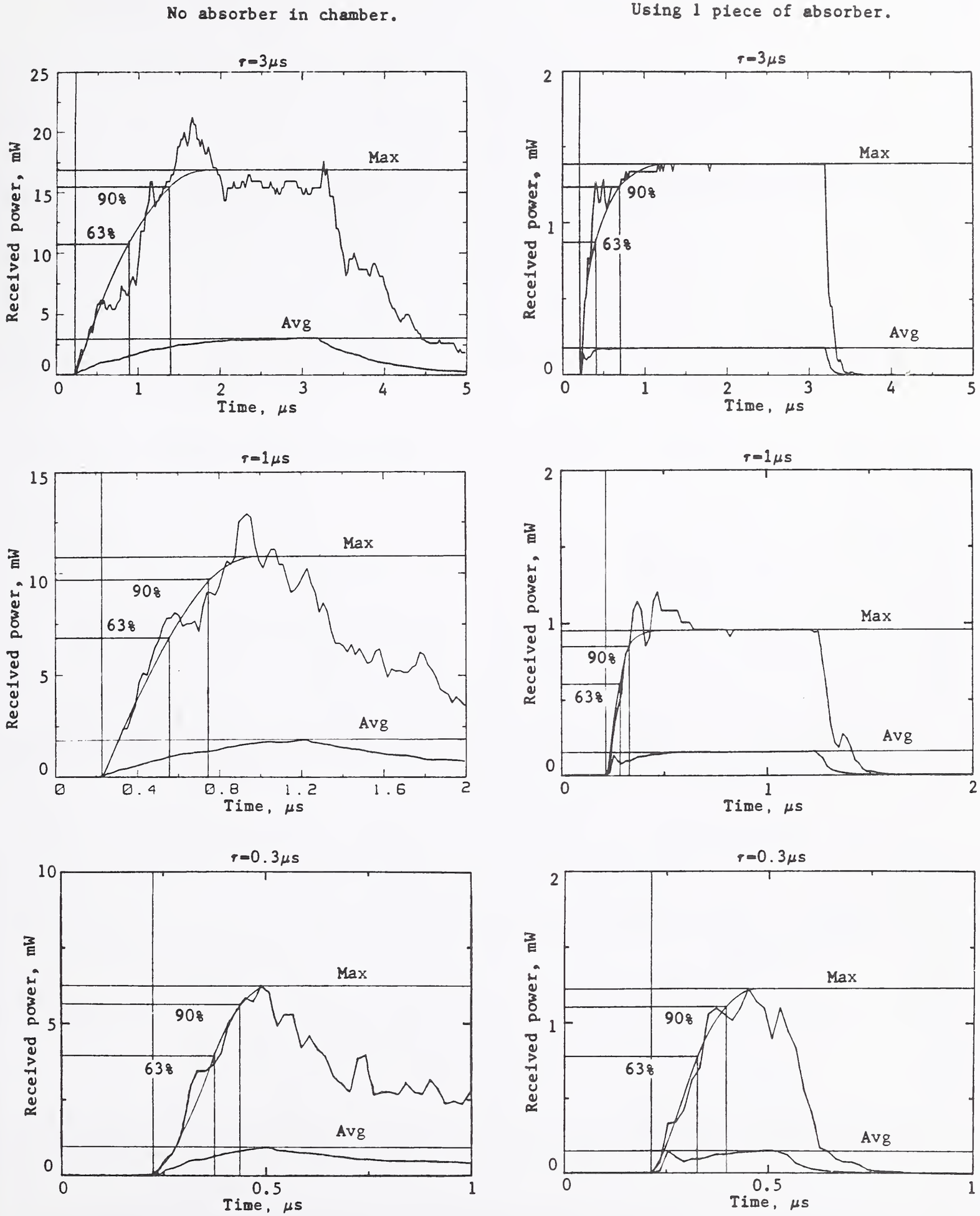

Figure 5.1(g) Maximum and average values of received rf pulse waveforms in the mode-tuned RADC small reverberating chamber using no rf absorber (chamber empty) and 1 piece of absorber; F = 8.9 GHz.

No absorber in chamber.

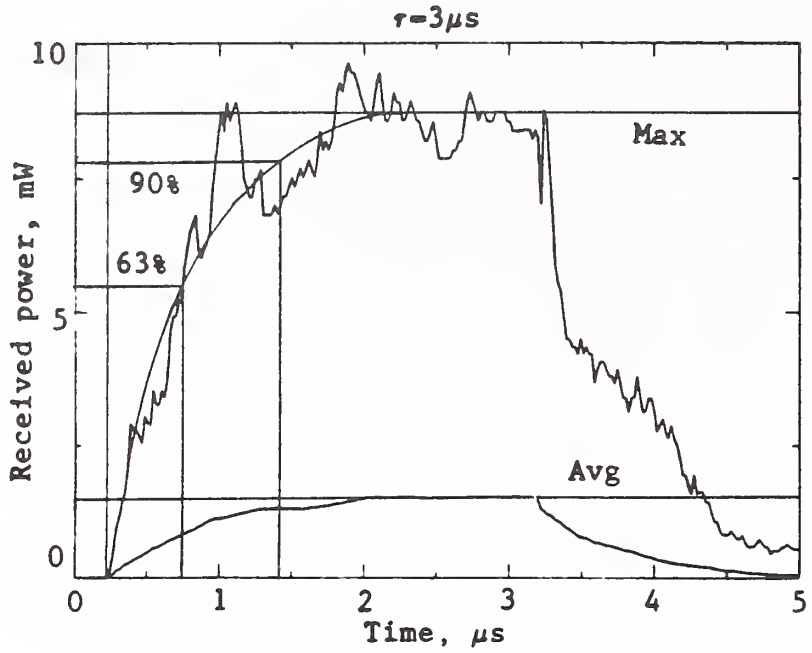

Using 1 piece of absorber.

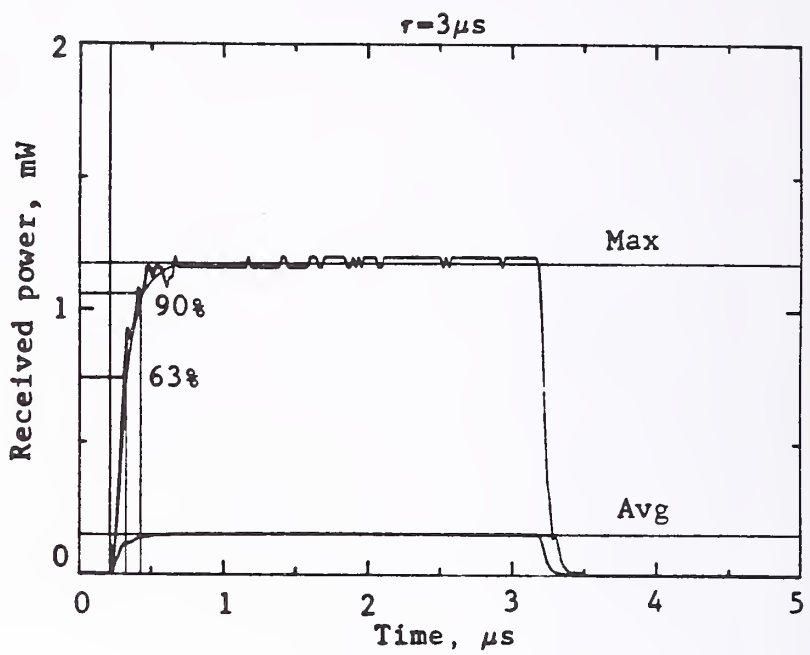

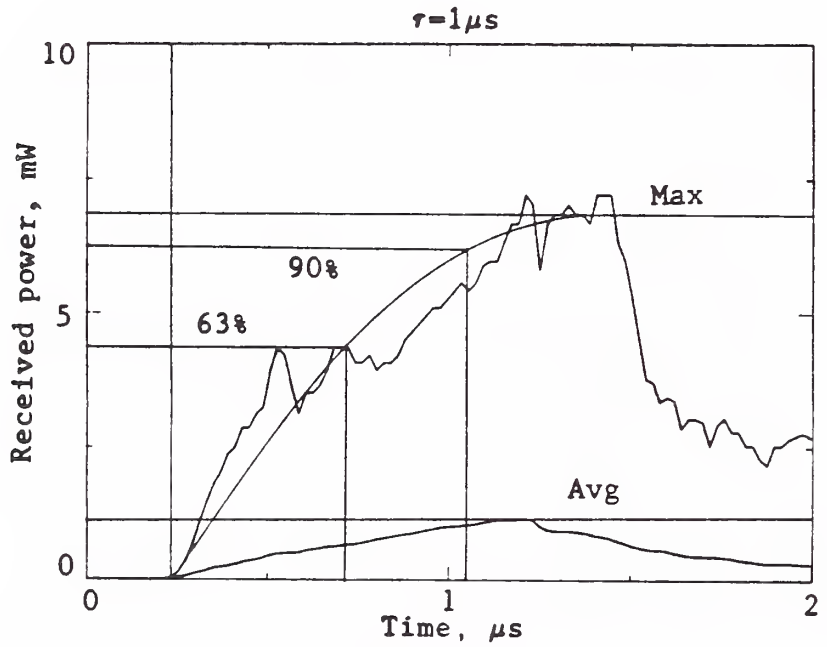

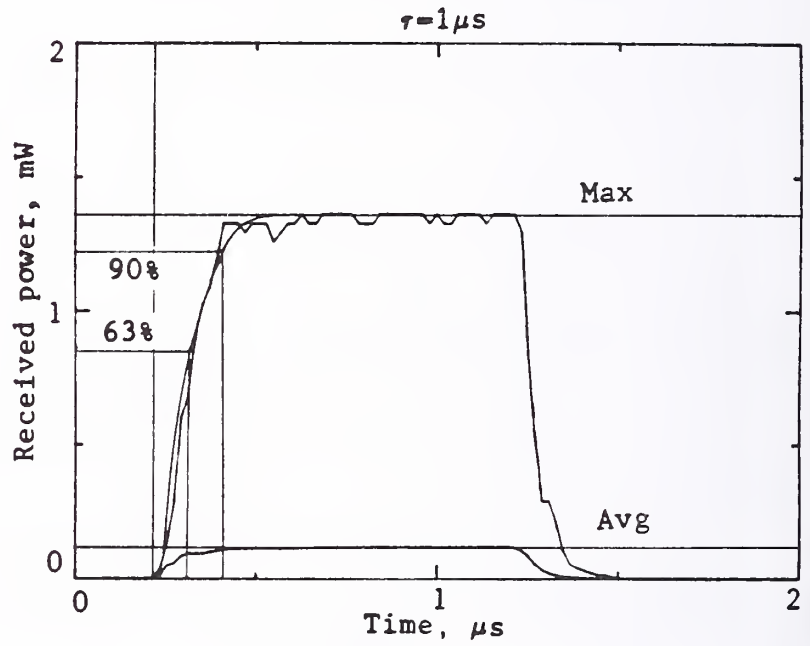

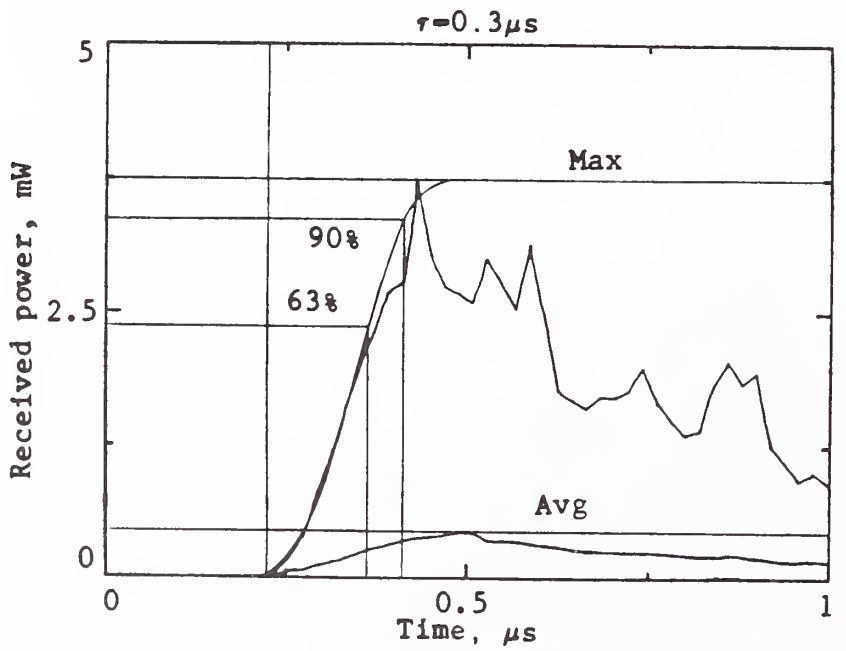

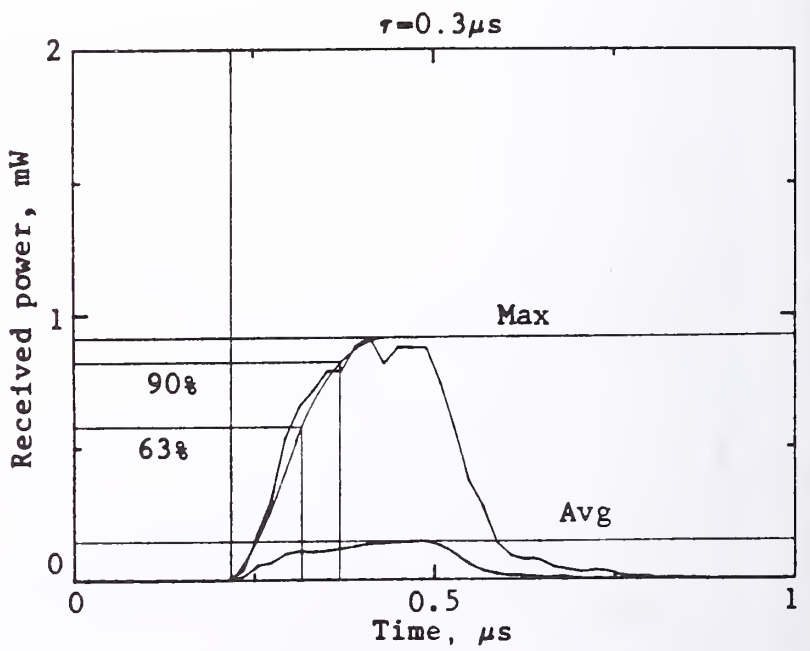

Figure 5.1(h) Maximum and average values of received rf pulse waveforms in the mode-tuned RADC small reverberating chamber using no rf absorber (chamber empty) and 1 piece of absorber; F = 12 GHz.

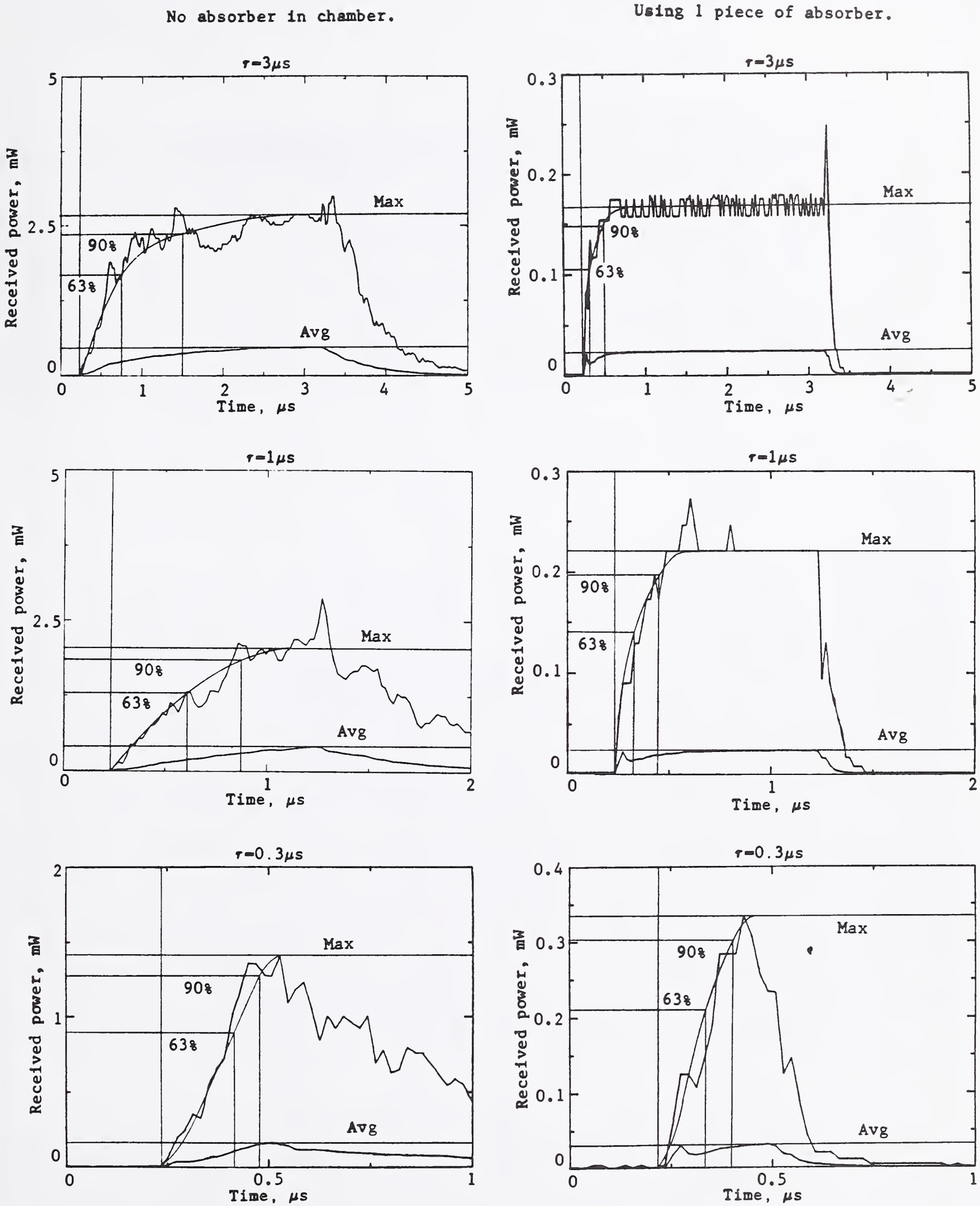

Figure 5.1(i) Maximum and average values of received rf pulse waveforms in the mode-tuned RADC small reverberating chamber using no rf absorber (chamber empty) and 1 piece of absorber; F = 16 GHz.

No absorber in chamber.

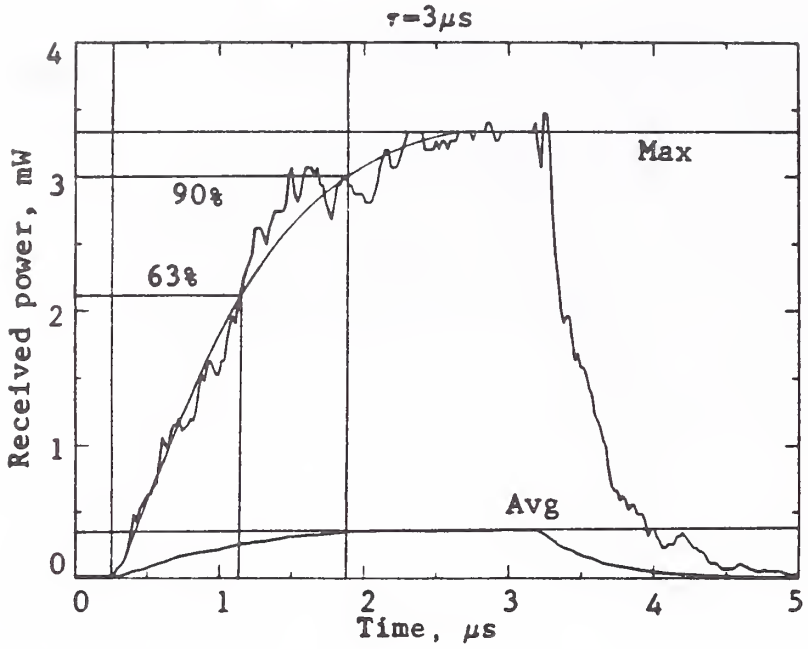

Using 1 piece of absorber.

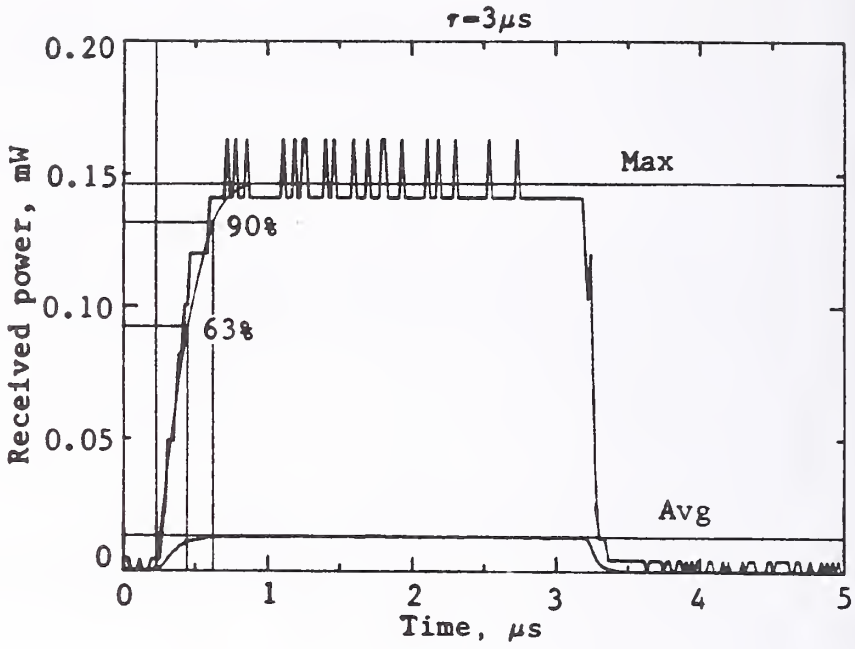

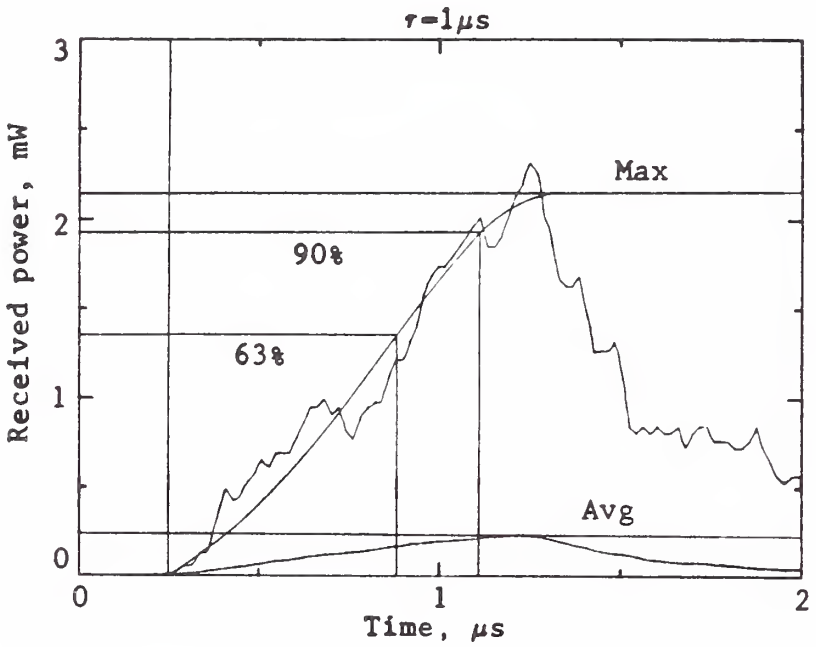

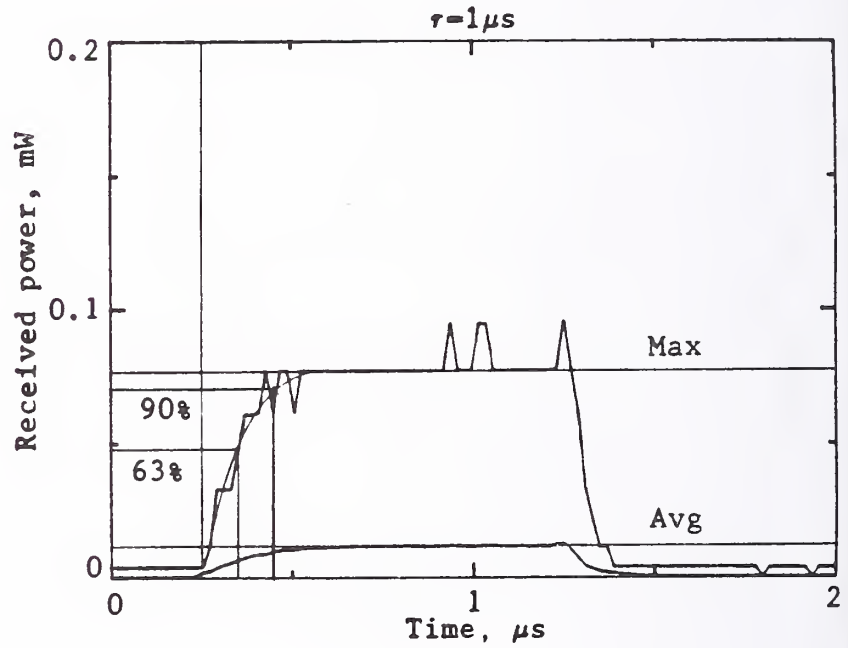

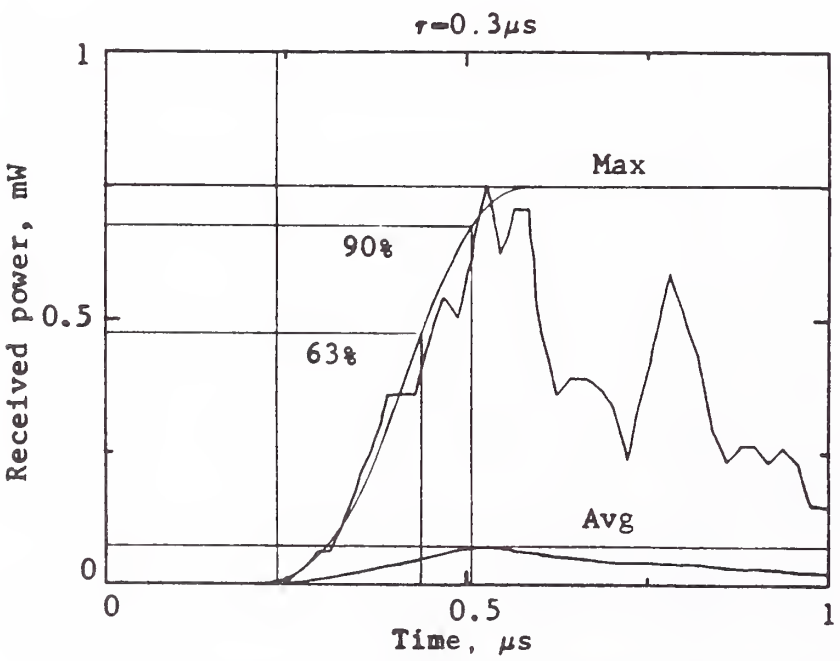

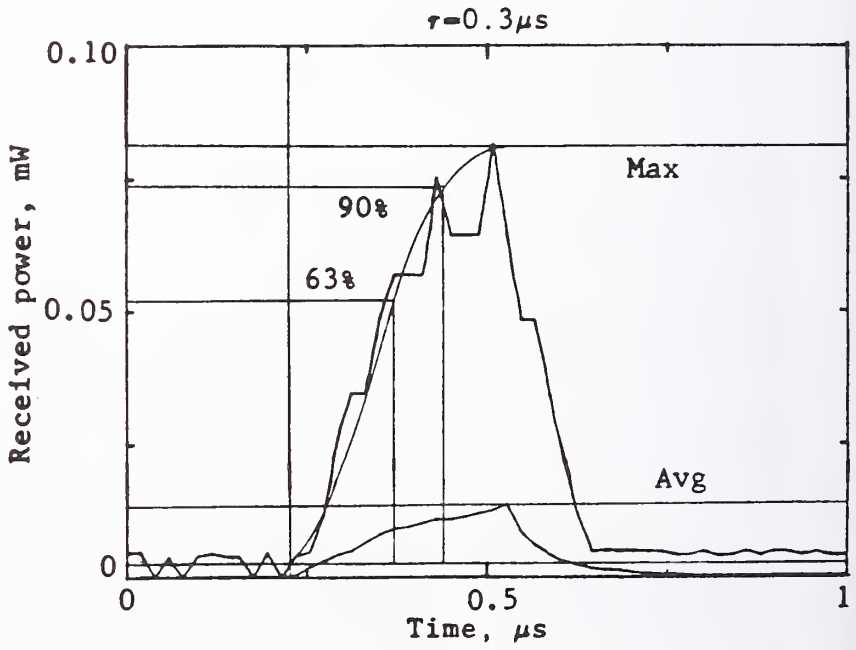

Figure 5.1(j) Maximum and average values of received rf pulse waveforms in the mode-tuned RADC small reverberating chamber using no rf absorber (chamber empty) and 1 piece of absorber; F = 18 GHz.

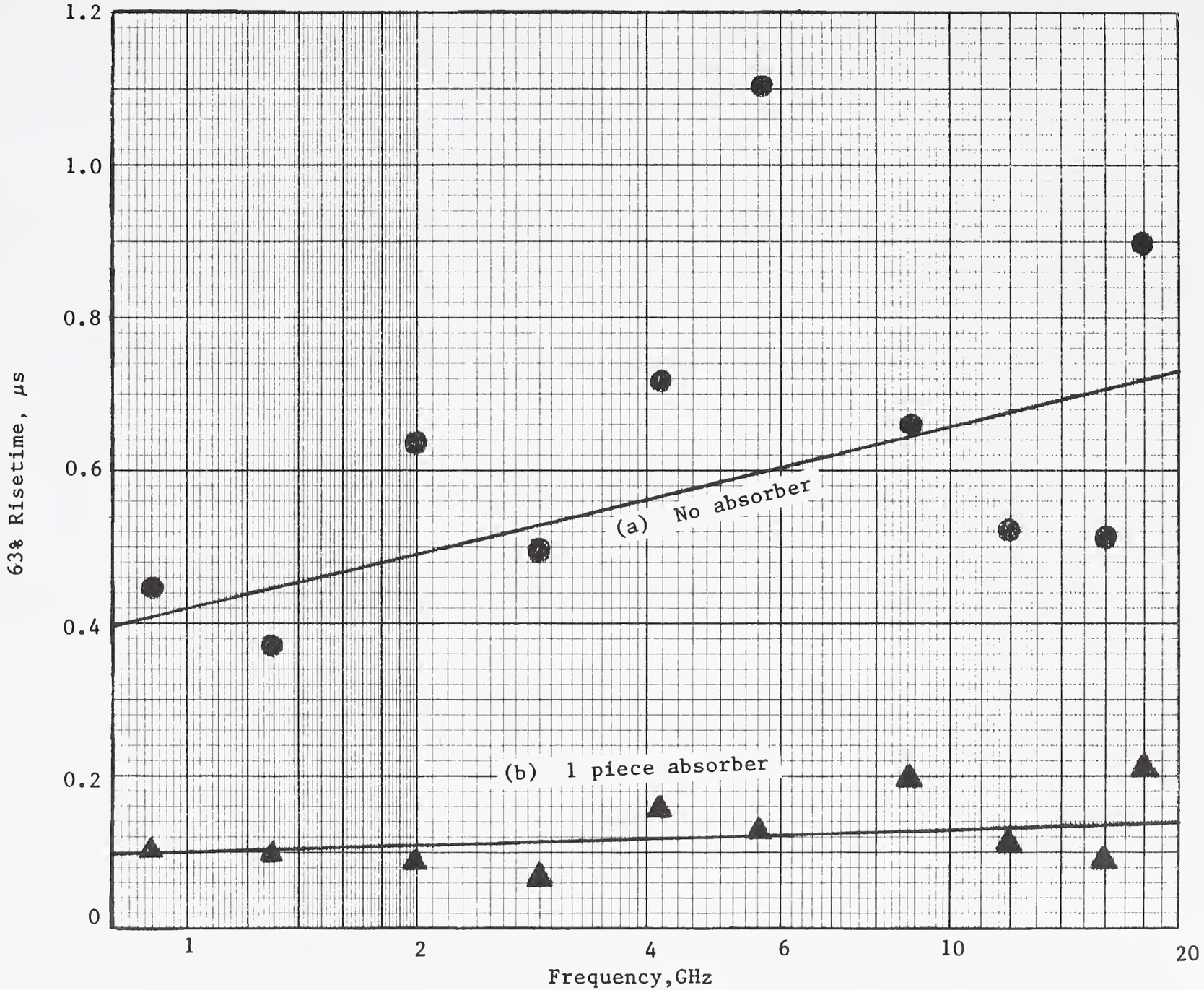

Figure 5.2 Graphs of data from figure 5.1 showing the time required for 3 μs rf pulses transmitted into the mode-tuned chamber to rise to 63 % of the steady state amplitude, using: (a) no absorber, and (b) 1 piece of 7.6 cm x 61 cm x 61 cm rf absorber.

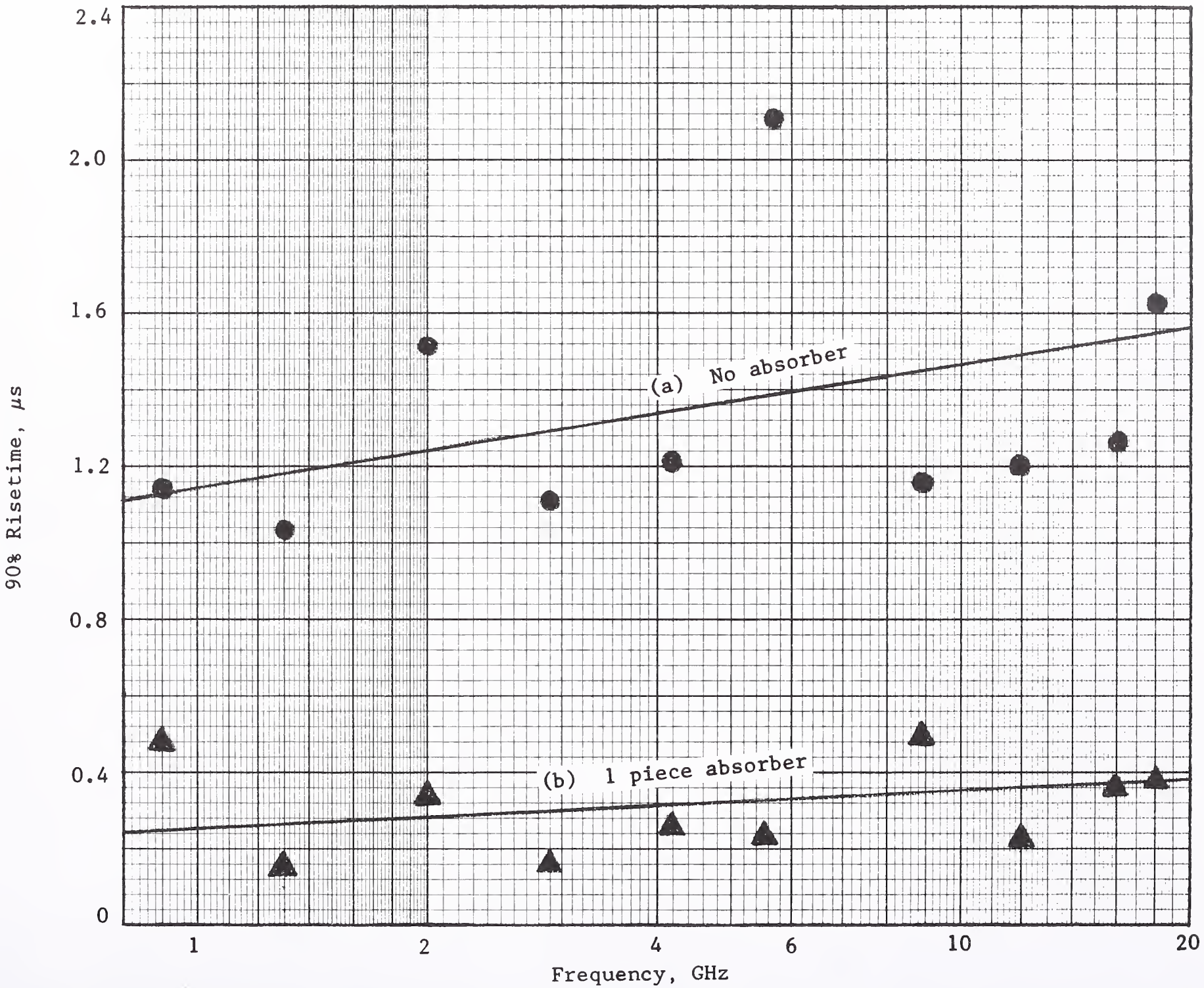

Figure 5.3 Graphs of data from figure 5.1 showing the time required for 3 μs rf pulses transmitted into the mode-tuned chamber to rise to 90 % of the steady state amplitude, using: (a) no absorber, and (b) 1 piece of 7.6 cm x 61 cm x 61 cm rf absorber.

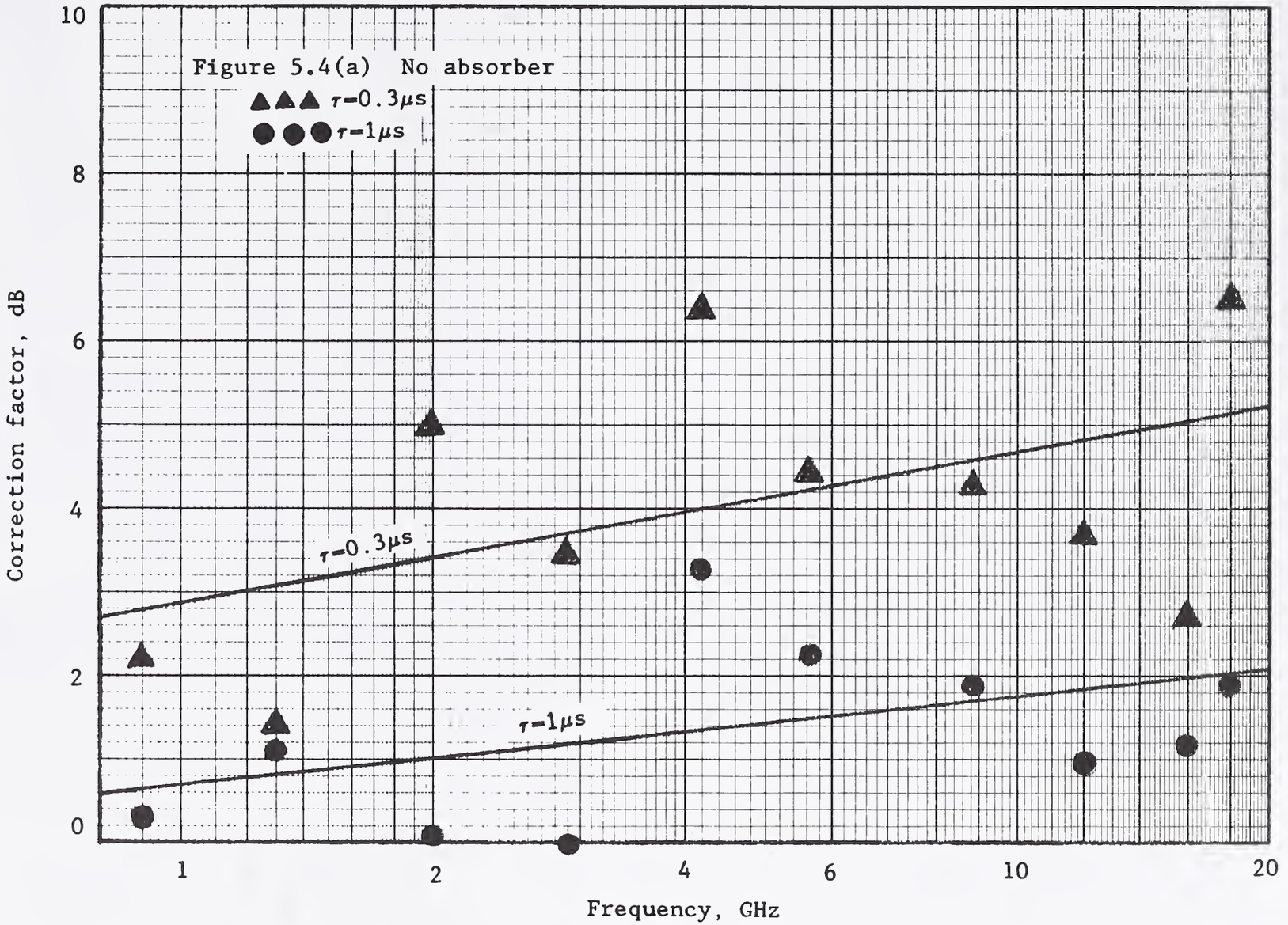

Figure 5.4(a) **Graphs of correction factors for response ammplitude of rf pulses in the mode-tuned chamber as a function of frequency, at selected pulse duration, using: (a) no absorber, and (b) 1 piece of 7.6 cm x 61 cm x 61 cm rf absorber.**

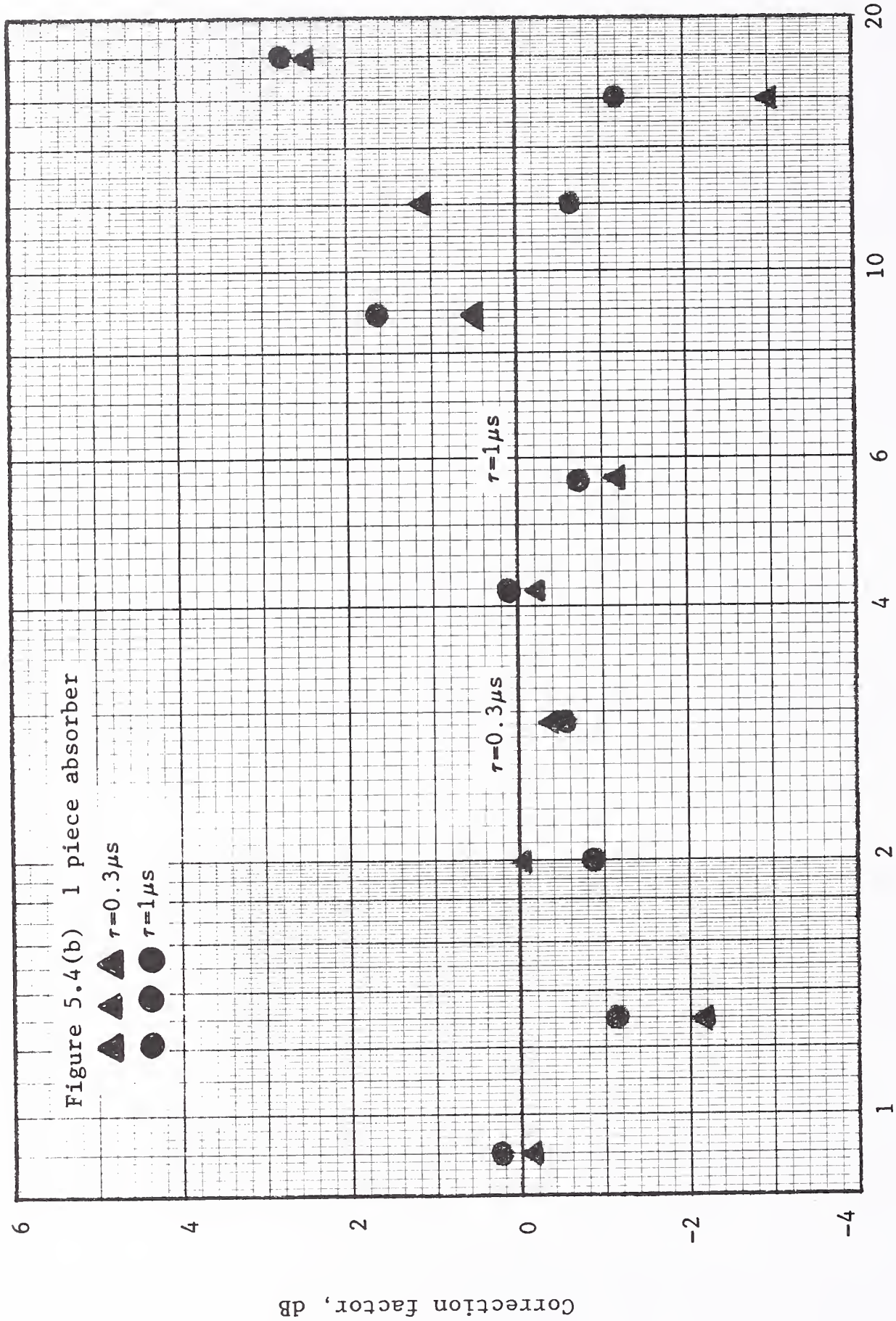

Figure 5.4(b) Graphs of correction factors for response ammplitude of rf pulses in the mode-tuned chamber as a function of frequency, at selected pulse duration, using: (a) no absorber, and (b) 1 piece of 7.6 cm x 61 cm x 61 cm rf absorber.

F = 0.9 GHz, using 10 dB pad

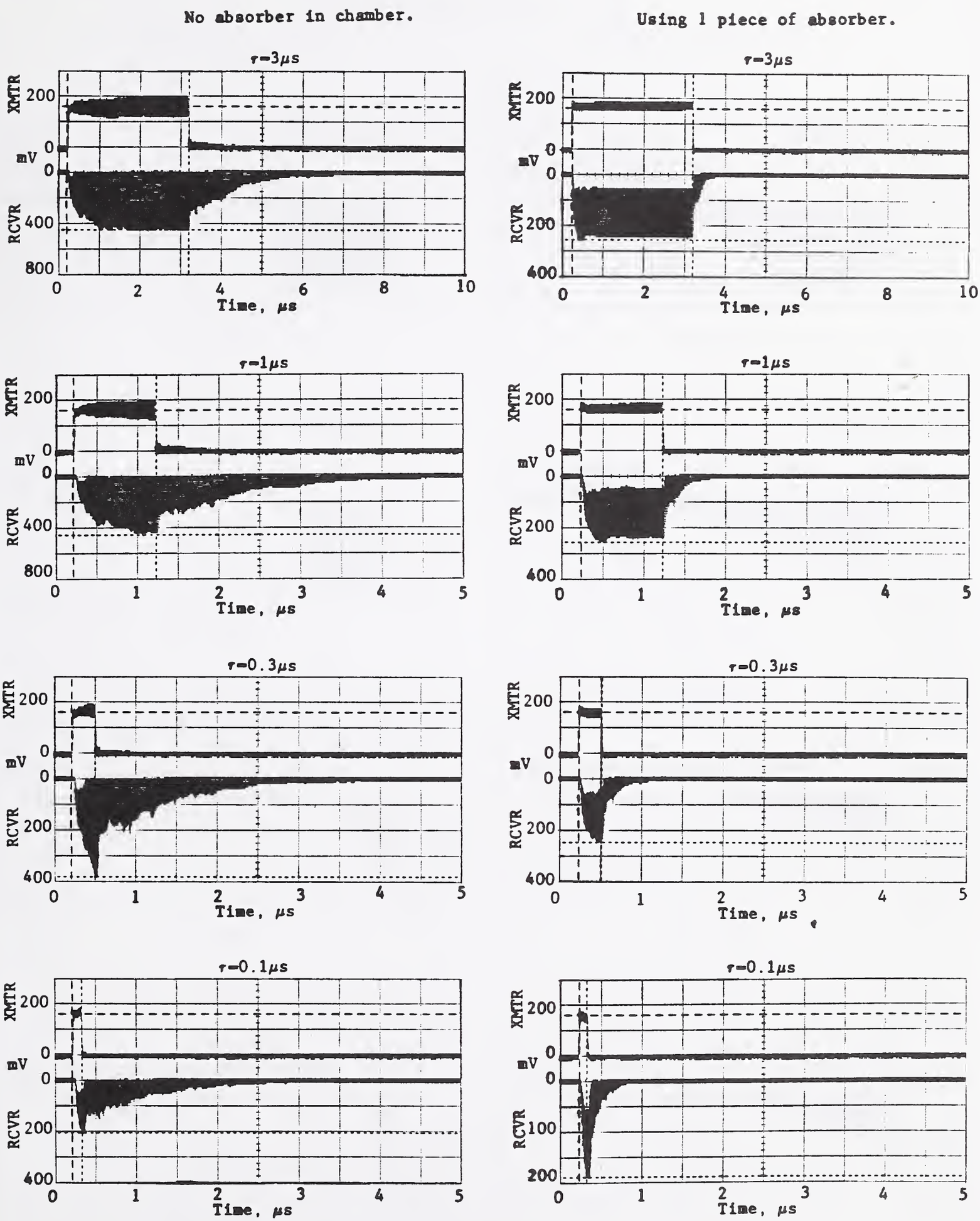

Figure 5.5(a) Maximum values of received rf pulse waveforms in the mode-stirred RADC small reverberating chamber using no rf absorber (chamber empty) and 1 piece of absorber; F = 0.9 GHz.

F = 1.3 GHz, using 10 dB pad

No absorber in chamber.

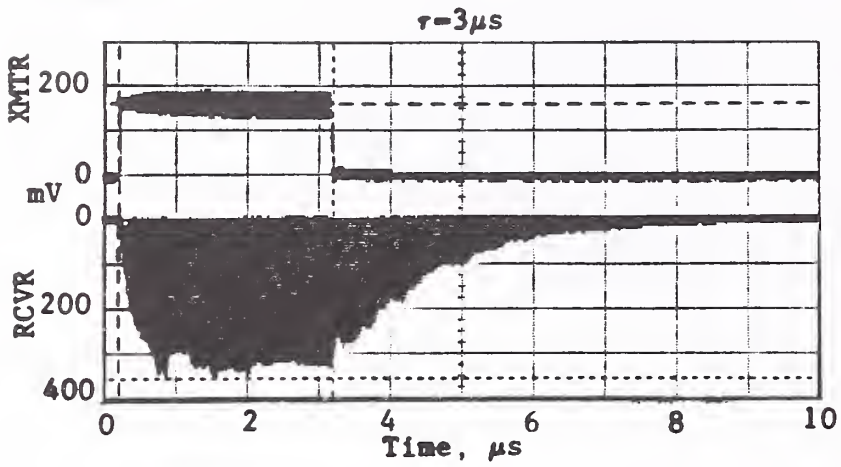

Using 1 piece of absorber.

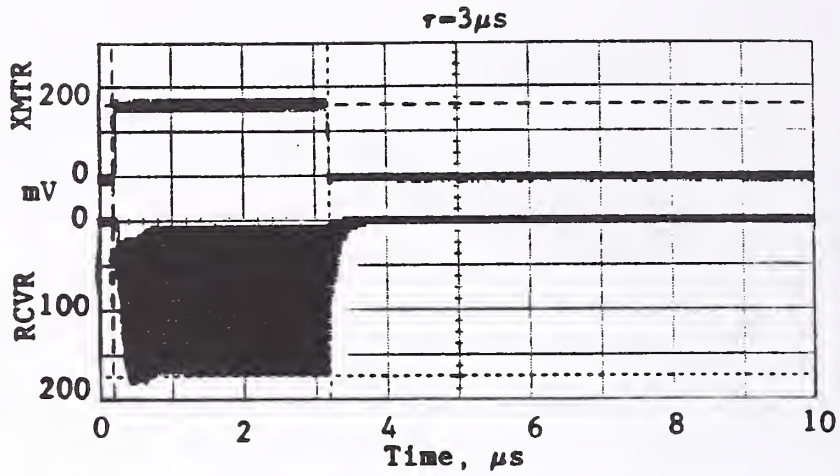

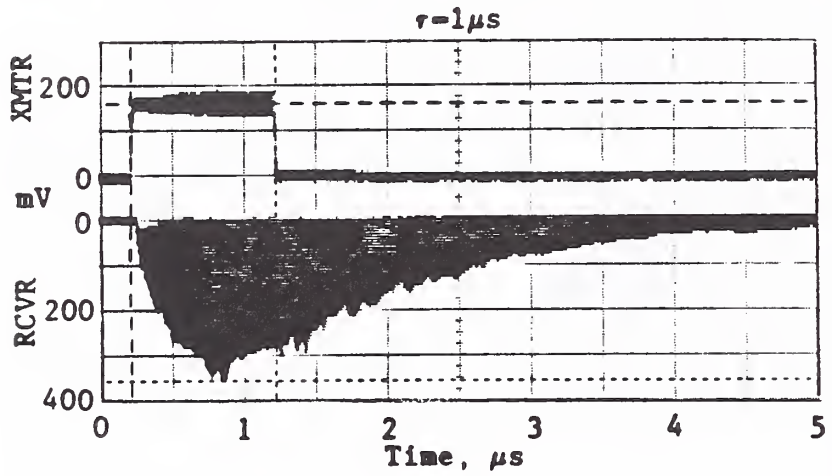

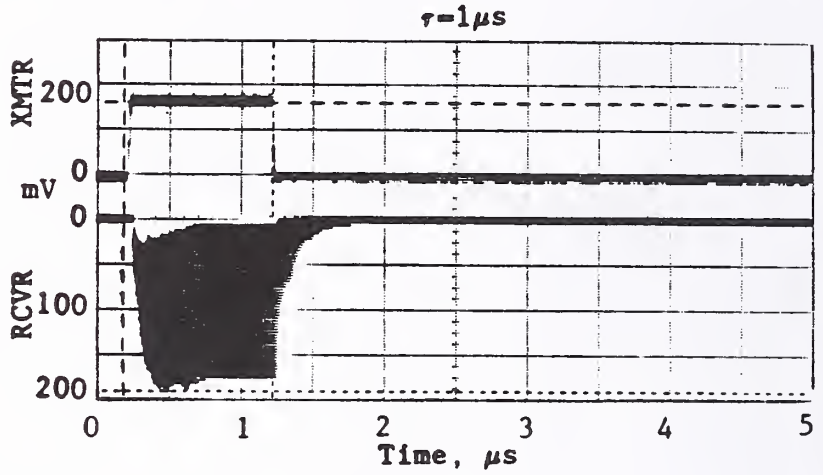

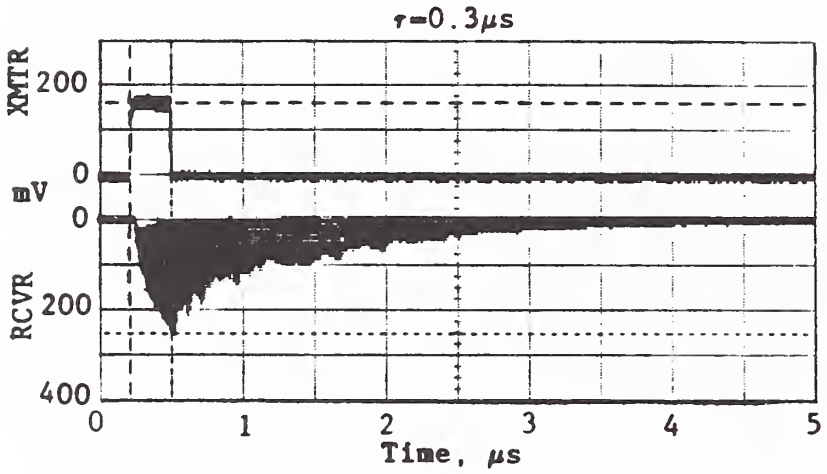

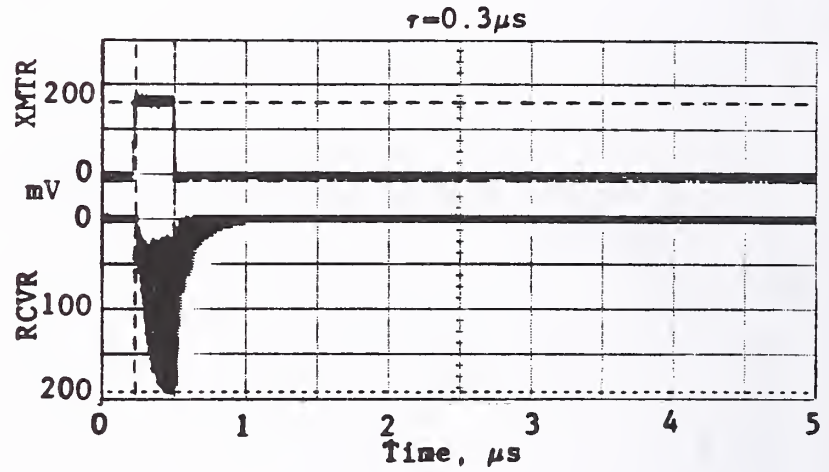

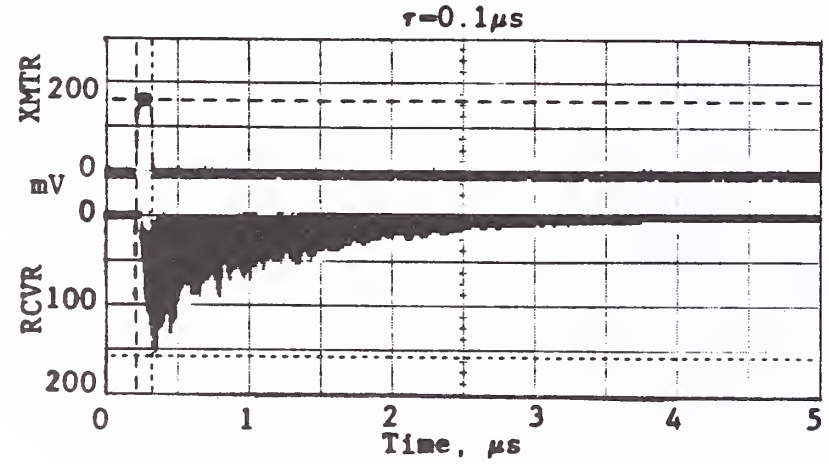

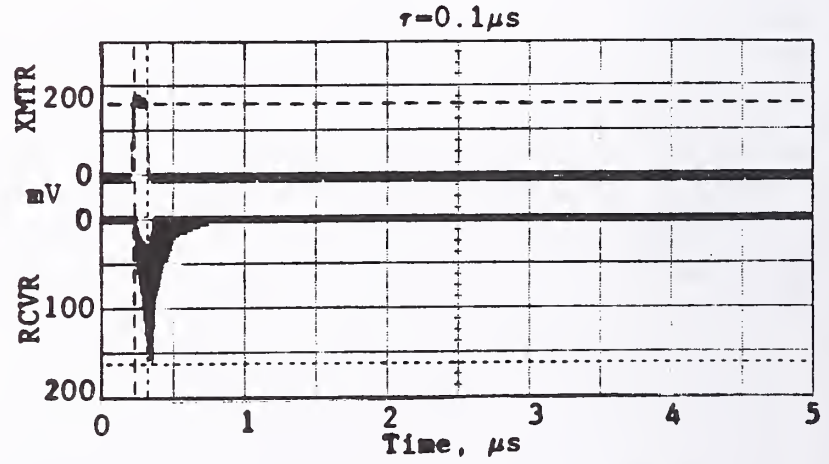

Figure 5.5(b) Maximum values of received rf pulse waveforms in the mode-stirred RADC small reverberating chamber using no rf absorber (chamber empty) and 1 piece of absorber; F = 1.3 GHz.

F = 2.0 GHz, using 10 dB pad

No absorber in chamber. **Using 1 piece of absorber.**

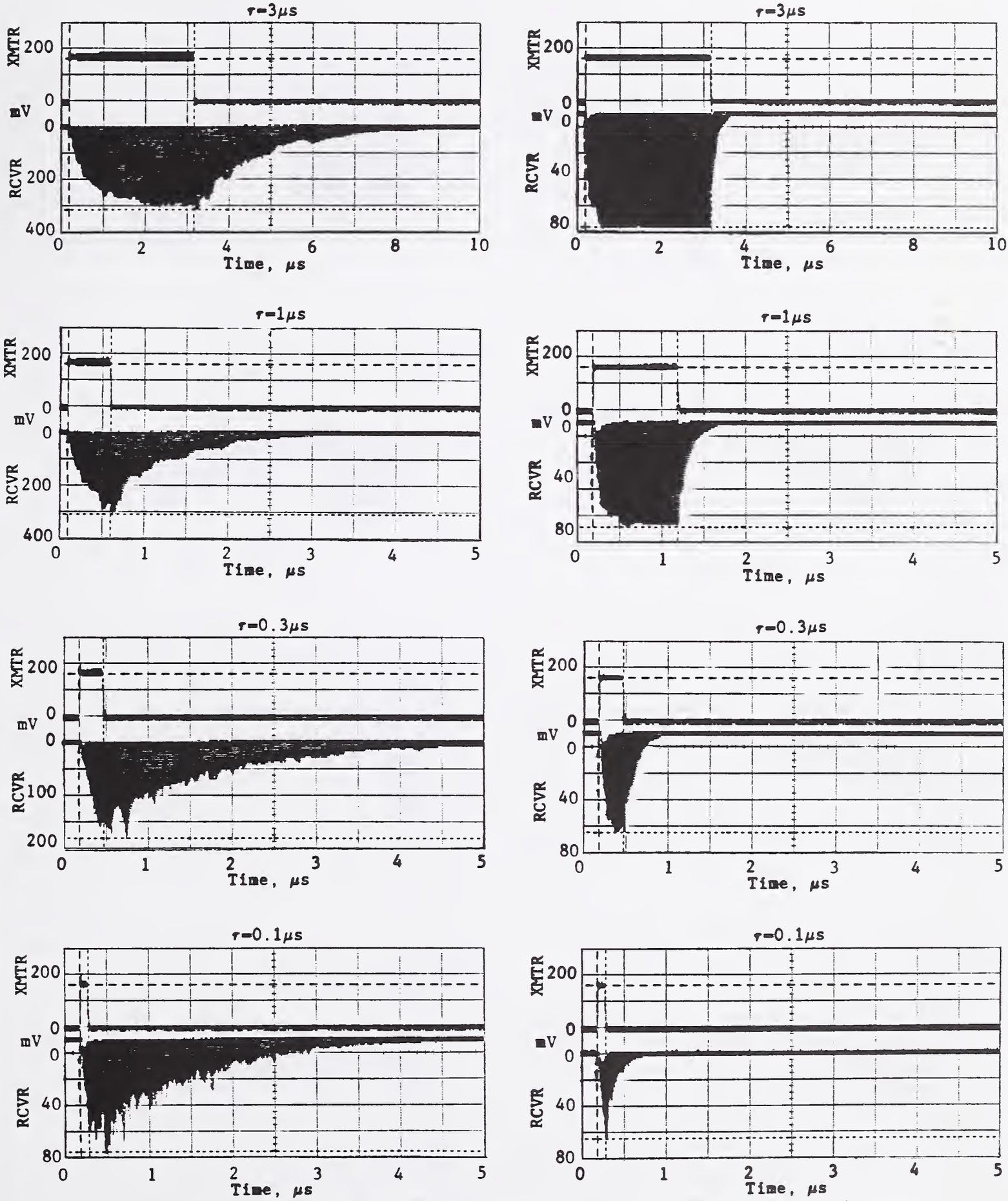

Figure 5.5(c) Maximum values of received rf pulse waveforms in the mode-stirred RADC small reverberating chamber using no rf absorber (chamber empty) and 1 piece of absorber; F = 2.0 GHz.

F = 2.9 GHz, using 10 dB pad

No absorber in chamber. **Using 1 piece of absorber.**

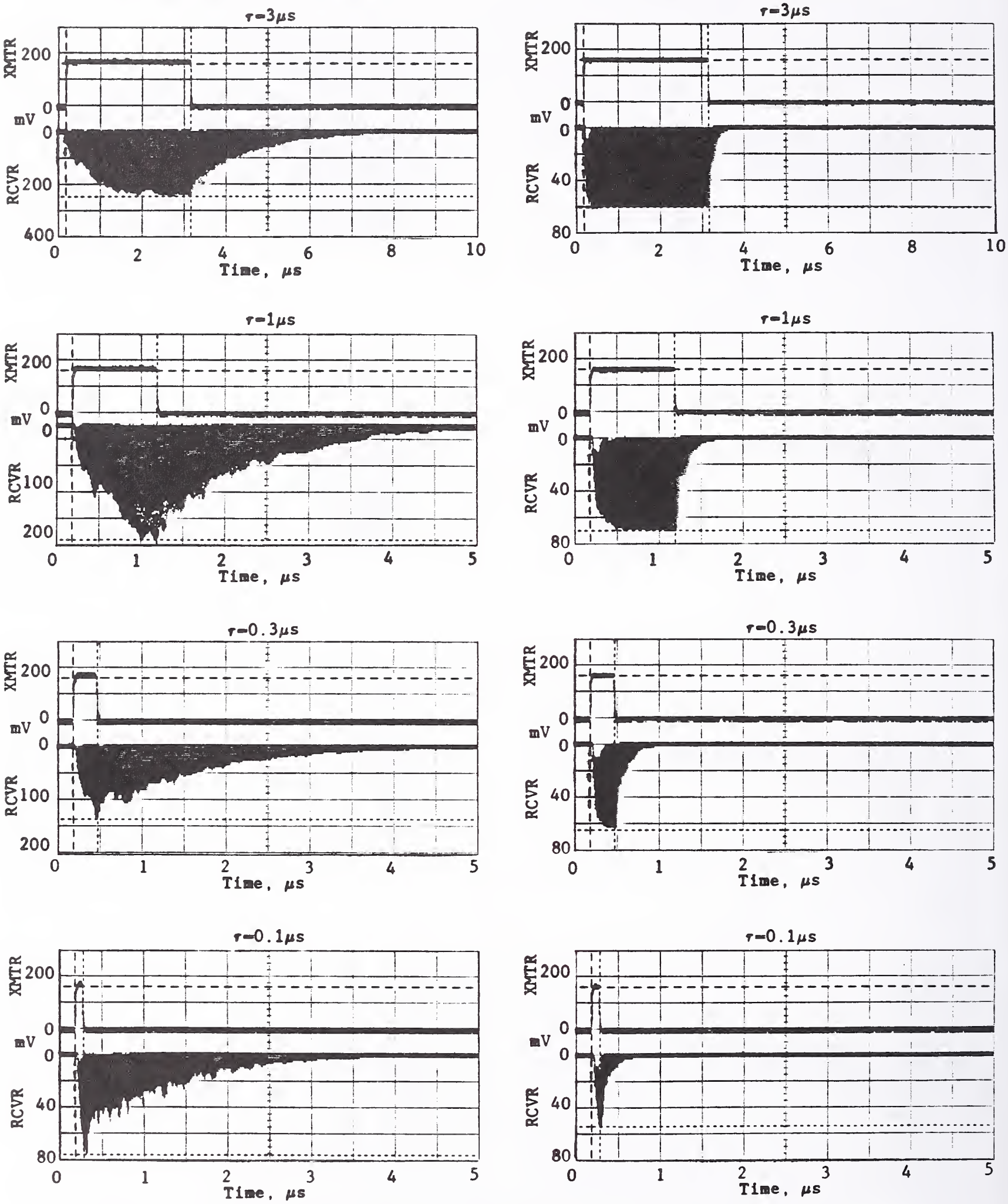

Figure 5.5(d) Maximum values of received rf pulse waveforms in the mode-stirred RADC small reverberating chamber using no rf absorber (chamber empty) and 1 piece of absorber; F = 2.9 GHz.

F = 4.2 GHz, using 10 dB pad

No absorber in chamber. **Using 1 piece of absorber.**

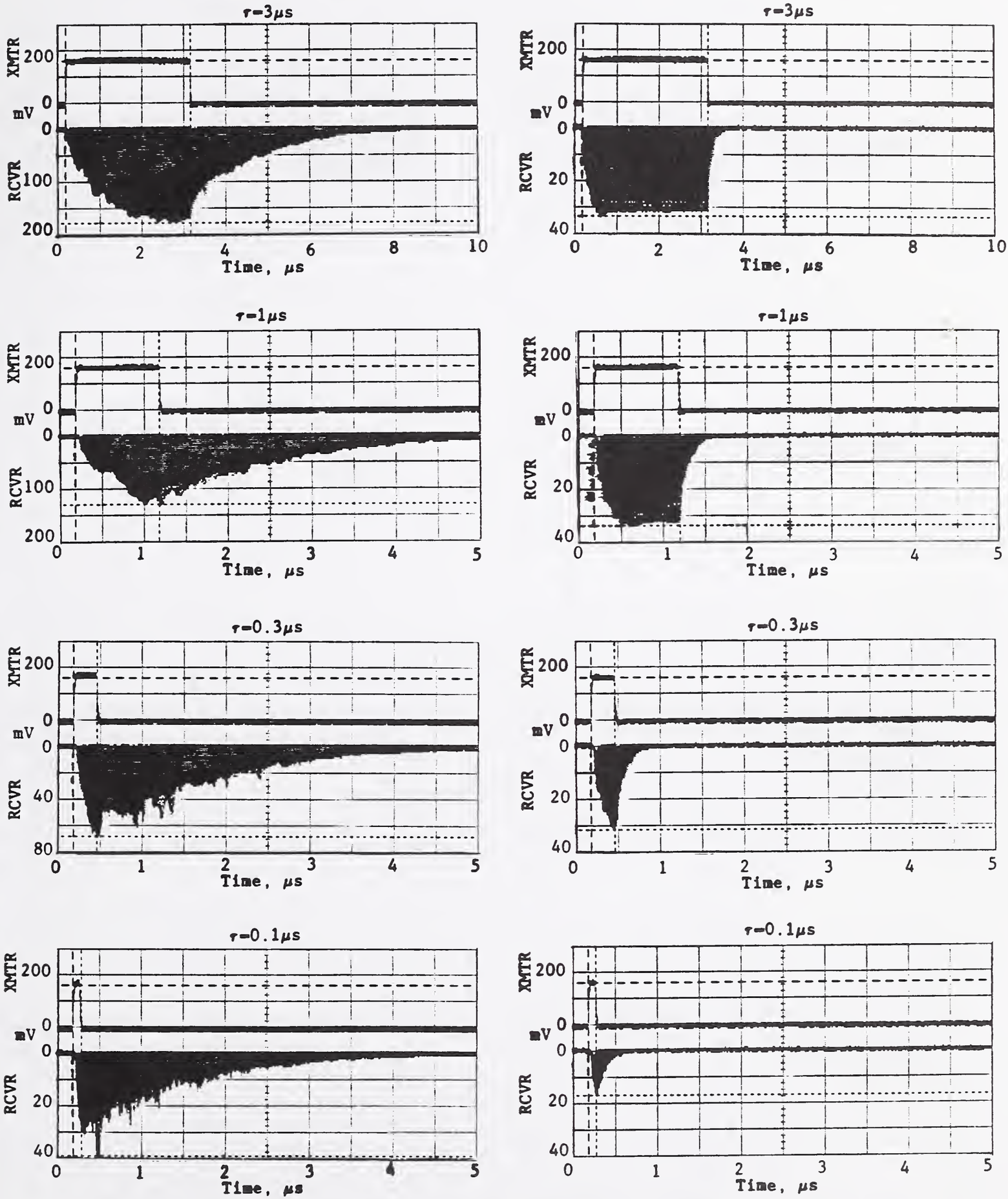

Figure 5.5(e) Maximum values of received rf pulse waveforms in the mode-stirred RADC small reverberating chamber using no rf absorber (chamber empty) and 1 piece of absorber; F = 4.2 GHz.

F = 5.65 GHz, using 10 dB pad

No absorber in chamber. **Using 1 piece of absorber.**

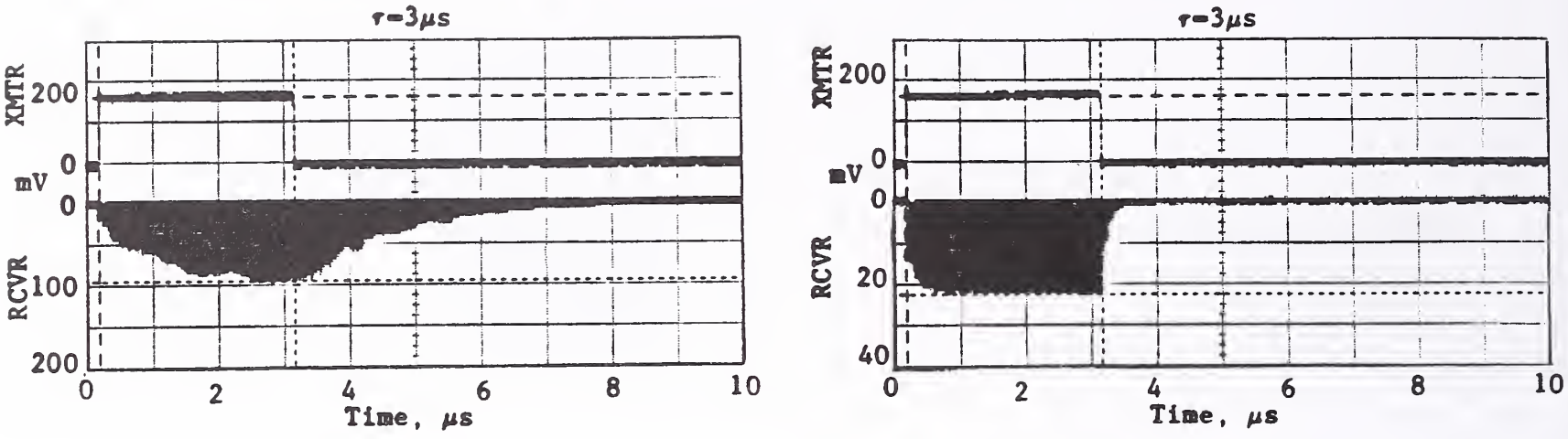

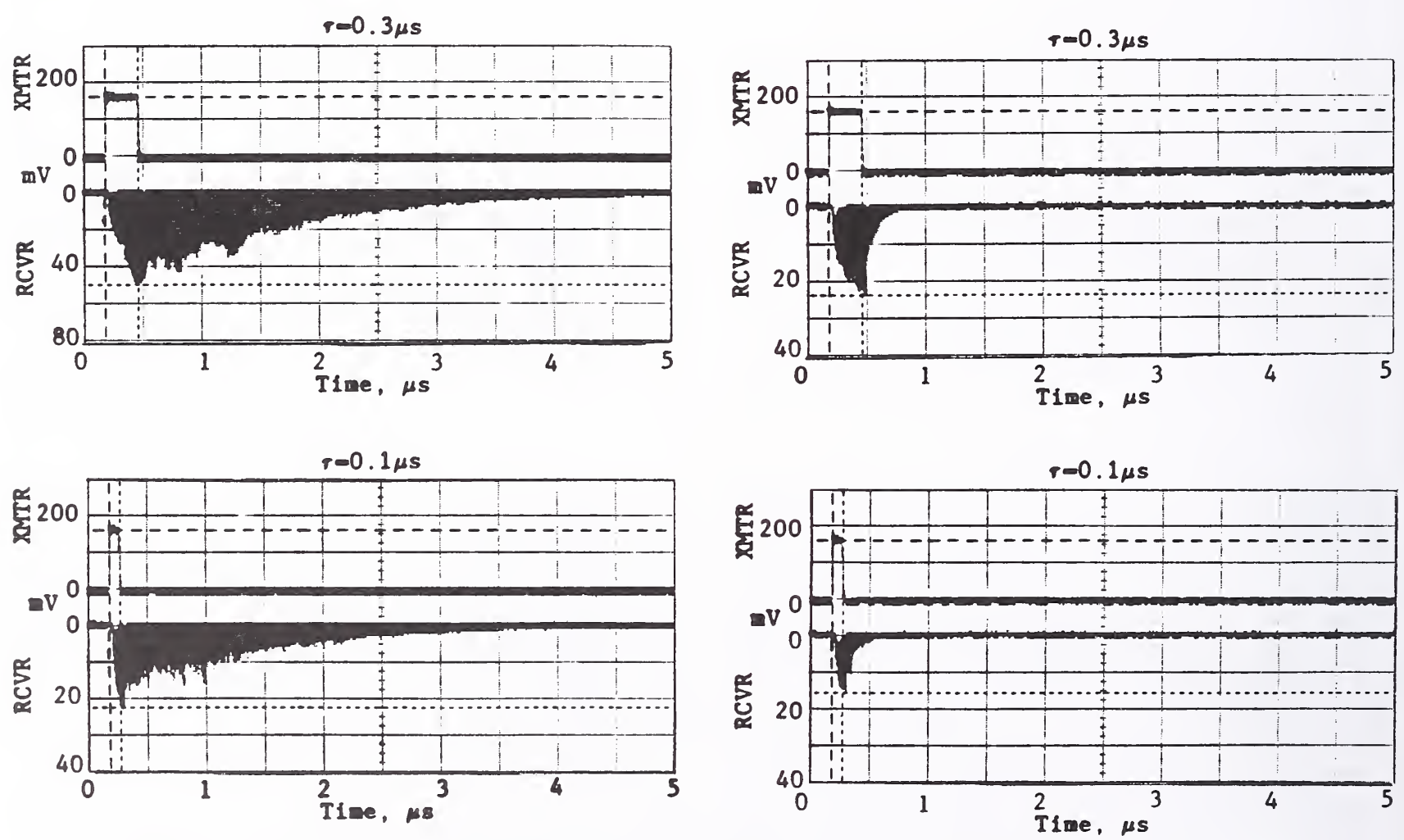

Figure 5.5(f) Maximum values of received rf pulse waveforms in the mode-stirred RADC small reverberating chamber using no rf absorber (chamber empty) and 1 piece of absorber; F = 5.65 GHz.

F = 8.9 GHz, using 3 dB pad

No absorber in chamber.

Using 1 piece of absorber.

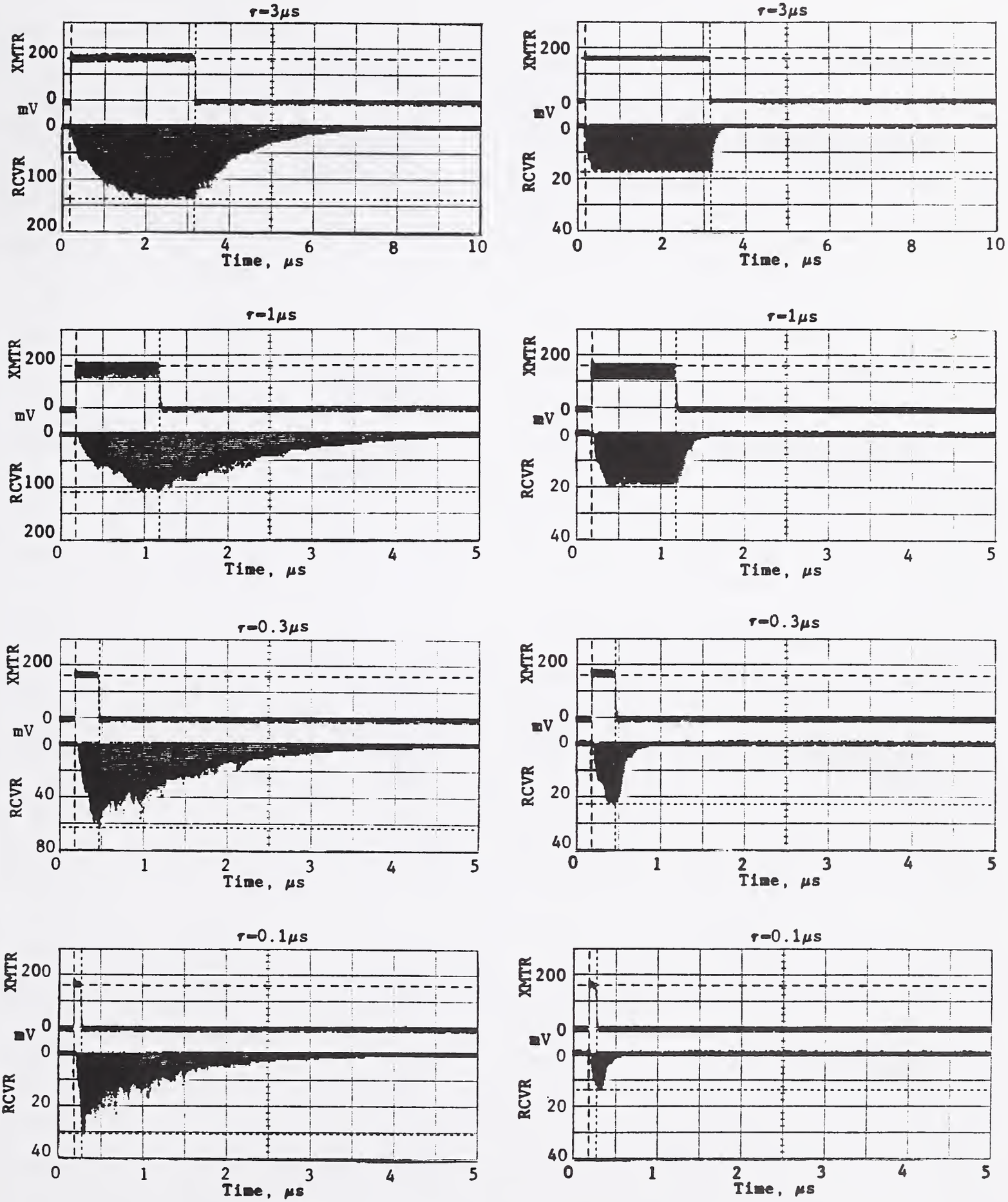

Figure 5.5(g) Maximum values of received rf pulse waveforms in the mode-stirred RADC small reverberating chamber using no rf absorber (chamber empty) and 1 piece of absorber; F = 8.9 GHz.

F = 12 GHz, using 3 dB pad

No absorber in chamber. **Using 1 piece of absorber.**

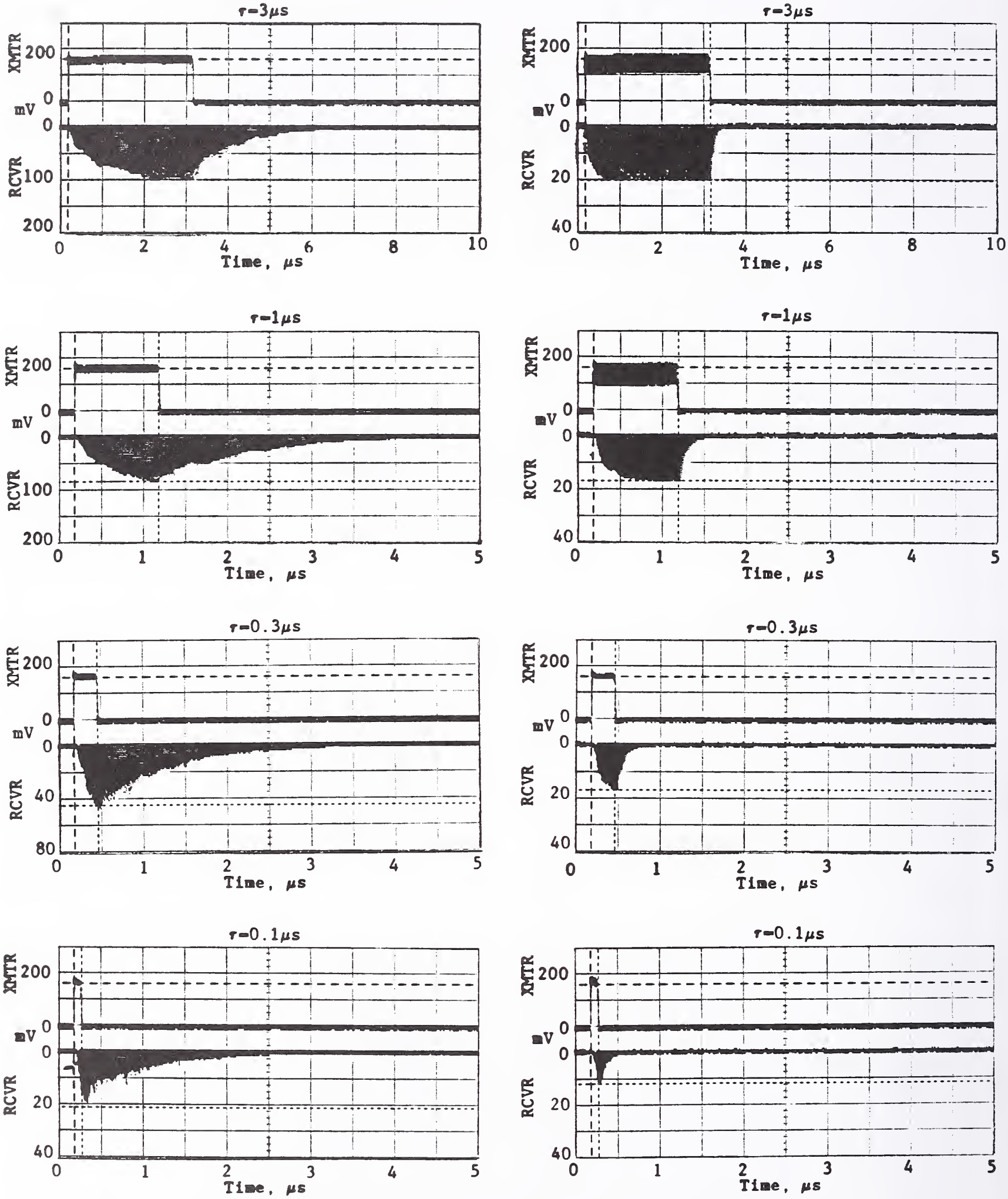

Figure 5.5(h) Maximum values of received rf pulse waveforms in the mode-stirred RADC small reverberating chamber using no rf absorber (chamber empty) and 1 piece of absorber; F = 12 GHz.

F = 16 GHz

No absorber in chamber.

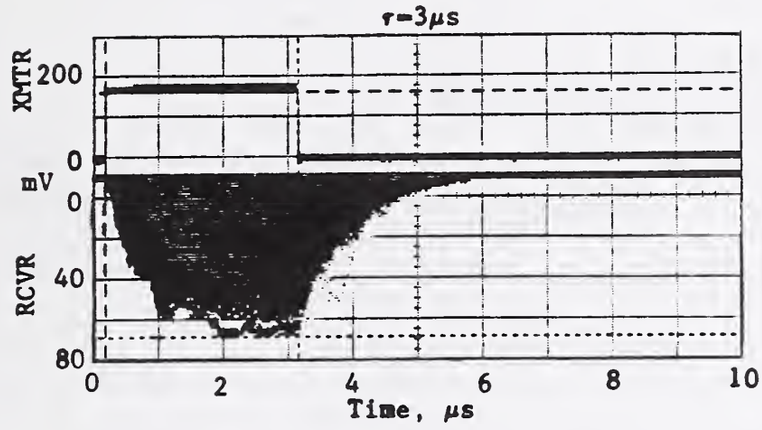

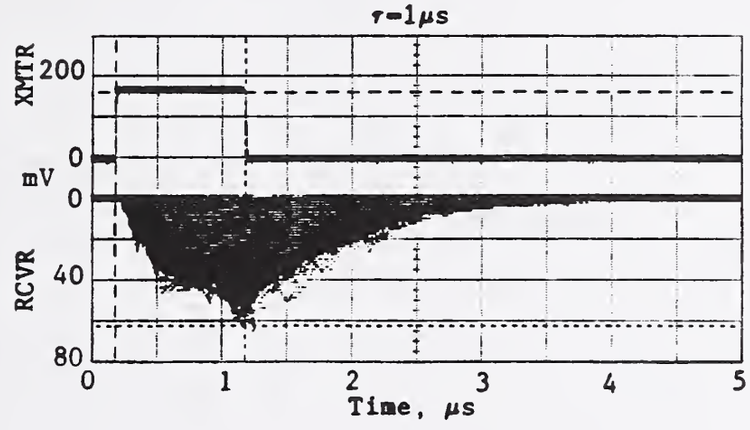

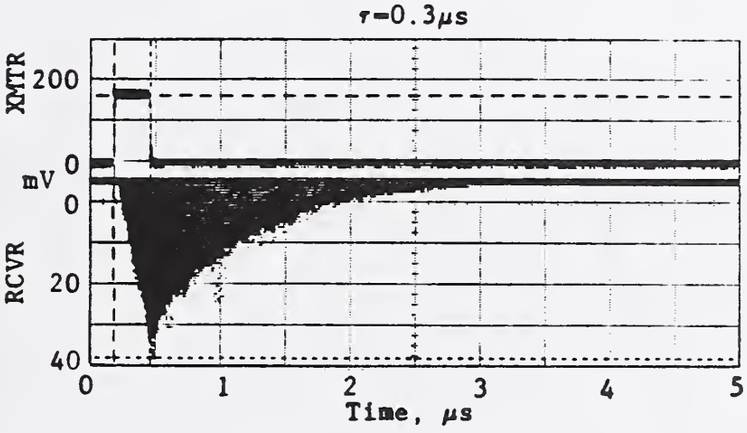

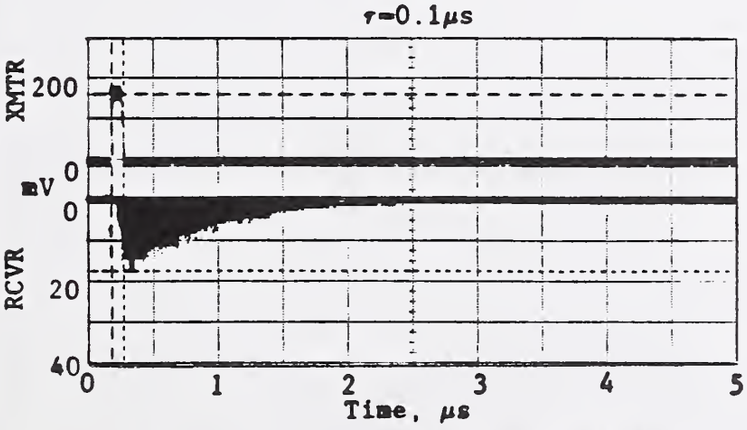

Using 1 piece of absorber.

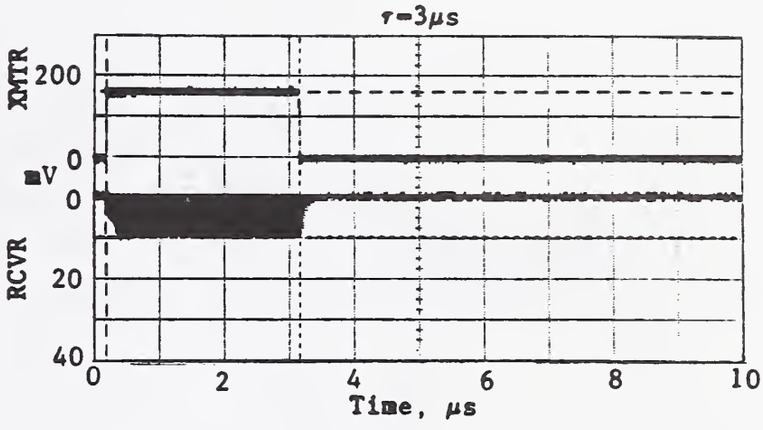

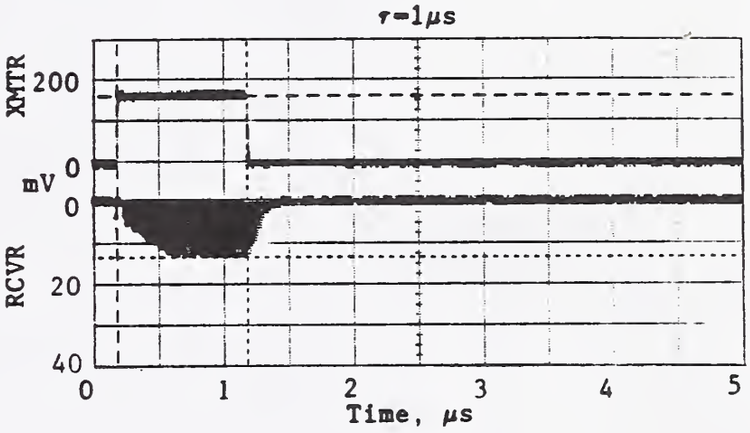

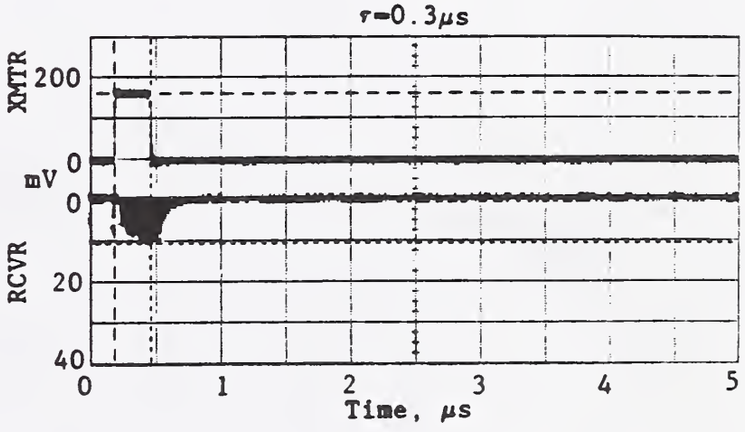

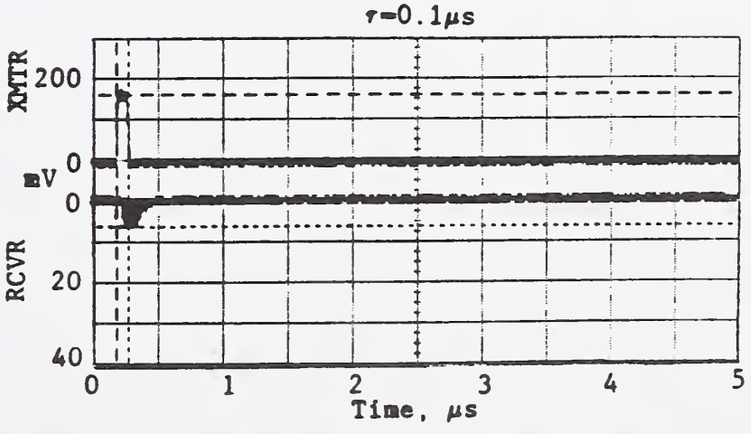

Figure 5.5(i) Maximum values of received rf pulse waveforms in the mode-stirred RADC small reverberating chamber using no rf absorber (chamber empty) and 1 piece of absorber; F = 16 GHz.

F = 18 GHz

No absorber in chamber.

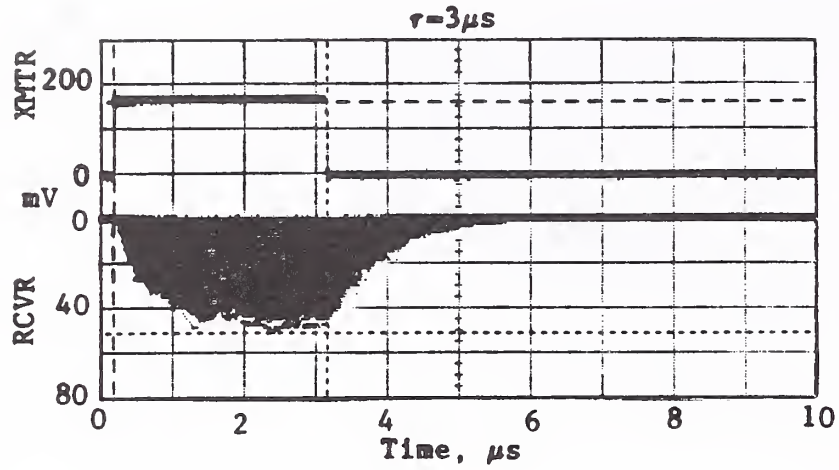

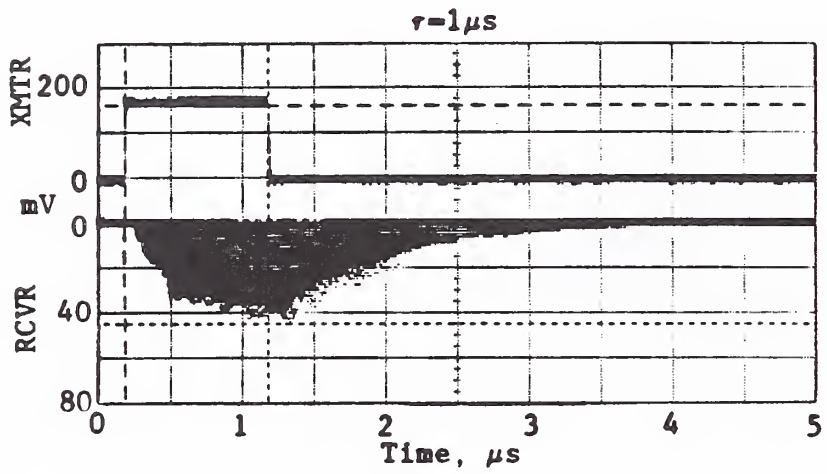

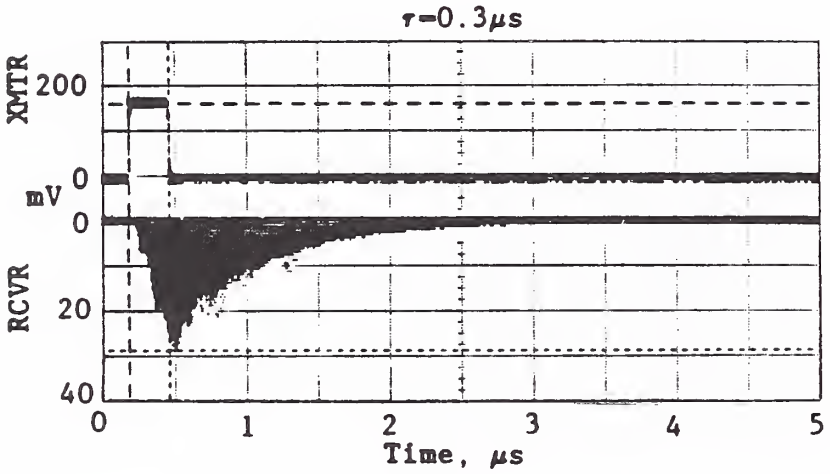

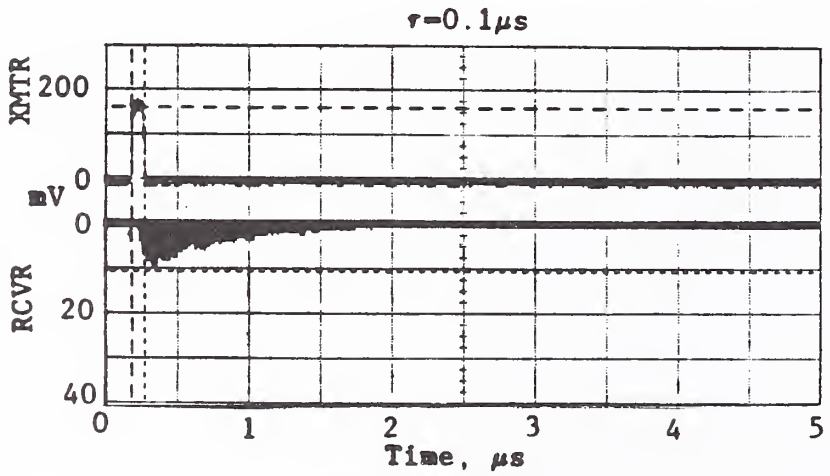

Using 1 piece of absorber.

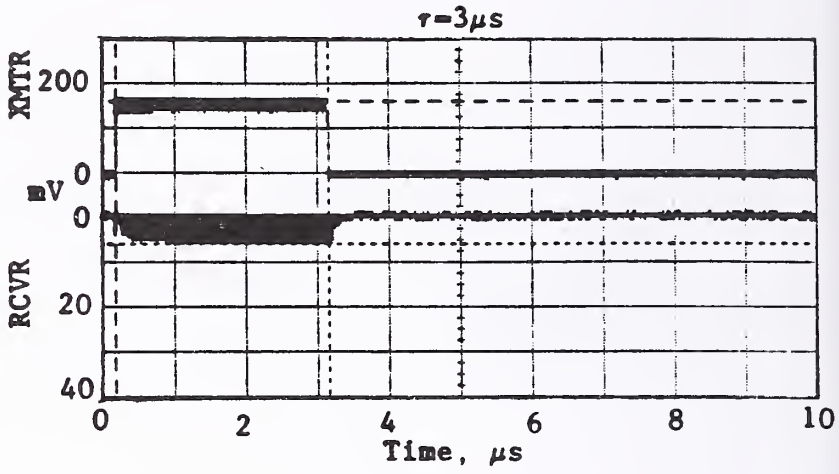

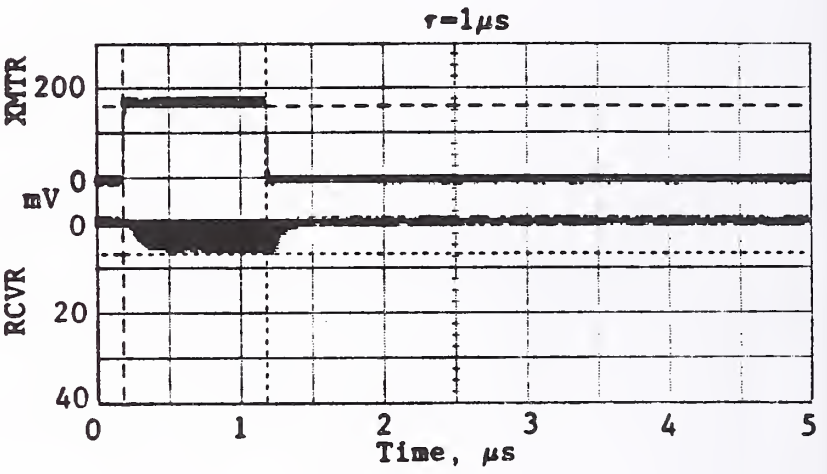

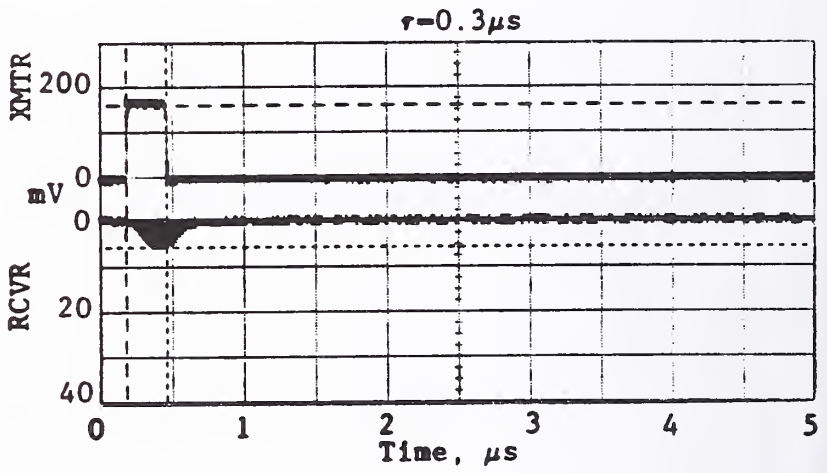

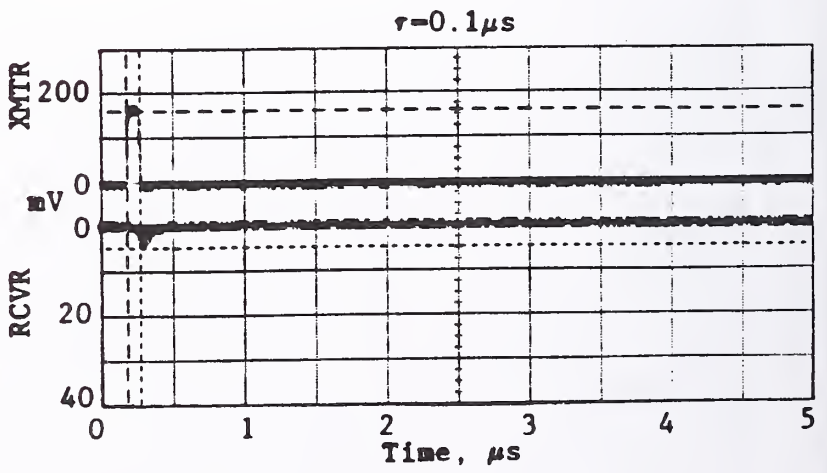

Figure 5.5(j) Maximum values of received rf pulse waveforms in the mode-stirred RADC small reverberating chamber using no rf absorber (chamber empty) and 1 piece of absorber; F = 18 GHz.

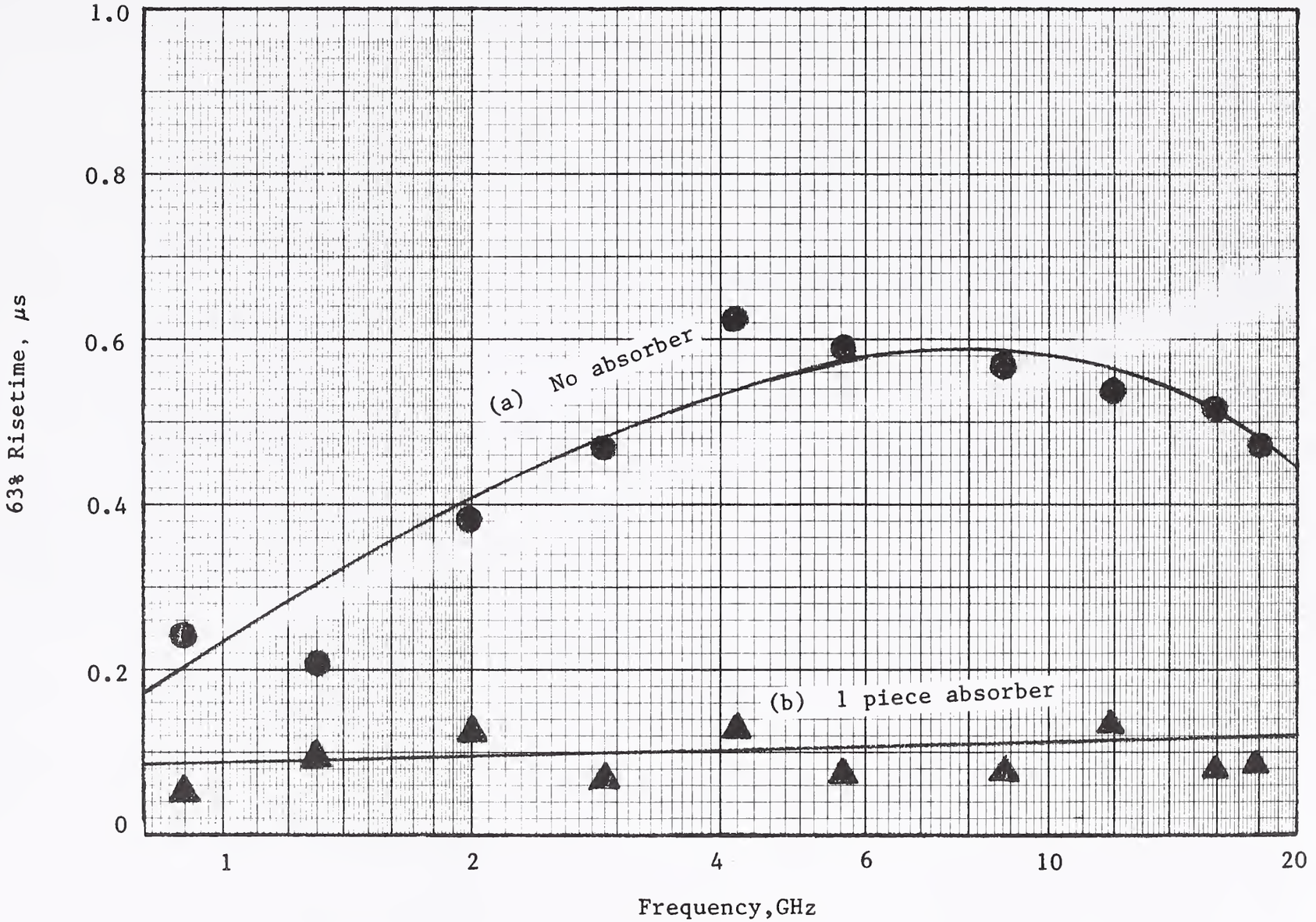

Figure 5.6 Graphs of data from figure 5.5 showing the time required for 3 μs rf pulses transmitted into the mode-stirred chamber to rise to 63 % of the steady state amplitude, using: (a) no absorber, and (b) 1 piece of 7.6 cm x 61 cm x 61 cm rf absorber.

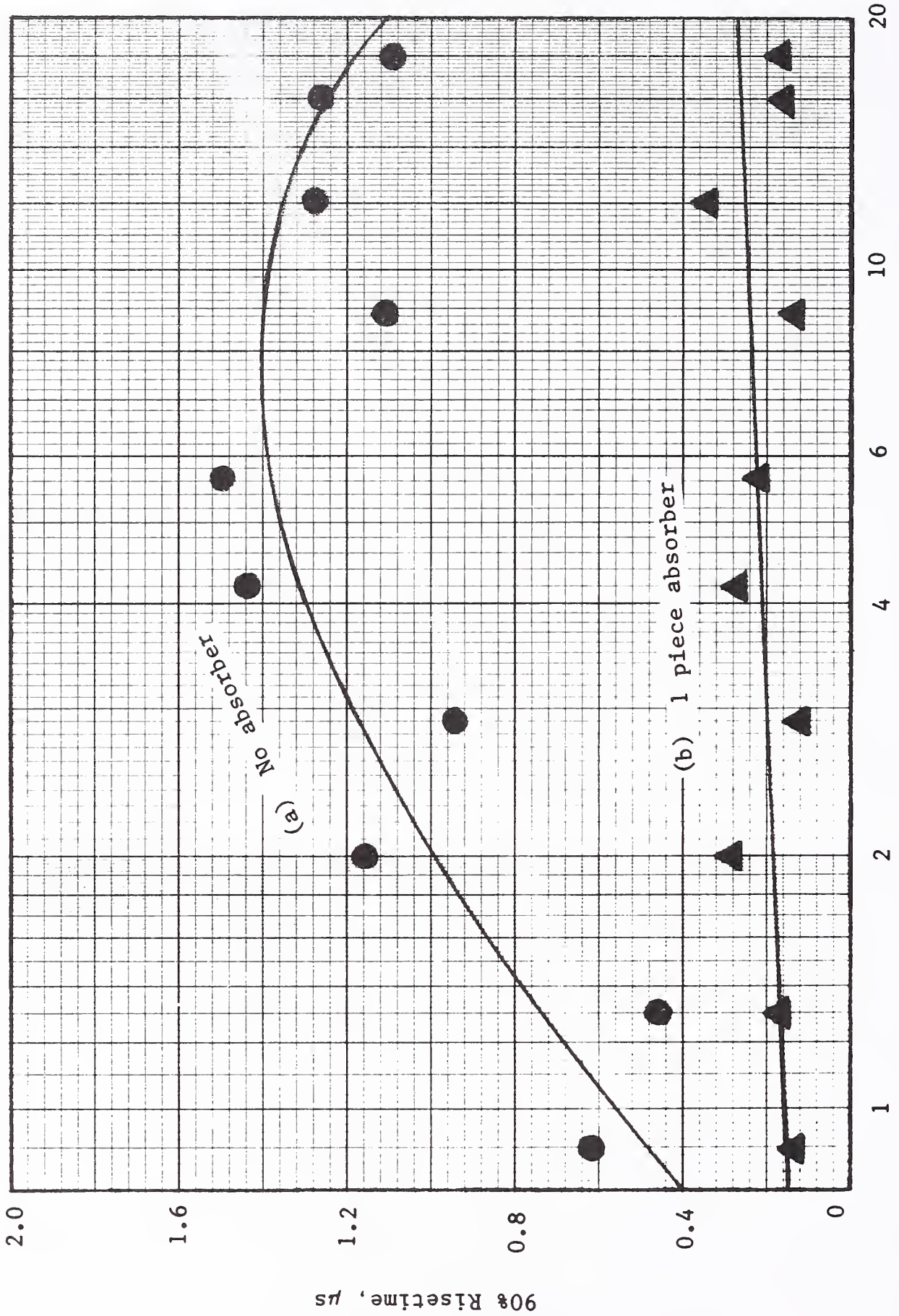

Figure 5.7 Graphs of data from figure 5.5 showing the time required for 3 μs rf pulses transmitted into the mode-stirred chamber to rise to 90 % of the steady state amplitude, using: (a) no absorber, and (b) 1 piece of 7.6 cm x 61 cm x 61 cm rf absorber.

Figure 5.8(a) No absorber

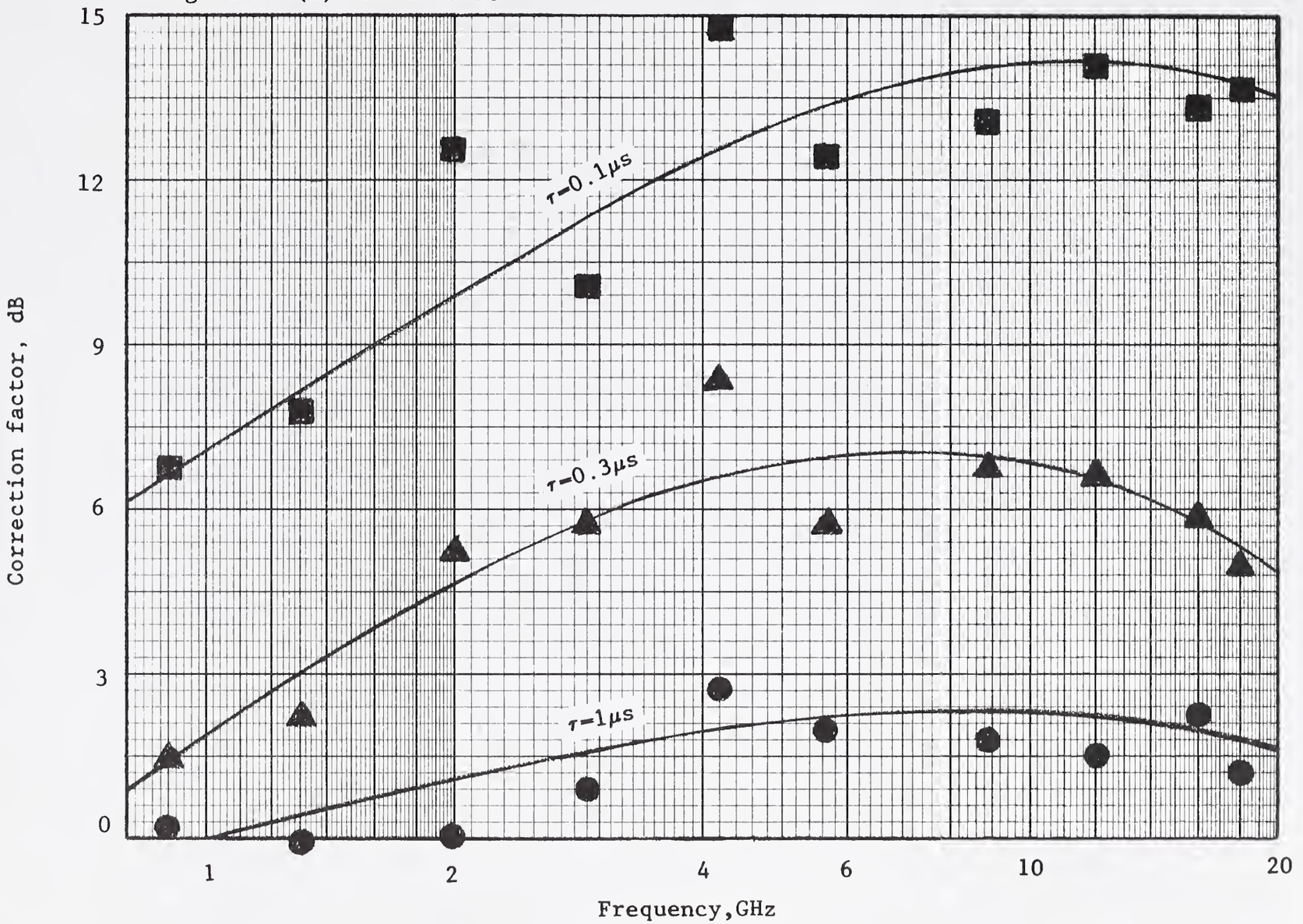

Figure 5.8(a) **Graphs of correction factors for response amplitude of rf pulses in the mode-stirred chamber as a function of frequency, at selected pulse durations, using: (a) no absorber, and (b) 1 piece of 7.6 cm x 61 cm x 61 cm rf absorber.**

Figure 5.8(b) 1 piece absorber

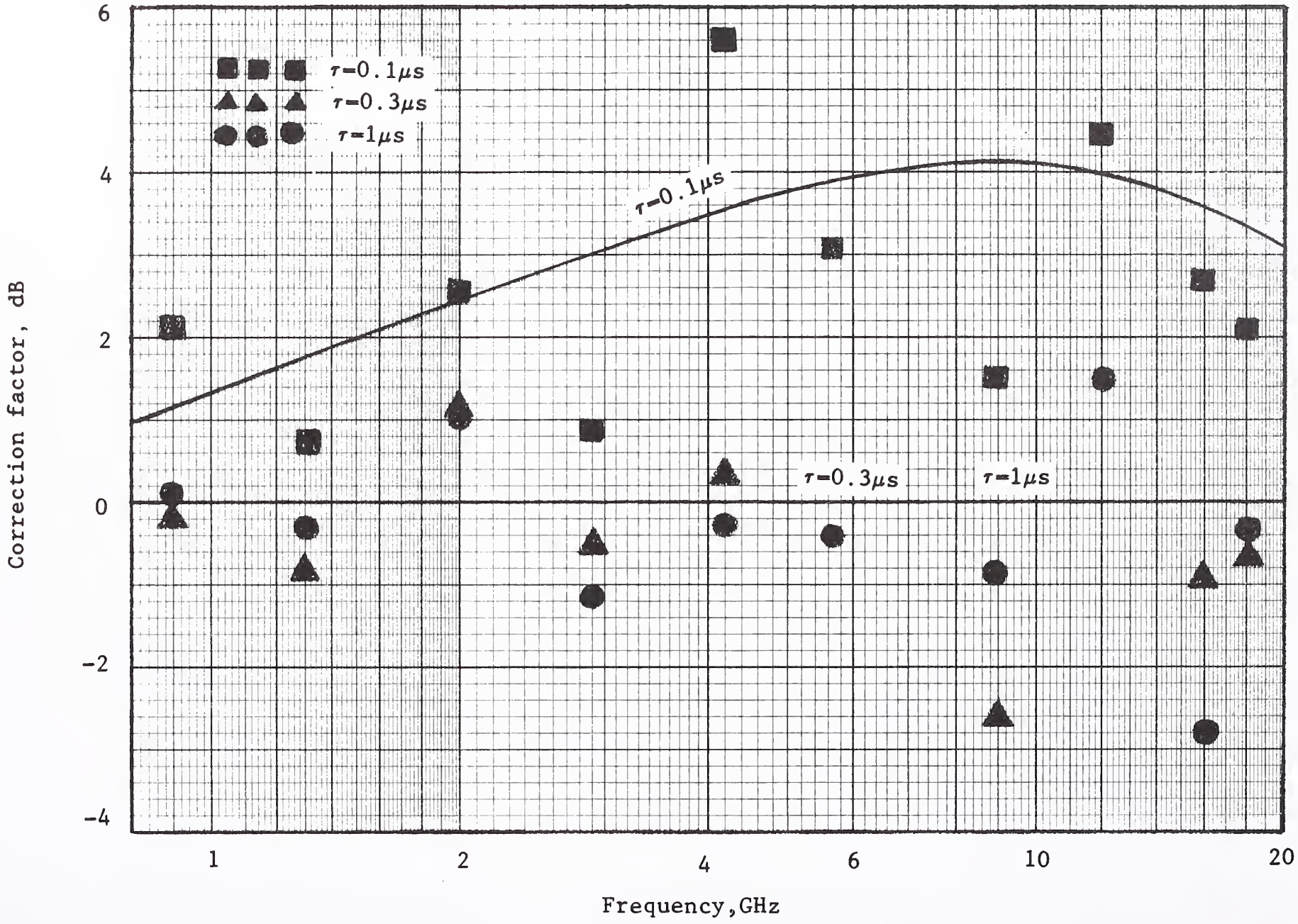

Figure 5.8(b) Graphs of correction factors for response amplitude of rf pulses in the mode-stirred chamber as a function of frequency, at selected pulse durations, using: (a) no absorber, and (b) 1 piece of 7.6 cm x 61 cm x 61 cm rf absorber.

Table 3.1. **Spatial variation of the cw E-field average and maximum values measured in the RADC small reverberating chamber.**

Frequency (GHz)	Variation in E-field (dB)
500	< ± 7.0
1000	< ± 5.0
1500	< ± 4.0
2000	< ± 3.0

Table 4.1. Summary of estimated uncertainties for determining the cw field strength inside the mode-tuned RADC small reverberating chamber (0.5 to 2.0 GHz).

Source of Error	Error (dB) 0.5 GHz Ave.	0.5 GHz Max.	1.0 GHz Ave.	1.0 GHz Max.	1.5 GHz Ave.	1.5 GHz Max.	2.0 GHz Ave.	2.0 GHz Max.
1a. Received Power								
Cable Loss	± 0.05		± 0.05		± 0.05		± 0.10	
Attenuator Cal.	± 0.10		± 0.10		± 0.10		± 0.10	
Antenna Efficiency	± 0.05		± 0.05		± 0.05		± 0.10	
Pwr. Meter Cal.	± 0.20		± 0.20		± 0.20		± 0.20	
Sub Total	± 0.40		± 0.40		± 0.40		± 0.50	
Mismatch	-3.0	-8.0	-3.0	-8.0	-2.0	-6.0	-2.5	-6.0
1b. E-Field Meas. 1-cm dipole probe	± 1.0							
2. Sampling Efficiency Spatial Field Var.	± 7.0		± 5.0		± 4.0		± 3.0	
Limited Sample Size (see [4])	±0.2	±0.5	±0.3	±1.0	±0.3	±1.2	±0.3	±1.5
Sub Total	±7.2	±7.5	±5.3	±6.0	±4.3	±5.2	±3.3	±4.5
3. Wave Impedance (see [4])	-2.0	-2.0	-2.0	-2.0	-2.0	-2.0	-2.0	-2.0
	+2.0	+6.0	+2.0	+4.5	+2.0	+3.5	+2.0	+3.0
E-Field Determined By Receiving Ant.								
Total Worst Case Error	-12.6	-17.9	-10.7	-16.4	-8.7	-13.6	-8.3	-13.0
	+9.6	+13.9	+7.7	+10.9	+6.7	+9.1	+5.8	+8.0
RSS Error	-8.1	-11.5	-6.4	-10.2	-5.2	-8.2	-4.6	-6.4
	+7.5	+9.6	+5.7	+7.5	+4.8	+6.3	+3.9	+5.4
E-Field Determined By Dipole Probe								
Total Worst Case Error	-10.2	-10.5	-8.3	-9.0	-7.3	-8.2	-6.3	-7.5
	+10.2	+14.5	+8.3	+11.5	+7.3	+9.7	+6.3	+8.5
RSS Error	-7.5	-7.8	-5.8	-6.4	-4.9	-5.7	-4.0	-5.0
	+7.5	+9.7	+5.8	+7.6	+4.9	+6.4	+4.0	+5.5

Table 4.2. Summary of estimated uncertainties for determining the cw field strength inside the mode-stirred RADC small reverberating chamber (2 to 18 GHz).

Source of Error	Error (dB) 2.0 GHz Ave.	2.0 GHz Max.	4.0 GHz Ave.	4.0 GHz Max.	8.0 GHz Ave.	8.0 GHz Max.	12.0 GHz Ave.	12.0 GHz Max.	18.0 GHz Ave.	18.0 GHz Max.
Max.1a.Received Power										
Cable Loss	± 0.10		± 0.10		± 0.15		± 0.15		± 0.20	
Atten. Calibration	± 0.10		± 0.15		± 0.15		± 0.20		± 0.20	
Antenna Efficiency	± 0.10		± 0.15		± 0.15		± 0.20		± 0.20	
Spec. Analyzer Cal.	± 1.00		± 1.50		± 1.50		± 1.50		± 1.50	
Sub Total	± 1.30		± 1.90		± 1.95		± 2.05		± 2.10	
Mismatch	-2.5	-6.0	-0.9	-2.4	-0.4	-0.8	-1.0	-1.5	-2.0	-2.3
1b. E-Field Meas.										
1-cm Dipole Probe	± 1.0		± 1.5		± 1.5		± 2.0		± 2.0	
2. Sampling Efficiency										
Spatial Field Var.	± 3.0		± 2.0		± 1.0		± 0.5		± 0.5	
0.5										
Limited Sample Size (see [4])	±0.1	±0.3	±0.2	±0.5	±0.3	±0.7	±0.3	±1.0	±0.3	±1.5
Sub Total	±3.1	±3.3	±2.2	±2.5	±1.3	±1.7	±0.8	±1.5	±0.8	±2.0
3. Wave Imped ≠ 120π (see [4])	Average ≤ ±2.0, -2.0 ≤ Maximum ≤ +3.0									
4. Input Power Var.	-1.2	-1.7	-0.8	-1.3	-1.6		-0.5		-1.0	
E-Field Determined By Receiving Ant.										
Total Worst	-10.1	-14.3	-7.8	-10.1	-7.3	-8.1	-6.4	-7.6	-7.9	-9.4
Case Error	+6.4	+7.6	+6.1	+8.9	+5.3	+6.7	+4.9	+6.6	+5.9	+7.1
RSS Error	-4.8	-7.5	-3.7	-4.6	-3.5	-3.7	-3.2	-3.6	-3.8	-4.3
	+3.9	+4.7	+3.5	+4.3	+3.1	+4.0	+3.0	+3.9	+3.0	+4.2
E-Field Determined By Dipole Probe										
Total Worst	-7.3	-8.0	-6.5	-7.3	-6.4	-6.8	-5.3	-6.0	-5.8	-7.0
Case Error	+6.1	+7.3	+5.7	+7.0	+4.8	+6.2	+4.8	+6.5	+4.8	+7.0
RSS Error	-4.0	-4.3	-3.4	-3.8	-3.2	-3.4	-3.0	-3.2	-3.1	-3.6
	+3.8	+4.6	+3.3	+4.2	+2.8	+3.8	+2.9	+3.9	+2.9	+4.1

Table 5.1(a). Mode-tuned data obtained from figure 5.1, giving rise times and correction factors for rf pulses in the RADC small reverberating chamber.

τ = Pulse Width ; CF ≡ Correction Factor

Freq. GHz	Nominal τ, μs	No Absorber				1 Piece Absorber			
		Rise Time, μs 63%	90%	MAX P_R mw	CF dB	Rise Time, μs 63%	90%	MAX P_R mw	CF dB
0.9	3	.445	1.139	531	0	.103	.481	167	0
0.9	1	.384	.687	500	0.26	.094	.295	158	0.24
0.9	0.3	.144	.227	320	2.20	.088	.152	171	-0.10
1.3	3	.375	1.075	408	0	.094	.149	104	0
1.3	1	.243	.493	317	1.10	.095	.148	136	-1.17
1.3	0.3	.152	.219	293	1.44	.105	.172	173	-2.21
2.0	3	.635	1.515	212	0	.087	.337	22.4	0
2.0	1	.470	.786	206	0.12	.134	.325	27.3	-0.86
2.0	0.3	.164	.252	67.2	4.99	.085	.144	22.6	-0.04
2.9	3	.495	1.108	116	0	.065	.166	19.3	0
2.9	1	.453	.833	116	0	.076	.244	22.0	-0.57
2.9	0.3	.111	.191	52.7	3.43	.067	.130	20.8	-0.33
4.2	3	.721	1.209	111	0	.161	.264	10.5	0
4.2	1	.421	.689	52.3	3.27	.153	.244	10.2	0.13
4.2	0.3	.144	.208	25.5	6.39	.150	.219	11.1	-0.24
5.65	3	1.111	2.113	52.0	0	.130	.236	4.18	0
5.65	1	.411	.677	31.1	2.23	.135	.286	4.88	-0.67
5.65	0.3	.203	.311	18.7	4.44	.109	.192	5.42	-1.13
8.9	3	.661	1.156	16.8	0	.198	.490	1.39	0
8.9	1	.330	.519	10.8	1.92	.071	.114	0.95	1.65
8.9	0.3	.150	.212	6.24	4.30	.113	.183	1.23	0.53
12	3	.524	1.195	8.70	0	.113	.209	1.17	0
12	1	.482	.815	6.85	1.04	.097	.191	1.36	-0.65
12	0.3	.138	.187	3.74	3.67	.098	.151	0.91	1.09
16	3	.517	1.267	2.67	0	.089	.276	.168	0
16	1	.376	.642	2.03	1.19	.096	.213	.221	-1.19
16	0.3	.180	.242	1.41	2.77	.117	.183	.334	-2.98
18	3	.897	1.630	3.33	0	.216	.392	.146	0
18	1	.633	.860	2.15	1.90	.100	.197	.077	2.78
18	0.3	.200	.269	0.75	6.47	.146	.215	.081	2.56

Table 5.1(b). Mode-tuned data obtained from figure 5.1, giving rise times and correction factors for rf pulses in the RADC small reverberating chamber.

τ = Pulse Width ; CF ≡ Correction Factor

		3 μs Pulses		1 μs Pulses			0.3 μs Pulses		
	Freq. GHz	63% Rise, μs	90% Rise, μs	63% Rise, μs	90% Rise, μs	CF dB	63% Rise, μs	90% Rise, μs	CF dB
No Absorber	0.9	.445	1.139	.384	.687	0.26	.144	.227	2.20
No Absorber	1.3	.375	1.075	.243	.493	1.10	.152	.219	1.44
No Absorber	2.0	.635	1.515	.470	.786	0.12	.164	.252	4.99
No Absorber	2.9	.495	1.108	.453	.833	0.00	.111	.191	3.43
No Absorber	4.2	.721	1.209	.421	.689	3.27	.144	.208	6.39
No Absorber	5.65	1.111	2.113	.411	.677	2.23	.203	.311	4.44
No Absorber	8.9	.661	1.156	.330	.519	1.92	.150	.212	4.30
No Absorber	12	.524	1.195	.482	.815	1.04	.138	.187	3.67
No Absorber	16	.517	1.267	.376	.642	1.19	.180	.242	2.77
No Absorber	18	.897	1.630	.633	.860	1.90	.200	.269	6.47
1-piece Absorber	0.9	.103	.481	.094	.295	0.24	.088	.152	-0.10
1-piece Absorber	1.3	.094	.149	.095	.148	-1.17	.105	.172	-2.21
1-piece Absorber	2.0	.087	.337	.134	.325	-0.86	.085	.144	-0.04
1-piece Absorber	2.9	.065	.166	.076	.244	-0.57	.067	.130	-0.33
1-piece Absorber	4.2	.161	.264	.153	.244	0.13	.150	.219	-0.24
1-piece Absorber	5.65	.130	.236	.135	.286	-0.67	.109	.192	-1.13
1-piece Absorber	8.9	.198	.490	.071	.114	1.65	.113	.183	0.53
1-piece Absorber	12	.113	.209	.097	.191	-0.65	.098	.151	1.09
1-piece Absorber	16	.089	.276	.096	.213	-1.19	.117	.183	-2.98
1-piece Absorber	18	.216	.392	.100	.197	2.78	.146	.215	2.56

Table 5.2(a). Mode-stirred data obtained from figure 5.5 giving rise times and correction factors for rf pulses in the RADC small reverberating chamber.

τ = Pulse Width ; CF ≡ Correction Factor

Freq. GHz	Nominal τ, μs	No Absorber				1 Piece Absorber			
		Rise Time, μs		MAX V_R mV	CF dB	Rise Time, μs		MAX V_R mV	CF dB
		63%	90%			63%	90%		
0.9	3	.246	.630	447	0	.056	.130	242	0
0.9	1	.173	.453	438	0.18	.054	.130	239	0.11
0.9	0.3	.144	.261	377	1.48	.068	.174	248	-0.21
0.9	0.1	.045	.064	206	6.73	.058	.098	189	2.15
1.3	3	.216	.466	328	0	.099	.168	174	0
1.3	1	.227	.447	331	-0.08	.121	.186	180	-0.29
1.3	0.3	.121	.231	254	2.22	.086	.134	192	-0.86
1.3	0.1	.055	.095	133	7.84	.073	.108	160	0.73
2.0	3	.388	1.157	300	0	.130	.302	86	0
2.0	1	.432	.837	300	0	.082	.194	76	1.07
2.0	0.3	.171	.267	165	5.19	.086	.151	75	1.19
2.0	0.1	.069	.151	71	12.52	.058	.091	64	2.57
2.9	3	.470	.945	236	0	.073	.130	60	0
2.9	1	.373	.734	212	0.93	.071	.168	68	-1.09
2.9	0.3	.127	.223	123	5.66	.065	.127	64	-0.56
2.9	0.1	.065	.097	74	10.07	.065	.093	54	0.92
4.2	3	.626	1.437	175	0	.125	.276	32	0
4.2	1	.440	.766	129	2.65	.119	.250	33	-0.27
4.2	0.3	.145	.219	66	8.47	.127	.243	31	0.28
4.2	0.1	.065	.097	32	14.76	.060	.089	16.8	5.60
5.65	3	.591	1.467	96	0	.073	.216	22	0
5.65	1	.291	.676	77	1.92	.086	.255	23	-0.39
5.65	0.3	.152	.247	50	5.67	.104	.240	23	-0.39
5.65	0.1	.058	.079	23	12.41	.050	.091	15.5	3.04
8.9	3	.574	1.118	134	0	.078	.142	17.1	0
8.9	1	.345	.669	109	1.79	.104	.175	18.8	-0.82
8.9	0.3	.144	.234	62	6.69	.122	.204	23	-2.57
8.9	0.1	.072	.106	30	13.00	.064	.118	14.3	1.55
12	3	.540	1.282	98	0	.130	.345	20	0
12	1	.324	.619	82	1.55	.127	.291	16.8	1.51
12	0.3	.159	.237	46	6.57	.110	.228	16.8	1.51
12	0.1	.072	.120	19.5	14.02	.063	.090	12.0	4.44
16	3	.514	1.265	77	0	.082	.164	9.7	0
16	1	.384	.794	59	2.31	.166	.324	13.3	-2.74
16	0.3	.201	.277	39	5.91	.088	.183	10.8	-0.93
16	0.1	.108	.144	16.6	13.33	.063	.090	7.1	2.71
18	3	.475	1.101	48	0	.086	.177	5.9	0
18	1	.306	.647	42	1.16	.101	.175	6.1	-0.29
18	0.3	.201	.281	27	5.00	.196	.279	6.4	-0.71
18	0.1	.095	.149	10.0	13.62	.077	.106	4.6	2.16

Table 5.2(b). Mode-stirred data obtained from figure 5.5 giving rise times and correction factors for rf pulses in the RADC small reverberating chamber.

τ = Pulse Width ; CF ≡ Correction Factor

	Freq. GHz	3 μs Pulses		1 μs Pulses			0.3 μs Pulses			0.1 μs Pulses		
		63% Rise, μs	90% Rise, μs	63% Rise, μs	90% Rise, μs	CF dB	63% Rise, μs	90% Rise, μs	CF dB	63% Rise, μs	90% Rise, μs	CF dB
No Absorber	0.9	.246	.630	.173	.453	0.18	.144	.261	1.48	.045	.064	6.73
No Absorber	1.3	.216	.466	.227	.447	-0.08	.121	.231	2.22	.055	.095	7.84
No Absorber	2.0	.388	1.157	.432	.837	0.00	.171	.267	5.19	.069	.151	12.52
No Absorber	2.9	.470	.945	.373	.734	0.93	.127	.223	5.66	.065	.097	10.07
No Absorber	4.2	.626	1.437	.440	.766	2.65	.145	.219	8.47	.065	.097	14.76
No Absorber	5.65	.591	1.467	.291	.676	1.92	.152	.247	5.67	.058	.079	12.41
No Absorber	8.9	.574	1.118	.345	.669	1.79	.144	.234	6.69	.072	.106	13.00
No Absorber	12	.540	1.282	.324	.619	1.55	.159	.237	6.57	.072	.120	14.02
No Absorber	16	.514	1.265	.384	.794	2.31	.201	.277	5.91	.108	.144	13.33
No Absorber	18	.475	1.101	.306	.647	1.16	.201	.281	5.00	.095	.149	13.62
1-pc. Absorber	0.9	.056	.130	.054	.130	0.11	.068	.174	-0.21	.058	.098	2.15
1-pc. Absorber	1.3	.099	.168	.121	.186	-0.29	.086	.134	-0.86	.073	.108	0.73
1-pc. Absorber	2.0	.130	.302	.082	.194	1.07	.086	.151	1.19	.058	.091	2.57
1-pc. Absorber	2.9	.073	.130	.071	.168	-1.09	.065	.127	-0.56	.065	.093	0.92
1-pc. Absorber	4.2	.125	.276	.119	.250	-0.27	.127	.243	0.28	.060	.089	5.60
1-pc. Absorber	5.65	.073	.216	.086	.255	-0.39	.104	.240	-0.39	.050	.091	3.04
1-pc. Absorber	8.9	.078	.142	.104	.175	-0.82	.122	.204	-2.57	.064	.118	1.55
1-pc. Absorber	12	.130	.345	.127	.291	1.51	.110	.228	1.51	.063	.090	4.44
1-pc. Absorber	16	.082	.164	.166	.324	-2.74	.088	.183	-0.93	.063	.090	2.71
1-pc. Absorber	18	.086	.177	.101	.175	-0.29	.196	.279	-0.71	.077	.106	2.16

NBS-114A (REV. 2-8C)

U.S. DEPT. OF COMM. **BIBLIOGRAPHIC DATA SHEET** *(See instructions)*	1. PUBLICATION OR REPORT NO. NISTIR 90-3939	2. Performing Organ. Report No.	3. Publication Date June 1990

4. TITLE AND SUBTITLE

EMR Test Facilities : Evaluation of a Small Reverberating Chamber Located at RADC , Griffiss AFB , Rome, New York .

5. AUTHOR(S) Myron L. Crawford, John M. Ladbury, Bill F. Riddle, and Ezra B. Larsen

6. PERFORMING ORGANIZATION *(If joint or other than NBS, see instructions)*

National Institute of Standards and Technology
~~NATIONAL BUREAU OF STANDARDS~~
DEPARTMENT OF COMMERCE
~~WASHINGTON, D.C. 20234~~ Boulder, Colorado 80303

7. Contract/Grant No.

8. Type of Report & Period Covered

9. SPONSORING ORGANIZATION NAME AND COMPLETE ADDRESS *(Street, City, State, ZIP)*

Compatibility and Measurements Division
RADC/RBC Griffiss AFB, New York 13441

10. SUPPLEMENTARY NOTES

☐ Document describes a computer program; SF-185, FIPS Software Summary, is attached.

11. ABSTRACT *(A 200-word or less factual summary of most significant information. If document includes a significant*

This report describes measurement procedures and results from evaluating a small reverberating chamber located at Rome Air Development Center (RADC), Rome, New York. The chamber was developed for measuring and analyzing the electromagnetic susceptibility/vulnerability (EMS/V) of weapon systems and the radio frequency (rf) shielding effectiveness of enclosures and materials. A brief description of the facility is given, including instrumentation for its calibration by the National Institute of Standards and Technology (NIST). Work was done earlier at NIST to evaluate the RADC large reverberating chamber. A follow-on project to construct and evaluate a small chamber is discussed in this report. Measurements include: (1) voltage standing wave ratio (VSWR) of the transmitting and receiving antennas; (2) coupling efficiency of the chamber; (3) effectiveness of the chamber tuner; (4) E-field uniformity in the test zone; (5) calibration of test E-fields based on receiving antenna power and calibrated dipole probe measurements; (6) responses of standard equipment under test (EUT) to test fields in the RADC reverberating chamber and the NIST anechoic chamber; and (7) performance of the reverberating chamber excited by rf pulses at ten frequencies from 0.9 to 18 GHz, four pulse widths from 0.1 to 3 μs, and for two values of chamber Q. Conclusions are that the chamber can be used at frequencies down to 500 MHz for cw testing, and for pulsed rf immunity testing with pulse widths as short as 0.3 μs. Estimates of measurement uncertainties are given.

12. KEY WORDS *(Six to twelve entries; alphabetical order; capitalize only proper names; and separate key words by semicolons)*

electromagnetic radiated susceptibility/vulnerability testing; pulsed rf measurements; reverberating chamber

13. AVAILABILITY

- [X] Unlimited
- [ ] For Official Distribution. Do Not Release to NTIS
- [ ] Order From Superintendent of Documents, U.S. Government Printing Office, Washington, D.C. 20402.
- [X] Order From National Technical Information Service (NTIS), Springfield, VA. 22161

14. NO. OF PRINTED PAGES 84

15. Price

☆ U.S. GOVERNMENT PRINTING OFFICE: 1990—776-075/25132

USCOMM-DC 6043-P80

AMERICAN BINDERY · EAST
1993